ANALYZING THE EFFECT OF REBAR HEATING ON BRIDGE STRUCTURES: SURFACE TEMPERATURE IMPLICATIONS

by
Pablo Andres Nunez Hernandez, B.S.
July, 2024

Director of Thesis: Suranga Gunerathne, Ph.D., P.E.

Major Department: Engineering

Abstract.

This study presents a comprehensive simulation-based analysis aimed at enhancing the serviceability of bridge decks in cold climates by preventing ice formation by applying an electrical power heat source (EPH) within transversal rebars. The objective is to identify the appropriate EPH capable of maintaining bridge surface temperatures above freezing under various climatic conditions.

The study uses "Mean Minimum Temperature" data from the U.S. Climate Normals dataset (1991-2020) to ensure simulations are applicable across diverse regions. By systematically varying the power of the embedded heat source, the research identifies the minimum required EPH input to maintain the bridge deck surface at 3°C, preventing ice formation. Key findings indicate that the developed 3D FEA model effectively avoids ice formation on bridge surfaces by using an external electrical energy source connected to transverse steel rebars. Parameters such as outside temperature, wind speed, and EPH location significantly influence the heating system's performance. A stress analysis confirms this method's feasibility, providing designers with guidelines.

The study concludes that maintaining a spacing of 12 inches (0.3048 meters) is optimal for the EPH placement, and for ensuring structural integrity, the EPH heat flow should be at most 1.22kW.

ANALYZING THE EFFECT OF REBAR HEATING ON BRIDGE STRUCTURES: SURFACE TEMPERATURE IMPLICATIONS

A Thesis

Presented to the Faculty of the Department of Engineering

East Carolina University®

In Partial Fulfillment of the Requirements for the Degree

Master of Science in Mechanical Engineering

by

Pablo Andres Nunez Hernandez, B.S.

July, 2024

Director of Thesis: Suranga Gunerathne, Ph.D., P.E.

Thesis Committee Members:

Kurabachew Duba, Ph.D.

Amin Akhnoukh, Ph.D.

Acknowledgements

First, I want to thank my parents for all the support and guidance they have always given me and for always trusting my decisions. They have made me the person I am today. To my siblings, for always helping and motivating me to surpass myself.

I want to thank to my dear girlfriend Andrea, who supports me unconditionally and always gave me words of encouragement to keep going despite all the adversities, words cannot fully convey how much I cherish her presence and love, which have been a constant source of inspiration. I also thank her family, who always made me feel welcome.

A special thanks to my advisor Dr. Gunerathne and Dr. Akhnoukh for their constant help, guidance, and recommendations in carrying out this thesis. Likewise, thanks to Dr. Duba for being part of my committee.

Thanks to Michael, Emre, and Ben, my master's classmates, and lifelong friends.

Finally, I want to thank God for all the blessings received during this stage and throughout my life. May your light continue to guide my path.

Contents

LIST OF TABLES..... vi
LIST OF FIGURES..... vii
ACRONYMS..... x
NOMENCLATURE..... xi
CHAPTER 1..... 1
INTRODUCTION..... 1
1.1 RESEARCH OBJECTIVES..... 3
1.1.1 RESEARCH QUESTIONS..... 4
1.1.2 HYPOTHESIS..... 4
CHAPTER 2..... 6
BACKGROUND..... 6
2.1 CONDUCTION..... 7
2.2 CONVECTION..... 10
2.2.1 Boundary layer..... 13
2.2.2 Reynolds number..... 14
2.2.3 Prandtl number..... 14
2.2.4 Nusselt number..... 15
2.2.5 Correlation for laminar flow over a flat surface..... 15
2.2.6 Correlation for turbulent flow over a flat surface..... 16
2.3 RADIATION..... 16
CHAPTER 3..... 18
RESEARCH METHODOLOGY..... 18
3.1 INTRODUCTION..... 18
3.2 TYPE OF INVESTIGATION..... 18
3.3 DESIGN AND DEVELOPMENT OF THE MODEL..... 19
3.4 SIMULATION RUNS..... 21
3.5 BOUNDARY CONDITIONS..... 22
3.6 MESHING TECHNIQUE..... 24

3.7 VALIDATION. 27

CHAPTER 4. 32

RESULTS AND ANALYSIS. 32

ANALYSIS OF DIFFERENT PARAMETERS FOR 5 REPRESENTATIVE STATES. 33

4.1. Electrical power heat source. 33

4.2 Wind speed. 45

4.3 Location of the EPH. 53

4.4 Stress analysis. 61

CHAPTER 5 67

CONCLUSION. 67

5.1 ANSWER TO THE RESEARCH QUESTIONS. 67

5.2 GENERAL CONCLUSIONS. 68

5.3 RECOMMENDATIONS. 68

5.4 FUTURE WORK. 69

References 70

APPENDIX A 75

Temperature distribution with the recommended EPH across the states of USA. 75

APPENDIX B 96

Table of ideal EPH for each state. 96

LIST OF TABLES.

Table 1. Values of convection heat transfer coefficient.....12
Table 2. Structural and thermal properties of the materials. 21
Table 3. Sensitivity analysis of the mesh. 26
Table 4. Datapoints of temperature for Alaska. 33
Table 5. Datapoints of temperature for Virginia.....36
Table 6. Datapoints of temperature for Missouri. 38
Table 7. Datapoints of temperature for Tennessee. 39
Table 8. Datapoints of temperature for South Carolina. 41
Table 9. Electrical power required at different ambient temperatures. 43
Table 10. Beauford scale. 46
Table 11. Convective film coefficient for each state. 46
Table 12. Electrical power in kW required for different wind speeds at different temperatures. 47
Table 13. Electrical power in kW required for different small values of wind speeds at different temperatures. 49
Table 14. Table of EPH required (kW) according to wind speed and temperature. 53
Table 15. Alternate heating method data in Alaska.....55
Table 16. Alternate heating method data in Virginia. 56
Table 17. Alternate heating method data in Missouri. 57
Table 18. Alternate heating method data in Tennessee.....58
Table 19. Alternate heating method data in South Carolina. 60
Table 20.Critical stress concentration in concrete and rebars.....64
Table 21. Ideal EPH for state. 96

LIST OF FIGURES.

Figure 1. Percentage of injuries and fatalities due to icy conditions. 2
Figure 2. Convection phenomenon in a plane surface. 11
Figure 3. Velocity along the boundary layer. 13
Figure 4. External dimensions of the bridge's deck. 20
Figure 5. Distribution of the rebars in the upper layer. 21
Figure 6. The faces of the transversal rebars are subjected to different heat flow. 22
Figure 7. Boundary conditions. 23
Figure 8. Relationship between temperature difference and convection coefficient. 24
Figure 9. Tetrahedrons mesh before sizing. 25
Figure 10. Tetrahedrons mesh after refinement sizing. 27
Figure 11. TR comparison of previous experimental data with the simulation. 29
Figure 12. TC comparison of previous experimental data with the simulation. 29
Figure 13. Temperature distribution applying constant heat flow. 30
Figure 14. Total deformation of the replicated specimen. 31
Figure 15. Temperature distribution in the left edge of the deck in Alaska 34
Figure 16. Temperature distribution in the top edge of the deck in Alaska. 35
Figure 17. Linear fit expression for minimum surface temperature vs power of the heat source in Alaska. 36
Figure 18. Temperature distribution in the left edge of the deck in Virginia 37
Figure 19. Linear fit expression for minimum surface temperature vs power of the heat source in Virginia. 37
Figure 20. Temperature distribution in the left edge of the deck in Missouri 38
Figure 21. Linear fit expression for minimum surface temperature vs power of the heat source in Missouri. 39
Figure 22. Temperature distribution in the left edge of the deck in Tennessee 40

Figure 23. Linear fit expression for minimum surface temperature vs power of the heat source in Tennessee. 41
Figure 24. Temperature distribution in the left edge of the deck in South Carolina 42
Figure 25. Linear fit expression for minimum surface temperature vs power of the heat source in South Carolina. 43
Figure 26. Electrical power required for avoiding icing formation. 44
Figure 27. EPH required at different wind speeds – polynomial fit. 48
Figure 28. EPH required per state at different wind speeds. 50
Figure 29. Trend analysis at lower wind speed velocities. 51
Figure 30. EPH required at different wind speeds – logarithmical fit. 52
Figure 31. Alternate heating of rebars. 54
Figure 32.Surface temperature distribution in Alaska with alternate rebar heating. 55
Figure 33. Surface temperature distribution in Virginia with alternate rebar heating. 57
Figure 34. Surface temperature distribution in Missouri with alternate rebar heating. 58
Figure 35. Surface temperature distribution in Tennessee alternate rebar heating 59
Figure 36. Surface temperature distribution in South Carolina alternate rebar heating. 60
Figure 37. Von-Mises stress distribution in the transversal rebar. 62
Figure 38. Stress distribution in the concrete. 64
Figure 39. Temperature distribution in the left edge of the deck in Alabama 75
Figure 40. Temperature distribution in the left edge of the deck in Arizona 76
Figure 41. Temperature distribution in the left edge of the deck in Arkansas 76
Figure 42. Temperature distribution in the left edge of the deck in California 77
Figure 43. Temperature distribution in the left edge of the deck in Connecticut 77
Figure 44. Temperature distribution in the left edge of the deck in Delaware 78
Figure 45. Temperature distribution in the left edge of the deck in Georgia 78
Figure 46. Temperature distribution in the left edge of the deck in Idaho 79
Figure 47. Temperature distribution in the left edge of the deck in Illinois 79
Figure 48. Temperature distribution in the left edge of the deck in Indiana 80
Figure 49. Temperature distribution in the left edge of the deck in Iowa 80
Figure 50. Temperature distribution in the left edge of the deck in Kansas 81
Figure 51. Temperature distribution in the left edge of the deck in Kentucky 81
Figure 52. Temperature distribution in the left edge of the deck in Louisiana 82
Figure 53. Temperature distribution in the left edge of the deck in Maine 82

Figure 54. Temperature distribution in the left edge of the deck in Maryland 83
Figure 55. Temperature distribution in the left edge of the deck in Massachusetts 83
Figure 56. Temperature distribution in the left edge of the deck in Michigan 84
Figure 57. Temperature distribution in the left edge of the deck in Minnesota 84
Figure 58. Temperature distribution in the left edge of the deck in Mississippi 85
Figure 59. Temperature distribution in the left edge of the deck in Montana 85
Figure 60. Temperature distribution in the left edge of the deck in Nebraska 86
Figure 61. Temperature distribution in the left edge of the deck in New Hampshire 86
Figure 62. Temperature distribution in the left edge of the deck in New Jersey 87
Figure 63. Temperature distribution in the left edge of the deck in New Mexico 87
Figure 64. Temperature distribution in the left edge of the deck in New York 88
Figure 65. Temperature distribution in the left edge of the deck in North Carolina 88
Figure 66. Temperature distribution in the left edge of the deck in North Dakota 89
Figure 67. Temperature distribution in the left edge of the deck in Ohio 89
Figure 68. Temperature distribution in the left edge of the deck in Oklahoma 90
Figure 69. Temperature distribution in the left edge of the deck in Oregon 90
Figure 70. Temperature distribution in the left edge of the deck in Rhode Island 91
Figure 71. Temperature distribution in the left edge of the deck in South Dakota 91
Figure 72. Temperature distribution in the left edge of the deck in Texas 92
Figure 73. Temperature distribution in the left edge of the deck in Utah 92
Figure 74. Temperature distribution in the left edge of the deck in Vermont 93
Figure 75. Temperature distribution in the left edge of the deck in Washington 93
Figure 76. Temperature distribution in the left edge of the deck in West Virginia 94
Figure 77. Temperature distribution in the left edge of the deck in Wisconsin 94
Figure 78. Temperature distribution in the left edge of the deck in Wyoming 95

ACRONYMS.

DOT. US Department of transportation.

FHWA. Federal highway administration.

NHTSA. National Highway Traffic Safety Administration

NaCl. Sodium chloride

$CaCl_2$. Calcium chloride

Na. Sodium.

EPH. Electrical power heat source.

FEA. Finite element analysis.

NOAA. National Oceanic and Atmospheric Administration

AASHTO. American Association of State Highway and Transportation Officials.

LFRD. Load and Resistance Factor Design.

ACI. American Concrete Institute.

NOMENCLATURE.

E: Internal energy.

$\dot{Q}$: Heat added to the system.

$\dot{W}$: Work done by the system.

c: Specific heat capacity.

ρ: Density.

q: Heat flux vector.

v: Velocity field.

D: Conductivity matrix.

T_∞: Temperature of the fluid far from the source.

T: The absolute temperature. (K or °R)

T_0: Absolute temperature of the surroundings or the ambient temperature. (K)

Q: Heat transfer rate. (W, watts)

k: Thermal conductivity of the material. (W/mk)

A: Cross-sectional area perpendicular to the heat transfer direction. (m^2)

h: Convection heat transfer coefficient. (W/m^2K)

S: Surface area where convection takes place.

u: Characteristic velocity of the fluid. (m/s)

L: Linear dimension where the fluid flows. (m)

μ: Dynamic viscosity of the fluid. (Pa s)

v: Kinematic velocity of the fluid. (m^2/s)

α: Thermal diffusivity. (m^2/s)

C_p: Specific heat capacity at a constant pressure. (J/kg K)

Nu_x: Local Nusselt number at a specific length.

N: Number of radiating surfaces.

P: Total power radiated by the black body.

σ: Stefan-Boltzmann constant, 5.67×10^{-8} (W/m^2K^4

CHAPTER 1.

INTRODUCTION.

Bridges play a crucial role in the transportation infrastructure, enabling the easy movement of people and goods from one place to another. When weather is harsh, specifically in winter climates, the potential formation of ice above these structures creates severe challenges for the safety of both people and the structure itself.

Diverse data shows a significant increase in accidents and crashes caused by icy conditions[1]. This results in human casualties because of the inherent danger of collisions and reduces transportation accessibility, leading to economic losses and inconvenience for commuters[2].

According to data from the DOT, a high number, exceeding 70% of the nation's road network, is in areas characterized by harsh environmental conditions that could lead to ice formation over the roads. Several factors associated with dangerous driving conditions because of the buildup of ice, such as low pavement friction, more distance needed for stopping, and compromised vehicle maneuverability, among others, result in reduced speeds, less roadway capacity, and an elevated percentage of accidents[3].

The consequences of this adverse weather are considerable, with over 1,300 fatalities and over 116,800 injuries reported annually, Figure 1, in vehicular incidents caused by these icy conditions[4].

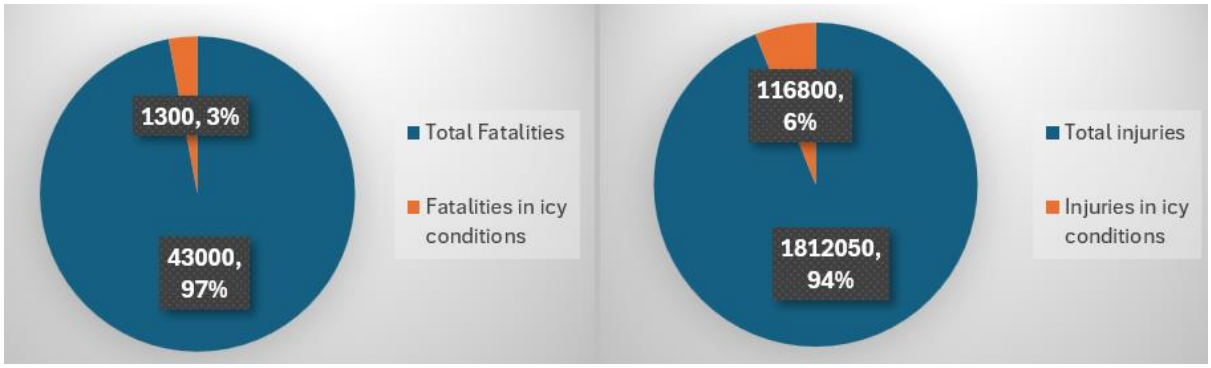

Figure 1. Percentage of injuries and fatalities due to icy conditions.

The current methods for deicing the bridges have primarily relied upon the utilization of deicing salts, such as NaCl or $CaCl_2$[5]. Although these salts have shown efficacy in the timely melting of ice and snow, it has also been shown that the application of salt and other chemicals does not melt snow when the temperature falls below $-3.9\ °C$ [6], which is a limitation of the use of salts. Moreover, the application of salts brings associated challenges. Primarily, the corrosive nature of deicing salts has been identified as a catalyst for the accelerated degradation of bridge structures[7]. This deterioration phenomenon reduces the overall service life of the infrastructure and incurs high maintenance costs[8]; approximately 20% of the DOT maintenance budgets are being used for winter road maintenance. State and local authorities collectively invest over 2.3 billion dollars annually in operations related to snow and ice control[4].

Other concerns about using salts include environmental damage to the surrounding areas, the accumulation of salts in the ecosystems raising ecological alarms, the risk of water body contamination, and threats to surrounding vegetation and wildlife[9]. The cumulative effect of these environmental hazards reveals the need for alternative, more sustainable deicing strategies.

To address these challenges, there is a growing need to explore alternative methods of deicing that are more sustainable, efficient, and environmentally friendly. In recent years, heat transfer has emerged as a promising approach for mitigating ice accumulation on bridge surfaces[10],[11]. Utilizing heat to avoid ice formation can minimize the effects associated with traditional deicing salts while maintaining the structural integrity of bridge components.

The thermal approach is an effective method for avoiding ice formation over bridges. Several studies have shown that ice and snow melt using hydronic heating systems, which use water, glycol, or another fluid circulated through pipes as the heat-transfer medium[12],[6], electrical heating cables or pipes, which consist of wires embedded in the bridge deck that generate heat when an electric current passes through them[11], and electrically conductive concrete[13].

While most research has focused on incorporating the previously mentioned elements into the design of bridge decks, there is limited information on heating the actual components of bridges; one research performed by Mehrabi[14] has studied the thermo-mechanical response of various components of the bridge in under thermal loading including the rebars. Therefore, this thesis aims to explore the temperature distribution on the surface of the bridge deck by heating the steel rebars, a structural component embedded within the structure.

1.1 RESEARCH OBJECTIVES.

This thesis aims to identify the appropriate EPH capable of preventing ice formation on bridges under established climatic conditions. This goal is directed toward analyzing the effect of rebar heating on bridge structures and evaluating its impact on the resulting surface temperatures. The research focuses on analyzing how various

environmental conditions, including temperatures, wind speeds, and the location of the EPH, impact the performance of this proposed heating system for bridges.

1.1.1 RESEARCH QUESTIONS.

- Is there a relationship between the EPH and the temperature on the surface of the bridge that can avoid the ice formation on the structure?
- How the different parameters used in the study affect the temperature distribution in the surface of the bridge's deck.
- Is there any thermo-mechanical limitation of the bridge's model?

1.1.2 HYPOTHESIS.

- A linear relationship exists between the EPH and the surface temperature of the bridge.
- The required EPH to prevent ice formation on bridge surfaces increases with higher wind speeds and decreases with higher outside temperatures.

By employing heat transfer principles, the research will explore the conductive properties of steel bars within bridges to transmit heat throughout the structure, effectively avoiding ice formation on the bridge's surface. The investigation will include a comprehensive analysis of the bridge's thermal behavior under different simulated conditions.

To achieve these objectives, the research will employ simulations in Ansys to model the heat transfer process within the steel bars of bridges. Various heating scenarios will be considered, including different heat flow intensities, wind speeds, and location of the EPH to predict the temperature distribution at the top of the bridge deck. The simulation results will be compared to understand the heat transfer mechanism and identify a relation between the EPH and the temperature distributions on the surface.

The outcomes of this investigation will offer significant results regarding the viability and efficacy of rebar heating as an innovative approach to deicing bridges. This research aspires to contribute substantially to advancing sustainable and ecologically deicing methodologies. The final goal is to increase the safety of individuals using bridges, underscoring the dual importance of environmental and public safety in the domain of infrastructure maintenance.

The results of the simulations will offer valuable information for decision-makers, bridge engineers, and relevant stakeholders to make informed choices regarding the best methods for deicing bridges in areas with harsh winter weather, considering the structure's structural integrity.

CHAPTER 2.

BACKGROUND.

Heat transfer is an innovative method currently being studied to address the challenge of ice formation on bridges in the wintertime. There are several studies that include the heat transfer process for deicing bridges. Most of them are studies that use geothermal energy and an external pump in a closed system for circulating a fluid through a pipe embedded in the bridge structure[15], the stable temperature of geothermal energy prevents ice formation by maintaining a surface temperature above freezing.

Using an external device can be a solution for avoiding ice formation; an electrical heat source can make the most of the characteristics of the thermal conductivity of the rebars, an essential element in a bridge. Several studies include the implementation of electric heating pipes embedded in the concrete layer[16], it has been demonstrated that an electrical heating source can effectively raise the temperature of the bridge components, resulting in no ice formation on the surface of it[17].

Heat transfer, in general terms, involves the movement of thermal energy from a region of higher temperature to a region of lower temperature[18], there are three primary types of heat transfer:

2.1 CONDUCTION.

The conduction phenomenon is a heat transfer process that occurs when there is direct contact between two or more materials. In the context of avoiding ice formation on a bridge, conduction is the primary heat transfer process because the electrical heat source will be directly exposed to the heat faces of the rebar. Then, there will be conduction between the rebars and the concrete, which are in direct bonded contact inside the bridge deck. Additionally, convection plays a vital role in this process, as it facilitates the transfer of heat from the concrete surface to the surrounding air, further aiding in the prevention of ice formation.

Conduction happens because of the movement of thermal energy from high-energy particles inside a material to lower-energy particles[19]. In a bridge deck, when the face of a steel rebar is exposed to an electrical energy source, there will be more thermal energy from the particles inside the rebar, and thus, they will start vibrating. The highly energetic particles near the heat source will collide with the neighboring particles, and because of this collision, there will be energy transfer in the process[20]. This chain reaction of energy transfer will continue through the material, propagating particle by particle. This phenomenon happens at a microscopic level and is quick, so the heat moves efficiently along the material. The rate at which this heat transfer happens depends on several factors. The most important ones are thermal conductivity (a physical property of the material), density, and temperature.

Materials with high thermal conductivity will conduct heat more efficiently. Steel rebars have a high thermal conductivity value, allowing heat to transfer quickly through them[21].

The thermal conduction equation is given by the first law of thermodynamics, as shown in Equation(1). The first law for a control volume can be stated as:

$$\frac{dE}{dT} = \dot{Q} - \dot{W} \tag{1}$$

For simplicity, we assume no work is done by the system ($\dot{W}$=0), and the heat added ($\dot{Q}$) results in a temperature change. The internal energy E, Equation(2) is related to temperature T by the specific heat capacity c and the density ρ.

$$E = \rho c T \tag{2}$$

Taking the time derivative:

$$\frac{dE}{dT} = \rho c \frac{\partial T}{\partial t}$$

Heat can be conducted and convected in a differential control volume, shown in Equation(3). Fourier's law describes heat conduction, and a convective term describes heat convection. Considering a source term representing internal heat generation. The heat transfer per unit volume can be written as:

$$\dot{Q} = -\nabla q + \rho c \mathrm{v} \ \nabla T + \dot{q} \tag{3}$$

According to Fourier's law of heat conduction, Equation(4):

$$q = -k \nabla T \tag{4}$$

The divergence of the heat flux is shown in Equation(5):

$$\nabla q = -\nabla (k \nabla T) \tag{5}$$

Substituting in the heat transfer equation:

$$\dot{Q} = \nabla (k \nabla T) + \rho c \mathrm{v} \ \nabla T + \dot{q}$$

Equating the rate of change of internal energy with the heat transfer term:

$$\rho c \frac{\partial T}{\partial t} = \nabla (k \nabla T) + \rho c \mathrm{v} \ \nabla T + \dot{q}$$

Generalizing the differential operators and variables in matrix form and denoting the gradient operator ∇ by L:

$$\rho c \frac{\partial T}{\partial t} + \rho c \mathrm{v} \,.\, LT + L^T q = \dot{q}$$

Note that v.LT is the dot product, that can be written as $\mathrm{v}^T LT$ in matrix form:

The equation becomes:

$$\rho c \left(\frac{\partial T}{\partial t} + \mathrm{v}^T \,.\, LT \right) + L^T q = \dot{q}$$

Then Fourier's law, Equation(4) is used to relate the heat flux vector to the thermal gradients, integrating D as the conductivity matrix:

$$q = -DLT$$

Then it is found Equation(6) which is the governing equation for conduction and convection.

$$\rho c \left(\frac{\partial \mathrm{T}}{\partial \mathrm{t}} + \mathrm{v}^T \,.\, LT \right) = L^T (DLT) + \dot{q} \tag{6}$$

There are three types of boundary conditions:

1. Specified temperatures acting over the surface.

2. Specified heat flows acting over the surface.

3. Specified convection surfaces acting over the surface or Newtons law of cooling shown in Equation(7).

$$\dot{q} = \mathrm{h}(\mathrm{T}\text{-}\mathrm{T}_\infty) \tag{7}$$

2.2 CONVECTION.

Convection is the transfer of heat through the movement of fluids, such as air or water[22]. While convection is minimally related to direct heat transfer between bridge structures, it will significantly impact the heat dissipation from the bridge surface to the surrounding environment.

When the rebar in the bridge gets hot, by conduction, there will be a rise in the temperature of the concrete as well, and it will heat the air or surrounding fluid around it. In this case, the fluid will be the air circulating through the bridge. The heat will be transferred to the particles of air that are directly touching the surface of the bridge's deck. Once these particles gain energy from the concrete, they will start moving vigorously, and when the particles of the air become heated, they tend to move apart from each other, becoming less dense. In gravity, less dense material always rises above denser material. As the hot air rises, it creates a space filled by the cooler air, which will happen along all the bridge surfaces. This is called natural convection or free convection[23].

An external force, the wind, inducing the movement of the air, increases the heat transfer ratio from or to the bridge structures. This aspect can be a crucial parameter when analyzing the temperature distribution on the surface of the bridge's deck. This process is called forced convection.

When wind blows across a bridge, it acts as an external force that moves the air particles around its surface. Usually, forced convection results in a higher heat transfer rate than natural convection[24] because the movement of the air is more vigorous than the slow and steady movement produced by natural convection.

The rate of heat transfer because of forced convection depends on several factors, including the wind speed magnitude and the direction of the wind[25][26]. Higher wind

speeds usually increase the heat transfer rate because they replace the warmed air on the bridge's surface faster. The direction of the air also plays a role. It affects the parts of the bridge most exposed to the wind current.

This factor needs special attention and consideration, specifically for bridges that do not have a structure or soil below them. They will have accelerated heat loss because of the forced convection[27] and the action of the winds blowing by the upper and lower parts of them.

Convection plays an essential role in the thermal behavior of bridge structures, especially when the conditions create more heat dissipation on the bridge's surface. When modeling the bridge's deck, some simplifications must be done to address the convection phenomena. The assumptions include creating a plane surface and wind flowing parallel to the surface. Figure 2 shows how the velocity variation of the air and temperature will affect the structure in ideal conditions of parallel air flow.

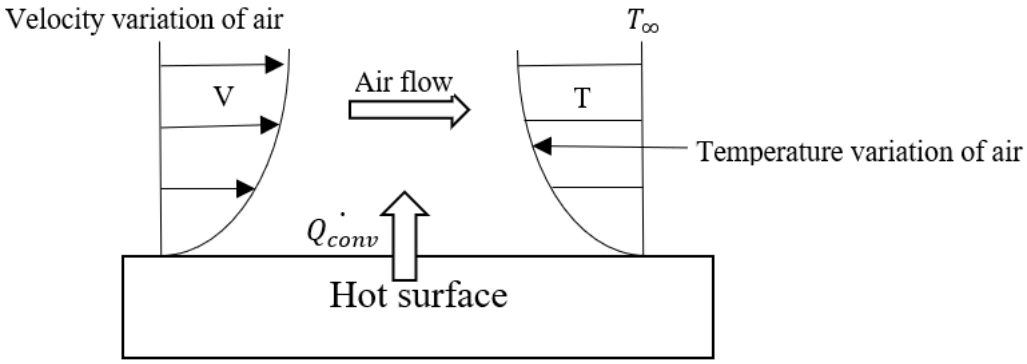

Figure 2. Convection phenomenon in a plane surface.

Usually, *h*, the convection heat transfer coefficient, is obtained by experiments, and it depends on several factors such as:

- Bulk fluid velocity.

Increasing the fluid's velocity will also increase the convective heat transfer coefficient. A higher velocity tends to disrupt the thermal boundary layer that forms on the object's surface.

- Properties of the fluid.

  The fundamental properties that affect the convective heat transfer coefficient include viscosity, thermal conductivity, specific heat, and density[28].

- Surface geometry.

  Different geometrical features can affect the convective heat transfer coefficient because they affect the fluid flow patterns and the overall transfer rate. The most important ones are usually the surface area, shape, and surface roughness. A rough surface area can promote the effect of turbulence, which will increase the heat transfer rate, especially in forced convection.

- Nature of the fluid motion.

  This is related to natural and forced convection. In natural convection, fluid motion is driven by density differences within the fluid, while in forced convection, fluid motion is generated by external means, such as a fan, pump, or blowing wind. Table 1 displays the predetermined values obtained from experiments that explain the convection heat transfer coefficient in different phases and states of matter.

Table 1. Values of convection heat transfer coefficient.

Process	Range of h [W/m^2 K]
Free convection.	
Vapors.	3-25
Liquids.	20-1000
Forced convection.	

Vapors.	10-500
Liquids.	100-15000
Phase change.	
Between liquids and vapor	5000-10000

2.2.1 Boundary layer.

The boundary layer in the fluid forms right next to the object's surface when a fluid flows past it, Figure 3. The velocity of the fluid within the boundary layer changes from zero at the surface (because of the no-slip condition where the fluid sticks to the surface) to nearly the free stream velocity (the velocity of the fluid far away from the surface) as you move away from the surface. In this layer, the effects of viscosity (the fluid's resistance to flow) are significant.

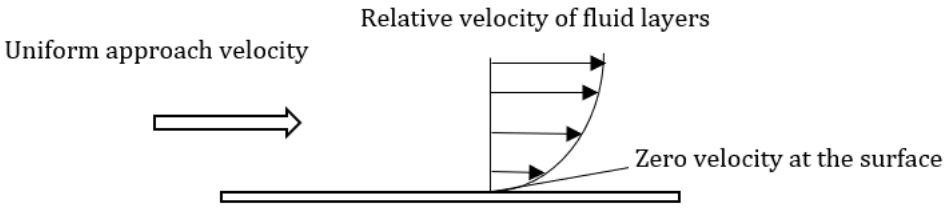

Figure 3. Velocity along the boundary layer.

The study of this layer is very complex, and extensive research has been performed on flat plates[29]. The importance of the velocity layer lies in the friction between the fluid and the surface. It is also essential in the momentum of the fluid, which is directly influenced by the Reynolds number[30].

Several dimensionless numbers are very important for characterizing the flow and heat transfer behavior in the study of heat transfer, especially in convection[31]. These

numbers allow the comparison of different physical situations and can be a tool for developing correlations for heat transfer coefficients.

Three main dimensionless numbers—the Reynolds number, Equation(8), the Prandtl number, Equation(9), and the Nusselt number, Equation(10)—are of paramount importance in the study of heat transfer and convection. Understanding these numbers is crucial for characterizing and predicting the flow and heat transfer behavior in various physical situations.

2.2.2 Reynolds number.

$$Re = \frac{\rho u L}{\mu} = \frac{u L}{v} \tag{8}$$

The Reynolds number is significant because the numerical results indicate the flow regime and determine whether it is laminar or turbulent. For flat surfaces, a Reynolds number of 500000 and below is considered laminar, and a Reynolds number over 500000 is considered turbulent[32].

2.2.3 Prandtl number.

$$Pr = \frac{v}{\alpha} = \frac{\mu C_p}{k} \tag{9}$$

The Prandtl number compares the momentum diffusivity to the thermal diffusivity of the fluid. It is essential in heat transfer, especially in studying the boundary layer behavior. “The Prandtl number represents a dimensionless value intrinsic to a fluid. Fluids with low Prandtl numbers exhibit high thermal conductivity and fluidity, making them suitable for heat-conducting liquids[33]”. For example, Na has a value of 0.01, air 0.72, and glycerol 7612.74.

2.2.4 Nusselt number.

$$Nu = \frac{hL}{k} \tag{10}$$

The Nusselt number compares the convective heat transfer to conductive heat transfer within the fluid. A higher Nusselt number shows more effective convective heat transfer relative to conduction[34].

Using specific correlations to calculate the convective heat transfer coefficient over flat surfaces in both laminar and turbulent flows is crucial for design and analysis in thermal engineering because of their accuracy and relevance in predicting thermal behavior across a broad range of applications[35]. These correlations, derived from theoretical and experimental solutions, enable engineers to estimate how changes in flow conditions confidently.

It is crucial to select appropriate correlations for calculating this coefficient. It depends on several factors, including the system's geometry, the nature of the fluid flow (laminar or turbulent), the temperature difference, and the fluid's physical properties.

Using correlations specifically derived or validated for flat geometries is essential for simulations involving plane surfaces. Plane surfaces have distinct characteristics in flow boundary layers and heat transfer dynamics compared to curved surfaces or complex geometries.

2.2.5 Correlation for laminar flow over a flat surface.

The local Nusselt number in a laminar flow over a flat plate is verified for values of the Re number < 500000 and is given by Equation(11):

$$Nu_x = 0.332 Re^{\frac{1}{2}} Pr^{\frac{1}{3}} \tag{11}$$

2.2.6 Correlation for turbulent flow over a flat surface.

A commonly used correlation is the Colburn correlation[36], also known as the Reynolds-Colburn analogy, Equation(12), to calculate the convective heat transfer coefficient on flat surfaces in turbulent flow. This correlation applies to turbulent flows over a flat plate. It is based on the concept that an analogy exists between heat transfer and momentum transport in turbulent flows.

$$Nu = 0.0296\, Re^{\frac{4}{5}} Pr^{\frac{1}{3}} \tag{12}$$

Findings from various sources in studies about how heat moves in fluids reveal an interesting pattern. When looking at how heat is transferred alongside flat surfaces and turbulent flow inside tubes, there are some similarities if the temperature is assumed to be at a specific layer, known as the 'film' temperature. This overlap in data highlights that, despite the different settings, the way heat moves in these situations shares fundamental similarities[36].

2.3 RADIATION.

Radiation is the transfer of heat through electromagnetic waves. It can contribute to heat transfer because electromagnetic waves penetrate the molecules and heat them at specific rates [37]. Other forms of radiation include infrared heaters, ultraviolet lamps, and others.

One of radiation's properties is that of other types of heat transfer; radiation does not require the presence of an intervening medium. This is because electromagnetic waves can travel through the vacuum of space, and when they hit an object, they can be absorbed, reflected, or transmitted[38].

The efficiency of solar radiation absorption depends on several factors, such as color, texture, and the angle at which the waves strike the surface[39]. Darker surfaces are known to absorb higher radiation. The color black results from a surface absorbing most of the wavelength of visible light that strikes it. This is not only happening with the visible spectrum but also the infrared radiation, which is the main component of thermal energy generated by the sun or other sources[40], lighter surfaces reflect more of the incoming radiation. The reflectivity of a surface is not only determined by color but also depends on the material surface properties, such as texture and composition, “albedo” is the term used for defining the reflectivity of solar radiation from a surface[41]. The range is from 0 to 1, where 0 indicates that a surface reflects all incoming light and absorbs none.

It is important to note that all bodies, solid, liquid, and gases, at temperatures above absolute zero, emit, absorb, or transmit radiation to varying degrees[42].

The radiation emitted by a body is based on the Stefan-Boltzmann Law, Equation(13):

$$P = \sigma A T^4 \tag{13}$$

CHAPTER 3.

RESEARCH METHODOLOGY.

3.1 INTRODUCTION.

In this section of the study, the methodology employed to develop a bridge deck model is presented, a bridge that functions as the pathway for vehicular traffic, cyclists, and pedestrians. This model's primary objective is to prevent ice formation on the bridge's surface. This goal will be achieved by strategically applying heat to the upper steel reinforcement bars embedded within the deck structure. The research focuses on simulating temperature variations across the deck's surface. By maintaining the surface temperature within a narrow range of 2 to 4 degrees Celsius, the model aims to avoid ice formation effectively[43],[44]. This temperature regulation is critical for ensuring the safety and integrity of the bridge during cold weather, potentially mitigating the risks associated with ice formation.

3.2 TYPE OF INVESTIGATION.

The investigation is based on computational simulations. Specifically, ANSYS FEA software is used to model the concrete bridge and check the temperature profiles across the surface of the bridge's deck[45]. The investigation will employ an EPH simulated by the program when applied directly to the structure's transversal reinforcement bars (rebars).

The main goal is to investigate the relationship between the EPH and the resultant temperature variations observed on the bridge deck. Exploring this method is necessary to evaluate the feasibility of heating a structural element in the bridges to avoid ice formation. Also, by doing this, there will be a better understanding of how heat transfer mechanisms impact the overall thermal behavior of a bridge.

3.3 DESIGN AND DEVELOPMENT OF THE MODEL.

For this study, the standards followed were the American Association of State Highway and Transportation Officials' "AASHTO LRFD Bridge Design Specifications"[46] and the ACI Committee 318's "ACI 318-19: Building Code Requirements for Structural Concrete"[47].

According to the DOT, "the specifications require that the minimum thickness of a concrete deck should not be less than 7 inches (0.1778m)"[4]. Usually, the range for the thickness of the deck is between 7 to 10 inches.

The thickness of the deck is set as 9 inches (0.2286m), the span will have a value of 100 inches (2.54m), and the lane width of the deck is set as the standard for freeways according to the FHWA 144 inches (3.6576m) for each lane[48]. Figure 4 shows the bridge's deck dimensions used for the simulations.

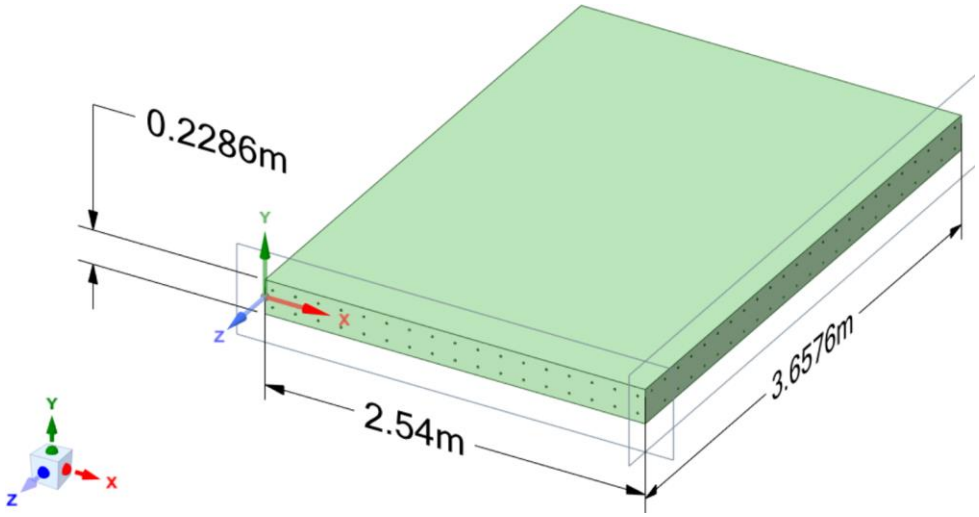

Figure 4. External dimensions of the bridge's deck.

Simulation of the bridge in ANSYS involved simulating one of the two halves and mirroring all components to create the final bridge model.

Starting from the top, the first layer is 1.5 inches thick, followed by a 1-inch-thick layer of concrete. Within this 1-inch layer, steel reinforcement bars are placed. The separation of these two layers serves only as a reference, and the model was considered just as one complete concrete layer. The span has 24 longitudinal bars spaced 6 inches (0.1524m) apart. Additionally, there are 17 transverse bars spaced 6 inches apart along the length of 2.54m[46],[47]. The longitudinal bars are positioned next to the top of the 1-inch concrete layer and have a diameter of 0.5 inches[47]. The transverse bars are adjacent to the bottom of the 1-inch layer, fitting perfectly within the structure. After, there is a 2-inch-thick layer. This configuration represents half of the bridge deck, with the lower half being an exact mirror of the upper layers. Figure 5 shows the distribution of longitudinal and transverse rebars used in the simulations.

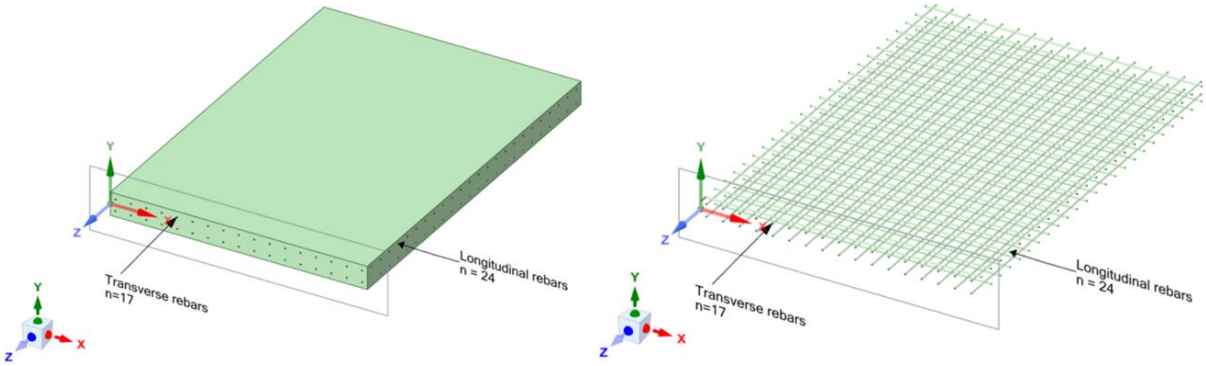

Figure 5. Distribution of the rebars in the upper layer.

The characteristic properties of the materials were assigned into the model according to the literature review[16],[49]. The reinforcement rebars utilized in the bridge deck construction are composed of structural steel[49]. The concrete is assumed to be a high-temperature-conductive Portland concrete[16]. The principal properties of the bridge components are shown in Table 2.

Table 2. Structural and thermal properties of the materials.

	Concrete	Structural steel
Thermal conductivity W/(m·°C)	2.75	60.5
Specific heat (J/Kg °C)	780	434
Density (Kg/m3)	2600	7850
Young's Modulus	3e10	2e11
Poisson's ratio	0.18	0.3
Bulk modulus (Pa)	1.5625e10	1.66e11
Shear modulus (Pa)	1.2712e10	7.69e10
Tensile yield strength (Pa)	N/A	2.5e8
Compressive yield strength (Pa)	N/A	2.5e8
Tensile ultimate strength (Pa)	5e6	4.6e8

3.4 SIMULATION RUNS.

Different EPHs at constant heat flow will be introduced to the 17 exposed faces of the transversal rebars. Figure 6 shows the "heat faces" of the corresponding 17 rebars to

check the temperature distribution at different power levels. The analysis iterates until finding an appropriate energy source capable of maintaining the lowest recorded temperature on the top of the bridge deck at the desired 3°C.

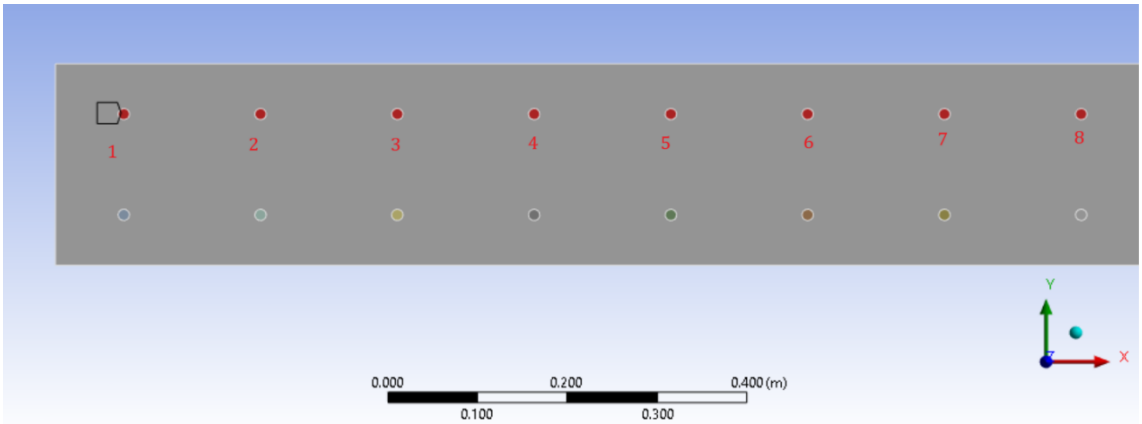

Figure 6. The faces of the transversal rebars are subjected to different heat flow.

A reference temperature was selected for each state to gather temperature data for the simulations. The coldest temperature corresponded to Alaska, with an average of -28.5°C. This information was obtained from the government website weather[50]. Specifically, the "Mean Min Temperature" data from the U.S. was used for this purpose. The U.S. Climate Normals offer a detailed collection of data products, presenting typical climate conditions at thousands of U.S. locations based on data collected from 1991 to 2020.

3.5 BOUNDARY CONDITIONS.

Figure 7 explains the boundary conditions in the model. Left and right surfaces are periodic boundaries, meaning the system extends infinitely in one or more dimensions. The top and bottom surfaces are exposed to the different external environment temperatures obtained from the dataset explained before. The simulations assume the same value for the convection and outside temperature. In this study, another consideration adopted is that when comparing the temperature of the concrete structure to the surrounding environment, there was no significant difference, so the impact of the

radiation on this model becomes negligible, meaning that the heat exchange between the concrete and its surroundings primarily occurs through both convection and conduction mechanisms. Because of this, the effect of the radiation was neglected in the simulated model.

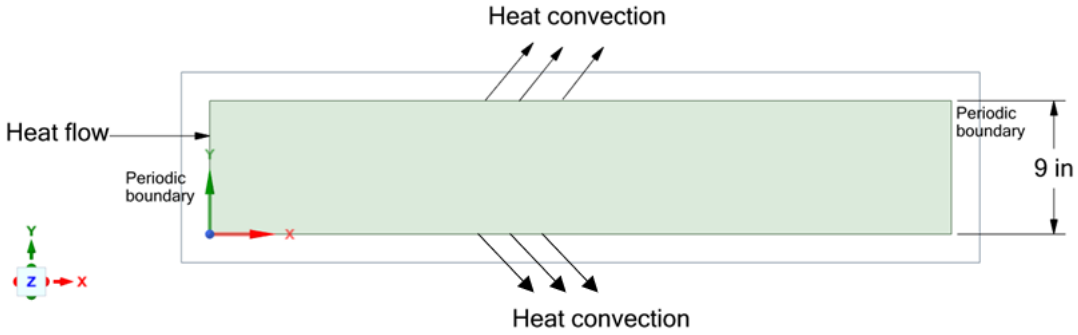

Figure 7. Boundary conditions.

Experiments were used to determine the heat convective transfer coefficient over a flat surface, it is important to note that the convection coefficient is temperature dependent, and the calculations for it were done by considering stagnant air at a velocity of 0.25 (m/s). Calculating the convection coefficient of the air depending on the temperature requires obtaining the thermodynamic properties of the air at specific temperatures. The thermodynamic tables from the book 'Thermodynamics: An Engineering Approach' were utilized for this purpose[51].

For a temperature of 1°C, we have:

ρ: 1.2874 (kg/m^3)

C_p: 1006 (J/kg K)

k: 0.0237

μ: 1.734e-5

Prandtl number: 0.73596

Using the Equation(8) for calculating the Reynolds number we got:

$$Re = \frac{\rho u L}{\mu} = 67889.19$$

Then, applying Equation(11):

$$Nu = 0.332 Re^{\frac{1}{2}} Pr^{\frac{1}{3}}$$

Finally, replacing the value in Equation(10) the value for h is: $1.24 \frac{w}{m^{2\circ}C}$

The Colburn relation expresses that there are similarities when assuming the film temperature for flat surfaces and horizontal cylinders in turbulent flows[36], then the film coefficient can be obtained from the data in horizontal cylinders and stagnant air[45], Figure 8 shows the non-linear relationship between the convection coefficient and the temperature.

Temperature[°C]	Convection coefficient [w/(m²°C)]
1	1.24
5	1.88
10	2.67
30	3.36
50	4.04
100	5.76
200	7.25
300	8.3
500	9.84
700	11.01
1000	12.4

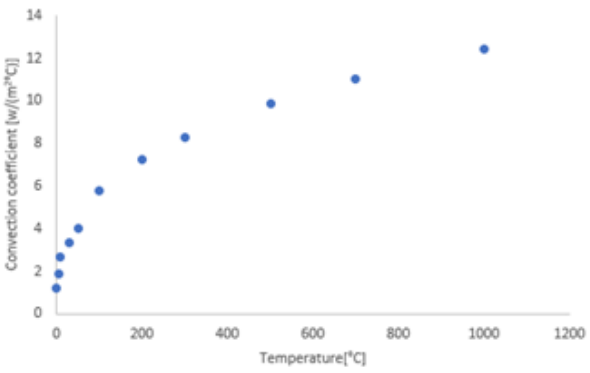

Figure 8. Relationship between temperature difference and convection coefficient.

3.6 MESHING TECHNIQUE.

A mesh sensibility analysis was performed. This is important in ANSYS because an accurate meshing technique and size ensure the reliability of the computer simulations. Determining the optimal mesh "density" can offer an adequate balance between computational efficiency and solution accuracy. One common technique for performing

mesh sensitivity analysis is to refine the mesh size and record the data. If the data do not change, this indicates convergence, which implies that similar values appear in the results even with further mesh refinement. When reaching that point there will be accurate results independent of the element size. This is important for accurately capturing the key phenomena studied in the thesis, such as thermal gradients and stress concentrations. Then, when evaluating the results, there will be areas where they become critical, and they will serve as a comparison point for critical values, such as the ultimate strength of the materials.

Figure 9 presents the finite element meshing, utilizing the tetrahedrons method. The choice of the tetrahedral method for meshing in this study is based on its capacity to accurately represent the geometries and details present in the model. The tetrahedral method's flexibility in capturing regular shapes and volumes is a key advantage, but its ability to allow a refined mesh in areas of importance, such as the transverse rebars where the EPH is connected[52], is particularly useful. The tetrahedral method is also suitable when accommodating domains characterized by varying material properties, ensuring precision in simulations encompassing thermal dynamics and structural mechanics.

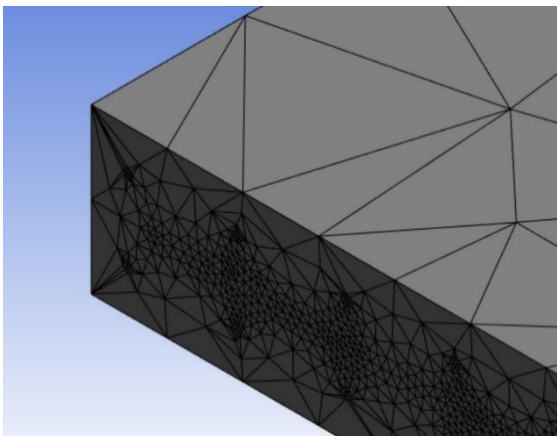

Figure 9. Tetrahedrons mesh before sizing.

Table 3 shows the sensitivity analysis of the mesh used for the simulations. The element size is significant when conducting the study, as the main criterion is trying to get a convergence value.

The 0.01m element size selection in the mesh analysis is justified based on a careful balance between accuracy and the computational resources used. The data shows a converging trend in the temperature values as the mesh size is refined. The temperature change from 0.03 m to 0.01 m is approximately 2.4%, while the change from 0.01 m to 0.005 m is only about 1.5%. The percentage error in temperature decreases from 3% at 0.01 m to 2% at 0.005 m, showing that the benefits of further refinement are minimal. The computational cost increases significantly with finer meshes, as seen with the jump from 951,933 elements and 2,061,024 nodes at 0.01 m to 1,049,871 elements and 2,229,142 nodes at 0.005 m. A 3% error is typically acceptable for practical engineering applications, making the 0.01 m mesh size a prudent choice.

Table 3. Sensitivity analysis of the mesh.

Element size (m)	# Elements	#Nodes	Temperature (°C)	% Error on temperature
Default-0.2225	848293	1880629	3.821	
0.1	894448	1961284	3.491	9%
0.06	909519	1987644	3.289	6%
0.03	920822	2007414	3.145	5%
0.01	951933	2061024	3.0682	3%
0.005	1049871	2229142	3.0221	2%

A finer mesh is necessary because it significantly increases the accuracy and resolution of computational simulations. A finer mesh allows a more detailed representation of the modeled geometry and physical phenomena. This improved detail

helps capture small-scale variations and complexities, leading to more precise results. The small element size in the heating area, shown in Figure 10, is adopted for having accurate results and for checking precisely any critical parameters in the design of the model.

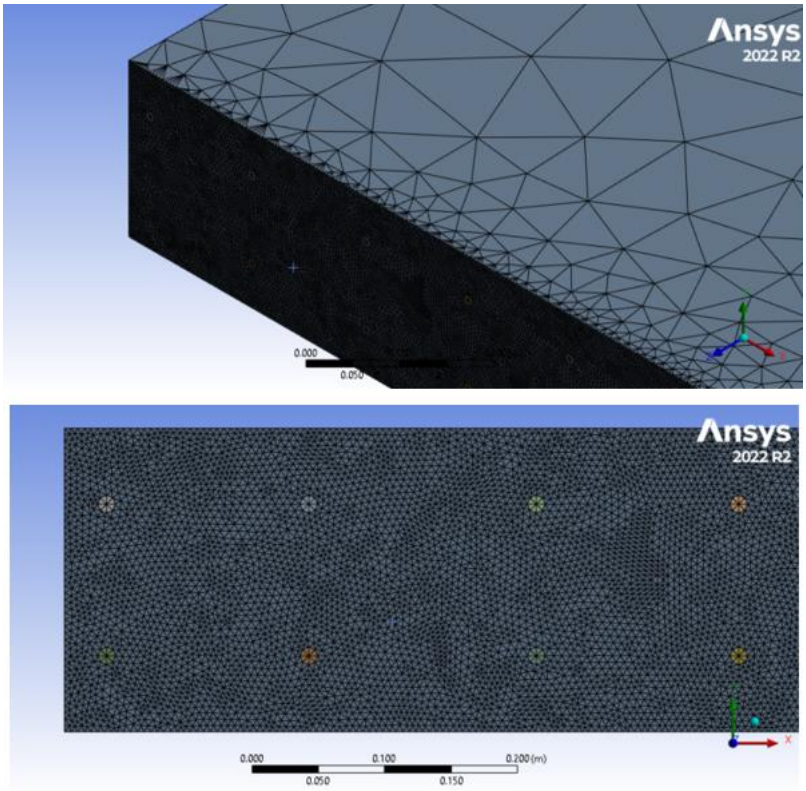

Figure 10. Tetrahedrons mesh after refinement sizing.

3.7 VALIDATION.

To validate the model, a prior study titled "Thermo-mechanical assessment of heated bridge deck under internal cyclic thermal loading from various heating elements: pipe, cable, rebar" was referenced[14]. In this study, boiling water served as the heat source due to its consistent temperature maintenance throughout the test.

The experimental setup used a cylindrical concrete specimen with a diameter of 150 mm and a length of 300 mm, containing a 400 mm long, 16 mm rebar embedded longitudinally at the center. The specimen was heated by immersing the rebar in boiling

water contained in a steel pot and heated using a portable pan stove. The specimen was positioned vertically on a plywood stand placed over the water pot. Water was continuously supplied through an opening in the plywood to account for water loss due to boiling. Temperature measurements were taken using thermocouples connected to a data acquisition system via amplifiers. The critical difference between the referenced study and this research is the form of heating. The referenced study used boiling water to heat the rebar, while this thesis employed a continuous flow into the rebars as the heating technique.

Comparing the thermocouples' readings allows for assessing the validity of the proposed model, simulating a real-world scenario. Two sets of thermocouples were analyzed: the first set, labeled "TR-X," was placed near the central rebar, and the second set, labeled "TC-X," was installed on the outer surface of the cylinder.

Figure 11 compares the experimental values obtained from the literature review to the results acquired for our simulations for the TR thermocouples. The maximum difference between the two is 6.03%, which indicates a generally good agreement between the simulated and experimental data. This discrepancy of 6.03% was observed at the TR (152) point, suggesting that while the simulation captures the overall trend accurately, there may be factors influencing higher temperature regimes that require further investigation.

Similarly, in Figure 12, the most significant deviation observed for the TC thermocouples is 6.18% at TC (279). This discrepancy, although slightly higher than that of the TR thermocouples, still suggests a reasonable agreement between simulation and experiment across the temperature range. This finding underscores the importance of

validating simulations against experimental data across various conditions to ensure robustness and accuracy in predictive models.

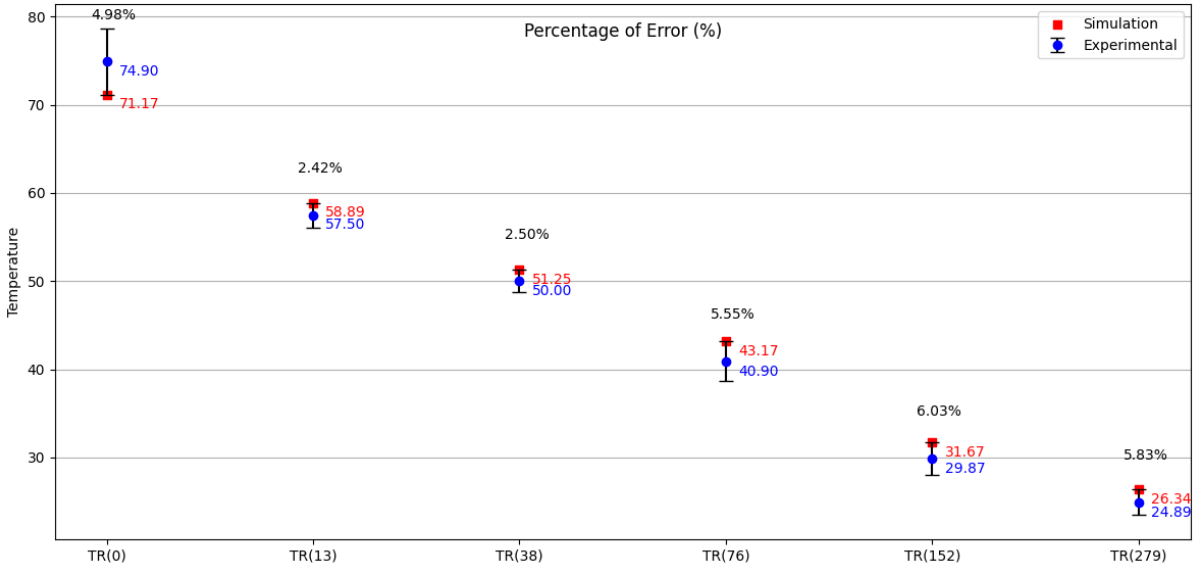

Figure 11. TR comparison of previous experimental data with the simulation.

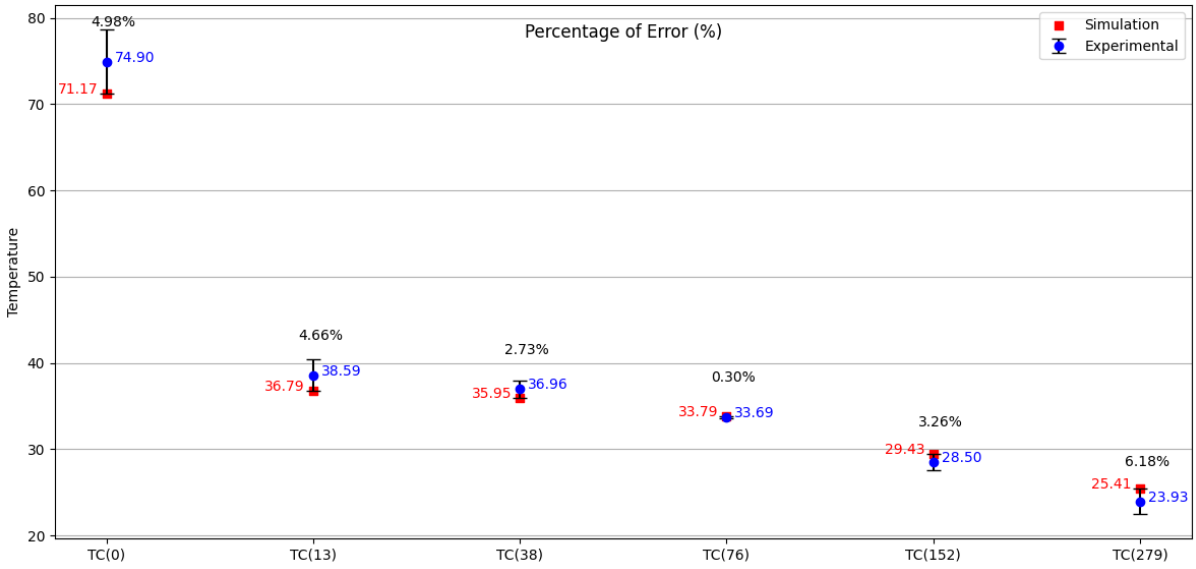

Figure 12. TC comparison of previous experimental data with the simulation.

Further analysis involved numerically modeling a transverse strip of a concrete deck slab. In their previous study, the authors simulated a strip with dimensions of 0.15 m width, 0.15 m depth (in the Z-direction), and a length of 2 m. The simulation applied a uniform heat source of 60°C throughout the traditional steel rebar. In contrast, our thesis simulations applied a uniform heat flow to the transverse face of the molybdenum bar.

Materials identical to those in the referenced research were employed to ensure consistency and comparability, specifically concrete and a molybdenum bar. This choice was due to the broad variability in concrete properties across literature sources. By utilizing the same concrete type as the original study, significant variables were controlled, ensuring any discrepancies in results stemmed solely from the method of heating rather than material properties. Using a molybdenum bar, characterized by a higher melting point and superior thermal conductivity than steel, significantly influenced heat absorption and dissipation dynamics.

Figure 13 replicates the previously stated research, demonstrating that the results align with the author's findings. This is evident through the temperature distribution, which shows similar values for two critical points reported in the original study: the temperature at the "concrete interface," or the area adjacent to the molybdenum rebar, is 55-57°C [14], and the "temperature at the external surface of the concrete slab" is 26°C.

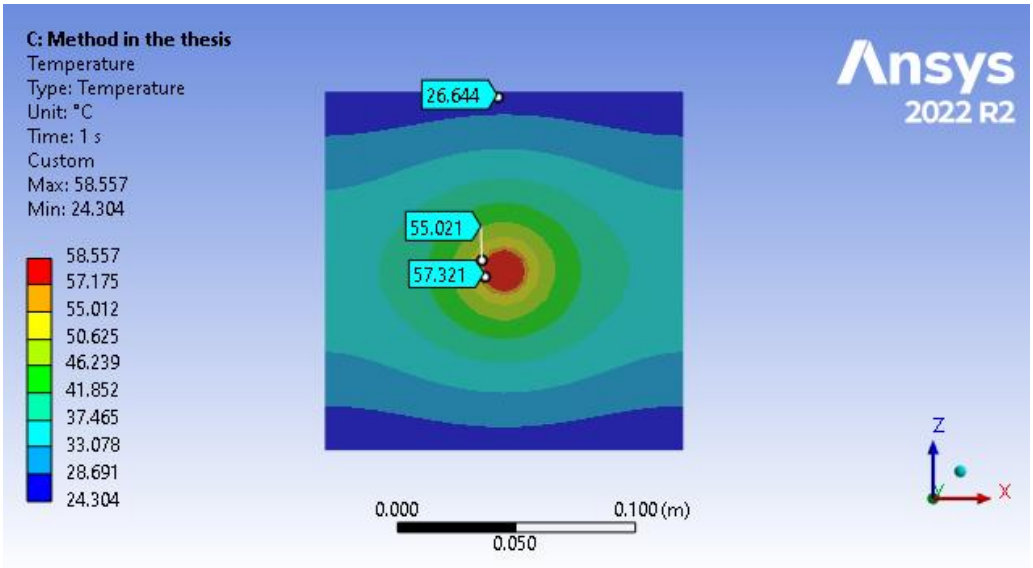

Figure 13. Temperature distribution applying constant heat flow.

The "temperature at the external surface of the concrete slab" (26°C) was used as a reference point for the subsequent analysis, as shown in Figure 14. After implementing the heat flow method, a parameter, specifically the total deformation, was compared. The total deformation from the previous research was 2.1116e-5 m; the results for the model used in the thesis show a total deformation of 2.0131e-5 m.

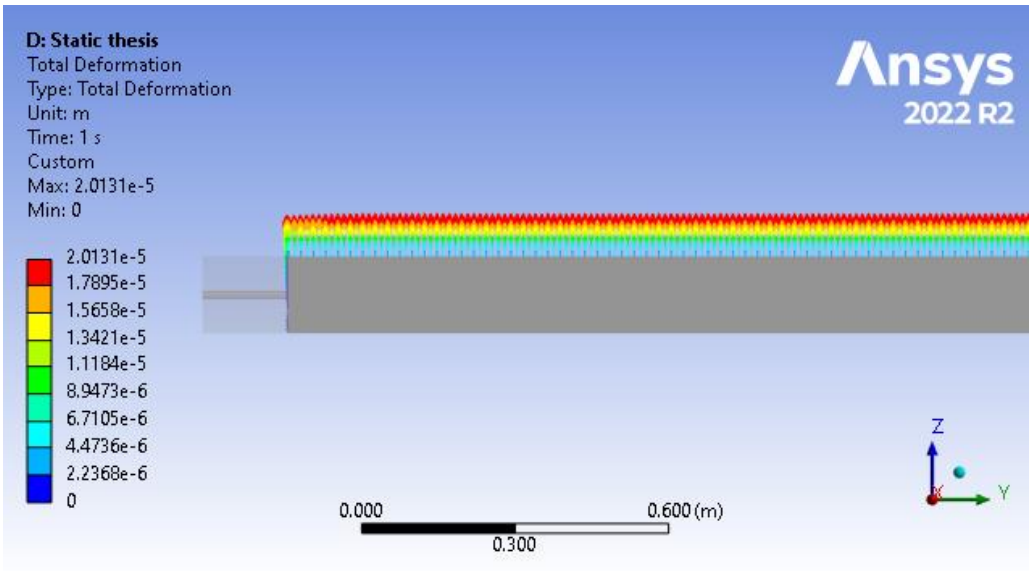

Figure 14. Total deformation of the replicated specimen.

To validate these results, a comparison was made, and the percentage error was calculated as follows:

$$\%\text{Error} = \frac{(2.1116e{-}5){-}(2.0131e{-}5)}{2.1116e{-}5} x100$$

$$\%\text{Error} = 4.66\%.$$

This low percentage error indicates that the results from the current study are in good agreement with the original research, further validating the methodology and findings.

CHAPTER 4.

RESULTS AND ANALYSIS.

This section discusses the results of the simulations performed with previously mentioned data. Understanding the relationship between the EPH and the resulting temperature distribution at the top of the bridge deck represents a complex task, especially understanding how environmental conditions can affect the structure. In the simulations, six data points were selected for each state. The interest is to explore a range of temperatures close to the actual value of 3°C to avoid ice formation over the bridges.

The parameters in these simulations include the range of temperatures of the data obtained from the "Mean Minimum Temperature" data from the U.S. Climate Normals dataset. It is noticed that the temperatures vary between ranges, where the lowest temperature recorded is a median temperature of -28.5°C.

Given the complexity and the computational time required for each simulation and the approach to conducting simulations for each state, limiting the number of data points to 6 per state is a pragmatic decision. It balances the necessity of detailed data against the constraints of time and computational resources.

ANALYSIS OF DIFFERENT PARAMETERS FOR 5 REPRESENTATIVE STATES.

In this section, the analysis will explore the results for different parameters in 5 states: Alaska, Virginia, Missouri, Tennessee, and South Carolina, with corresponding ambient temperatures of -28.5, -16.5, -10.444, -4.667, and -0.278°C, respectively. The states were chosen based on their representative temperature variations. Analyzing each state individually will enhance understanding of the influence of the other parameters involved in the study.

4.1. Electrical power heat source.

Table 4 shows the values for the power heat source and minimum surface temperature in Alaska.

Table 4. Datapoints of temperature for Alaska.

Alaska (-28.5°C)	
Power of the heat source (kW)	Minimum temperature in the Surface (°C)
10	4.69
9	3.54
8.6	3.06
8	2.27
7	0.76
6	-0.9

In Alaska, as shown in Figure 15 , the state with the recorded lowest temperature, an 8.6kW EPH, is necessary to achieve the target temperature, specifically 3.0682°C. It is important to note the temperature decreases exponentially as it moves away from the area where the reinforcement bar is in contact with the power source, which aligns with expectations. Upon analyzing the results, the hottest part is observed on the surface where the power source is applied, registering a temperature of 541.33°C in the concrete.

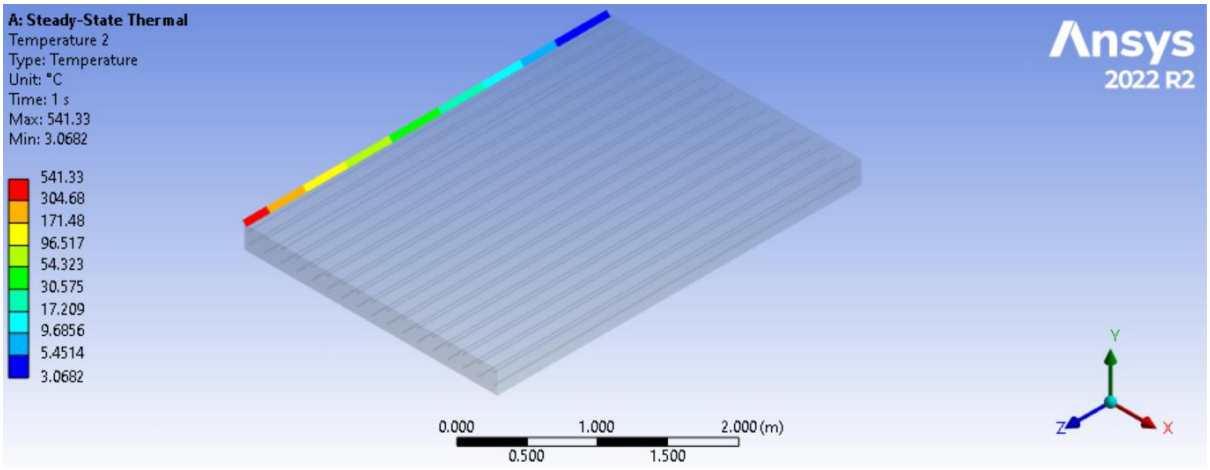

Figure 15. Temperature distribution in the left edge of the deck in Alaska using a 8.6 kW power energy source.

Figure 16 displays the temperature distribution along the edge farthest from the EPH. This edge was chosen due to its distance from the heat source, which contains the coldest point on the entire upper surface of the bridge deck. A uniform temperature distribution pattern is evident longitudinally, which helps minimize the risk of warping, cracking, or other structural deformations due to differential expansion or contraction. The maximum temperature difference observed is 0.0079°C.

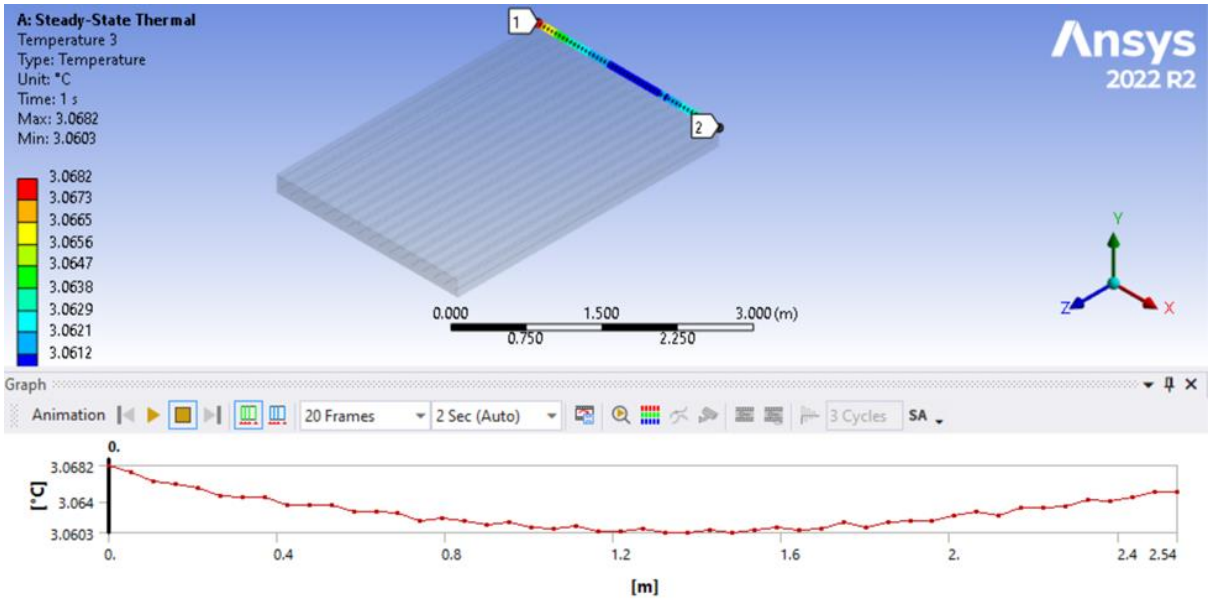

Figure 16. Temperature distribution in the top edge of the deck in Alaska.

The mathematical relationship between the power of the heat source and the minimum surface temperature is observed in Figure 17. At lower power levels, the minimum surface temperature falls below zero, indicating that the power of the heat source is insufficient to keep the surface above the freezing point under the conditions tested. For this case, even high values of the EPH, 6kW, are not enough to reach the desired temperature, giving us a clear idea of how difficult it is to reach the desired value under extremely cold climates.

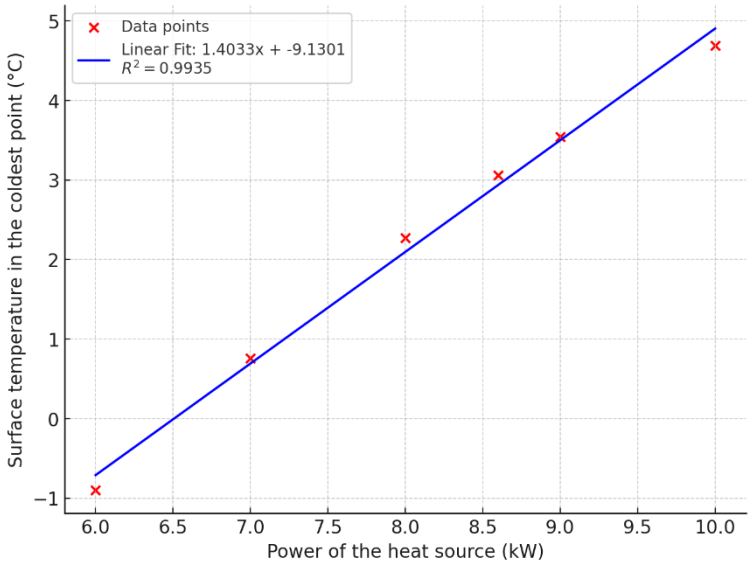

Figure 17. Linear fit expression for minimum surface temperature vs power of the heat source in Alaska.

Table 5 shows the results for the next state, Virginia, with a median temperature of -16.5℃.

Table 5. Datapoints of temperature for Virginia.

Virginia (-16.5°C)	
Power of the heat source (kW)	Minimum temperature in the Surface (°C)
5.5	5.38
5	4.62
4.5	3.76
4	2.86
3.5	1.86
3	0.74

Figure 18 shows that in Virginia, applying a 4000W EPH is necessary for achieving the desired target temperature of 2.856°C. Additionally, the maximum temperature on the deck's surface is 278.99°C, a significant reduction compared to Alaska.

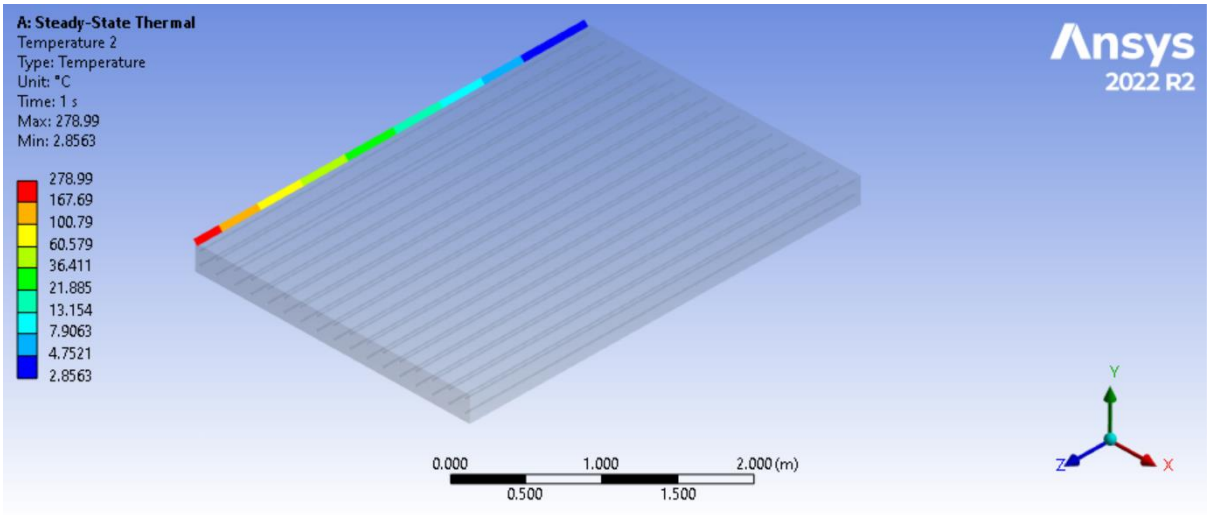

Figure 18. Temperature distribution in the left edge of the deck in Virginia using a 4 kW power energy source.

Continuing the analysis, Figure 19 shows that the state's initial temperature implies a decreased need for electrical power to achieve the desired temperature; at -16.5°C, a power of approximately 4kW will be enough. When evaluating the curve for fitting the target temperature, the result is an EPH of 4.14kW.

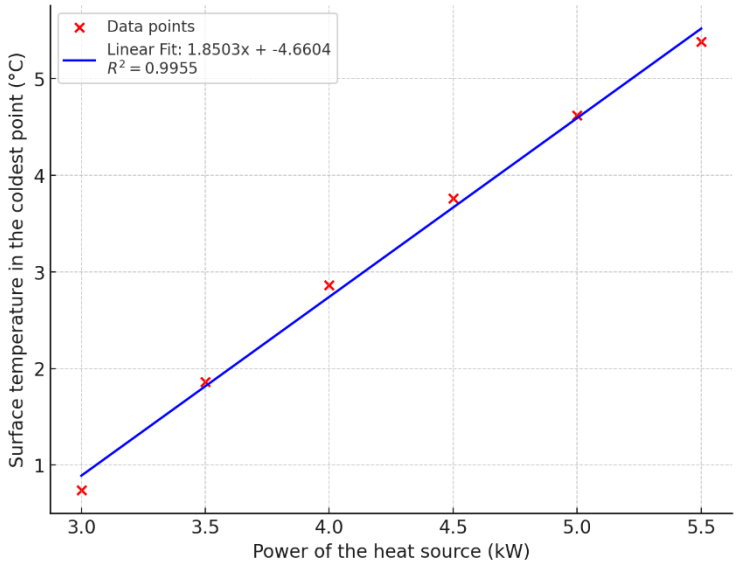

Figure 19. Linear fit expression for minimum surface temperature vs power of the heat source in Virginia.

The next state analyzed is Missouri, Table 6 shows the values that were generated by the simulations.

Table 6. Datapoints of temperature for Missouri.

Missouri (-10.444°C)	
Power of the heat source (kW)	Minimum temperature in the Surface (°C)
4	6.28
3.5	5.41
3	4.45
2.5	3.35
2	2.05
1.5	0.45

At a temperature of -10.444°C, it is observed in Figure 20 that the requirement for the EPH is around 2.5kW. The maximum temperature recorded in this simulation is 187.55°C, which follows the tendency as the ambient temperature keeps decreasing.

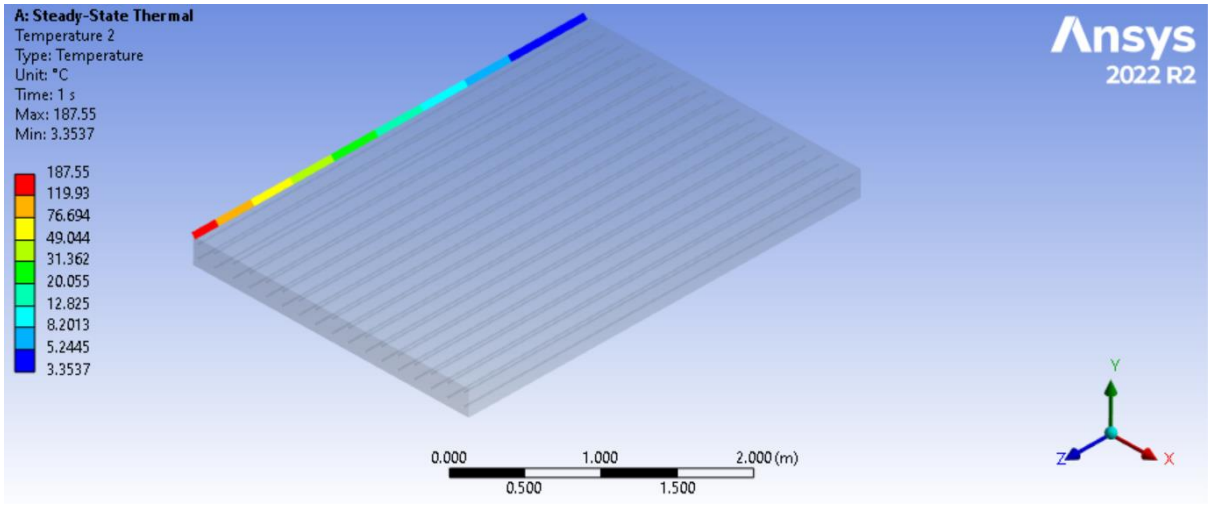

Figure 20. Temperature distribution in the left edge of the deck in Missouri using a 2.5 kW power energy source.

Consistent with the graphs analyzed previously, Figure 21 shows a linear relationship. The reduction of the power of the heat source is a direct response to the decreasing temperature of the state; a heat flow of 2.46kW will be enough to reach the temperature to avoid ice formation over the bridge's deck. The model gives a value of

0.9869, suggesting that approximately 98.69% of the variation in the dependent variable (surface temperature at the coldest point) can be explained by the independent variable (power of the heat source). This strongly indicates that the model is a good fit for the data.

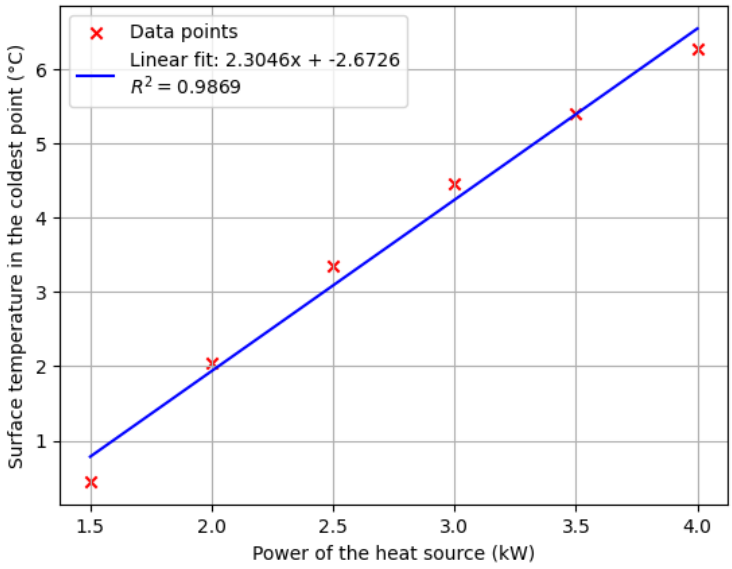

Figure 21. Linear fit expression for minimum surface temperature vs power of the heat source in Missouri.

The following state analyzed is Tennessee, Table 7 shows the values that were generated by the simulations.

Table 7. Datapoints of temperature for Tennessee.

Tennessee (-4.667°C)	
Power of the heat source (W)	Minimum temperature in the Surface (°C)
1.8	4.97
1.6	4.48
1.4	3.92
1.2	3.29
1	2.58
0.8	1.76

According to Figure 22, utilizing a 1.2kW EPH results in a minimum surface temperature of 3.29°C. This observation contributes to our understanding of the thermal

effects induced by varying the electrical power input. Specifically, it highlights how a relatively low power setting can still achieve temperatures above freezing under specific conditions related to “warmer” temperatures.

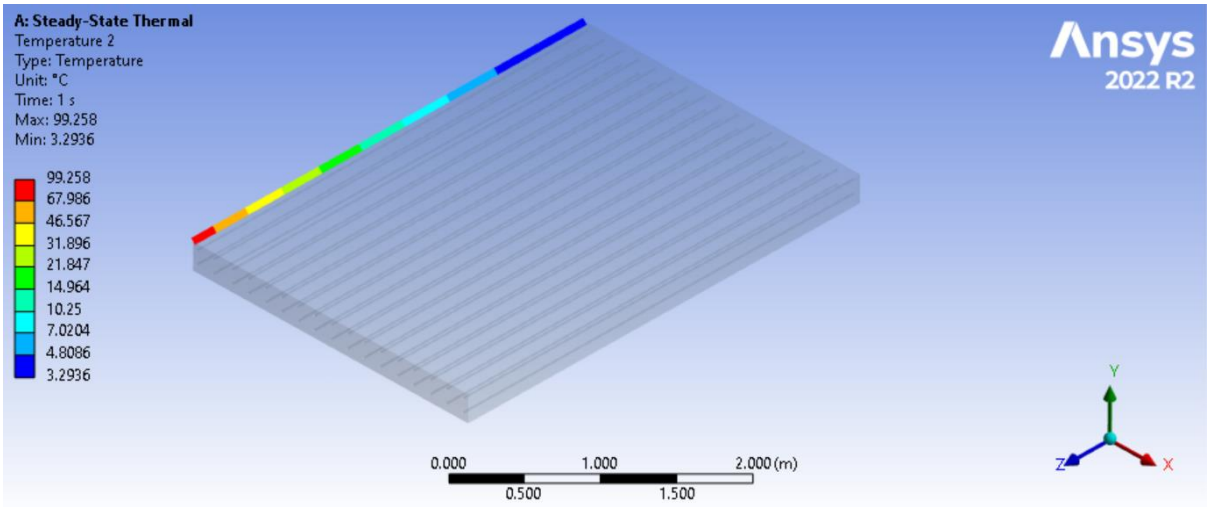

Figure 22. Temperature distribution in the left edge of the deck in Tennessee using a 1.2 kW power energy source.

In Figure 23, the positive linear coefficient shows a direct relationship between power and temperature. For each 0.1 kW increase in the power of the heat source, the surface temperature in the coldest point increases by approximately 0.31971 degrees Celsius. When fitting the data into the linear expression the value of the EPH required for this state is 1.14kW.

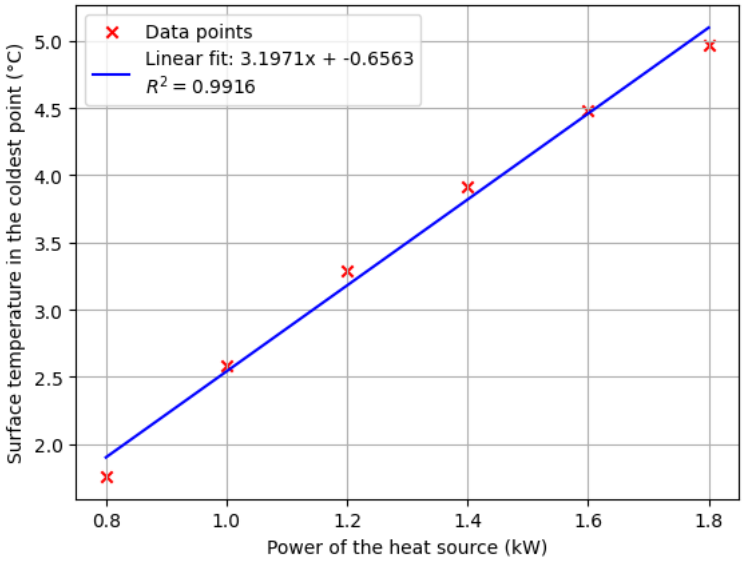

Figure 23. Linear fit expression for minimum surface temperature vs power of the heat source in Tennessee.

Finally, the last state analyzed is South Carolina and the corresponding values are shown in Table 8.

Table 8. Datapoints of temperature for South Carolina.

South Carolina (-0.278°C)	
Power of the heat source (W)	Minimum temperature in the Surface (°C)
1.2	5.41
1	4.92
0.8	4.44
0.6	3.74
0.4	2.91
0.2	1.87

In Figure 24, the ambient temperature of the state of South Carolina is close to 0°C. As a result, the energy source's power requirement is the lowest among the states analyzed. The graph displays the temperature distribution using a 400W constant heat flow for each bar. The maximum temperature value recorded is 37.705°C. This illustrates the heating system's efficiency even at a lower power setting. Achieving significant heating with a reduced energy input underscores the importance of adjusting power

levels based on environmental conditions to optimize energy use while achieving the desired thermal outcomes.

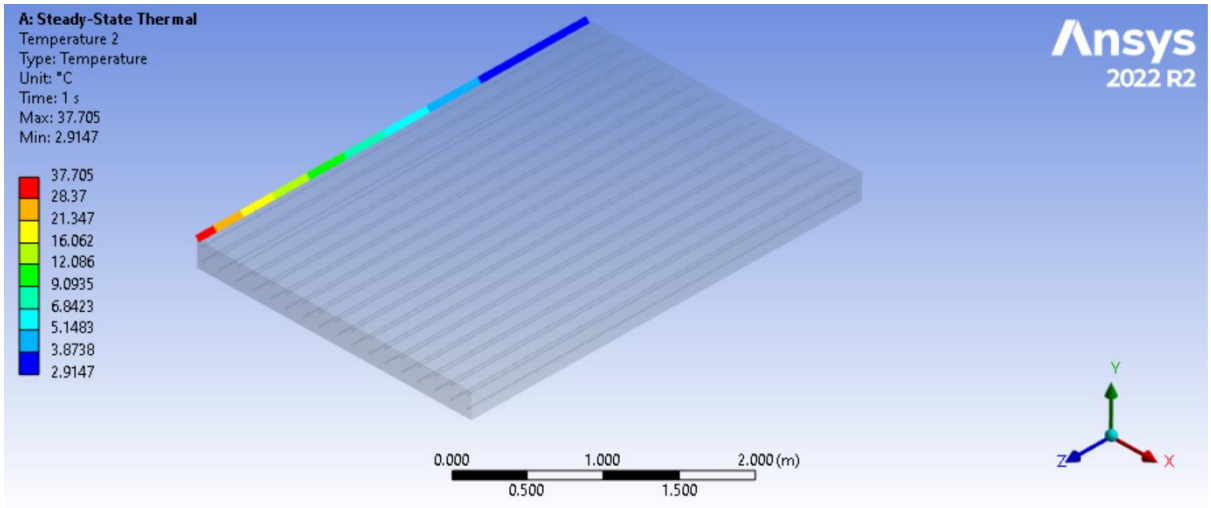

Figure 24. Temperature distribution in the left edge of the deck in South Carolina using a 0.4 kW power energy source.

The variation in surface temperature with these data falls within a range of approximately 3.5°C. The distribution exhibits a consistent behavior across all instances, characterized by a linear trend line, as shown in Figure 25. This consistency in the temperature distribution pattern, regardless of the specific conditions or power settings, underscores the robustness of the linear model in predicting the thermal response. The relatively narrow temperature range observed in this instance illustrates the precision with which thermal effects can be managed and anticipated, facilitating more efficient and targeted control of heating systems in various environmental conditions.

The ideal EPH for this state is a value of 447W.

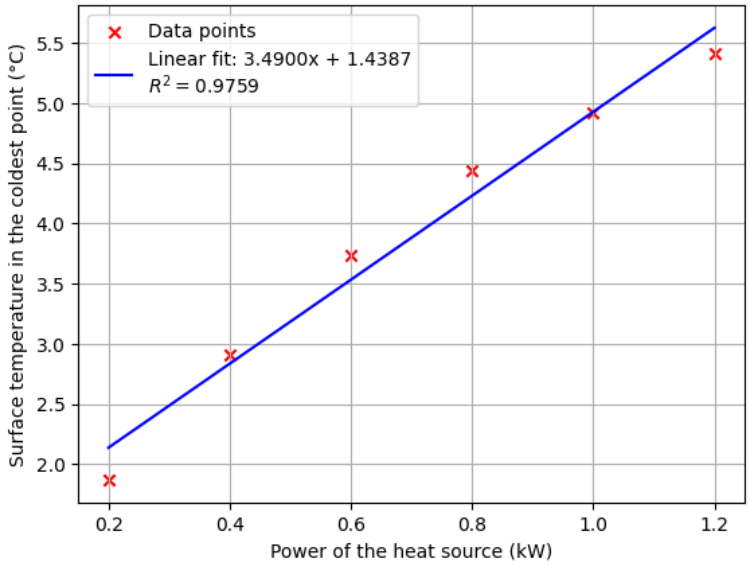

Figure 25. Linear fit expression for minimum surface temperature vs power of the heat source in South Carolina.

Once the EPH analysis for each state was completed, an analysis was conducted starting from the freezing point down to the lowest recorded value (-28.5°C) in increments of -2°C. The results here show the whole range of temperatures related to the value of the EPH for achieving the target temperature of 3°C and avoiding ice formation; it is essential to note that the simulation included the properties of the air under 1atm of pressure and the wind speed as a fixed value of 0.25m/s (stagnant air). Table 9 shows the values obtained from 0°C and subsequent increments of 2°C.

Table 9. Electrical power required at different ambient temperatures.

Ambient temperature (°C)	Electrical power required (kW)
0	0.39
-2	0.57
-4	1.01
-6	1.38
-8	1.80
-10	2.26
-12	2.78
-14	3.35
-16	3.97
-18	4.65
-20	5.37

-22	6.12
-24	6.9
-26	7.72
-28	8.57

Figure 26 shows an exponential fit applied to the data concerning temperature and the required power to achieve a temperature of 3°C. This analysis is shown in Equation(14).

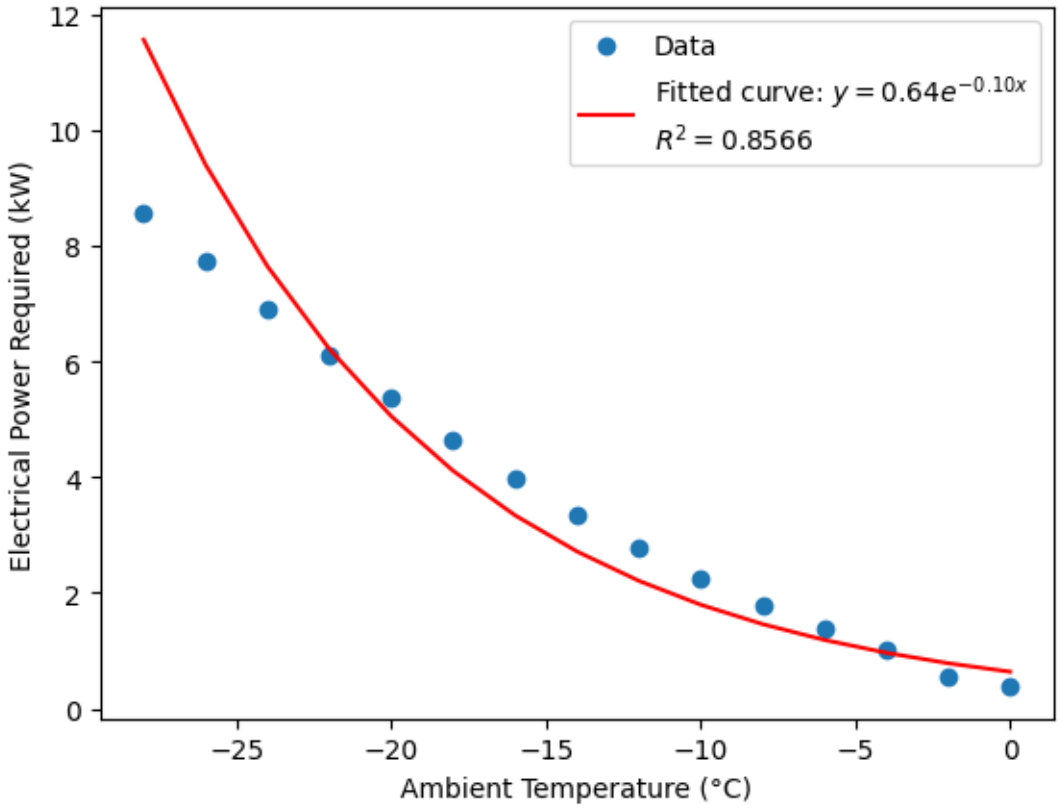

Figure 26. Electrical power required for avoiding icing formation.

$$y(x) = 0.64e^{-0.10x} \tag{14}$$

The value of R^2 (coefficient of determination) indicates that approximately 85.66% of the variance in the electrical power required can be explained by the ambient temperature using this model. A high value, such as 0.8566, suggests a strong correlation between the variables and that the model fits the data well. The remaining 14.34% of the variance is due to other factors not captured by the model, such as measurement errors

or other variables influencing the power requirement. This high value validates the effectiveness of the exponential model in predicting electrical power requirements based on ambient temperature.

As the ambient temperature drops, the EPH increases, indicating that heating systems become less efficient in colder climates. The non-linear behavior can be explained by the convection heat transfer coefficient, indicating that colder temperatures require more energy to maintain the desired temperature of the deck's surface due to increased heat loss to the surroundings.

Appendix A, corresponding to Figure 39 to Figure 78 shows the temperature distribution for each state at the recommended EPH. Similarly , Table 21 in Appendix B shows the ideal EPH corresponding to each state's temperature.

4.2 Wind speed.

The following analysis examines the impact of wind on the temperature distribution across the surface of the bridge deck. All previous calculations were conducted under stagnant air conditions, with a wind speed of 0.25 m/s. However, wind speed variations can influence the amount of power required for the heat source to avoid ice formation. Wind can significantly influence the heat transfer rate from the surface, potentially altering the effectiveness of the heating strategies. The increased convective heat loss in environments with high wind speeds could necessitate higher power inputs to maintain desired temperature levels.

To conduct this analysis, a range of wind speeds will be considered using the values obtained from the Beaufort scale[50], which estimates wind speeds based on the observed conditions of the sea or land, as shown in Table 10.

Table 10. Beauford scale.

Beaufort Scale	Description	Average Wind Speed (mph)	Average Wind Speed (m/s)
0	Calm	0 - 1	0 - 0.45
1	Light Air	1 - 3	0.45 - 1.34
2	Light Breeze	4 - 7	1.79 - 3.13
3	Gentle Breeze	8 - 12	3.58 - 5.36
4	Moderate Breeze	13 - 18	5.81 - 8.05
5	Fresh Breeze	19 - 24	8.50 - 10.73
6	Strong Breeze	25 - 31	11.18 - 13.87
7	Near Gale	32 - 38	14.32 - 16.99
8	Gale	39 - 46	17.43 - 20.57
9	Severe Gale	47 - 54	21.01 - 24.14
10	Storm	55 - 63	24.59 - 28.16
11	Violent Storm	64 - 73	28.61 - 32.62
12	Hurricane	74+	33.06+

This analysis considers different wind speeds: 0.25 m/s, 1 m/s, 5 m/s, 10 m/s, 15 m/s, and 20 m/s. This range was chosen to encompass a broad condition from calm air to gale-force winds. Investigating these varying wind speeds aims to capture a broad spectrum of real-world scenarios. The lowest speed, 0.25 m/s, represents the initial stagnant air environment. Incrementally increasing the wind speed allows us to observe the progressive impact of wind-induced convective cooling on our ability to maintain the desired surface temperature of 3°C.

Table 11 shows the convective film coefficient with the different wind speeds for each state, the calculations of the convection coefficient for each state are performed evaluating the Reynolds number in each case. When checking the results for the Reynolds number, the transition to a turbulent flow occurs at 1.85m/s.

Table 11. Convective film coefficient for each state.

	1 (m/s)	5 (m/s)	10 (m/s)	15 (m/s)	20 (m/s)
Alaska	4.386	15.894	27.673	38.277	48.183
Virginia	4.303	15.594	27.15	37.554	47.272
Missouri	4.247	15.39	26.796	37.063	46.655

Tennessee	4.196	15.205	26.473	36.616	46.092
South Carolina	4.156	15.06	26.222	36.27	45.656

Consistent with expectations, shows that increased wind speed necessitates a corresponding elevation in the EPH for keeping the deck's surface at a non-freezing temperature. The following results, derived from data collection and simulations, are presented for the five states.

Table 12 shows that increased wind speed necessitates a corresponding elevation in the EPH for keeping the deck's surface at a non-freezing temperature. The following results, derived from data collection and simulations, are presented for the five states.

Table 12. Electrical power in kW required for different wind speeds at different temperatures.

Temperature (°C) / Wind speed (m/s)	Alaska (-28.5)	Virginia (-16.5)	Missouri (-10.444)	Tennessee (-4.667)	South Carolina (-0.278)
0.25	8.64	4.14	2.46	1.14	0.45
1	10.16	5.3	3.39	1.81	1.07
5	11.61	6.39	4.27	2.44	1.65
10	12.95	7.41	5.08	3.03	2.19
15	13.82	8.07	5.6	3.41	2.54
20	14.46	8.56	6	3.69	2.79

Some key findings come from Figure 27; the tendency is consistent in the different states analyzed, and the key factor differentiating the curves is the initial temperature of each state. It is noted that Alaska needs a more significant increase of electrical power for archiving the target temperature compared to the other states, with a value of 5.82kW for mitigating the cooling effects of wind at 20m/s; this can be explained by a thermodynamic approach in colder climates, especially those with high wind speeds, the

forced convection effect becomes significant. The value of h increases with wind speed, which means that the colder and windier it is, the more heat is lost from the bridge. An increase in the heat losses is compensated by adding more heating power to the EPH.

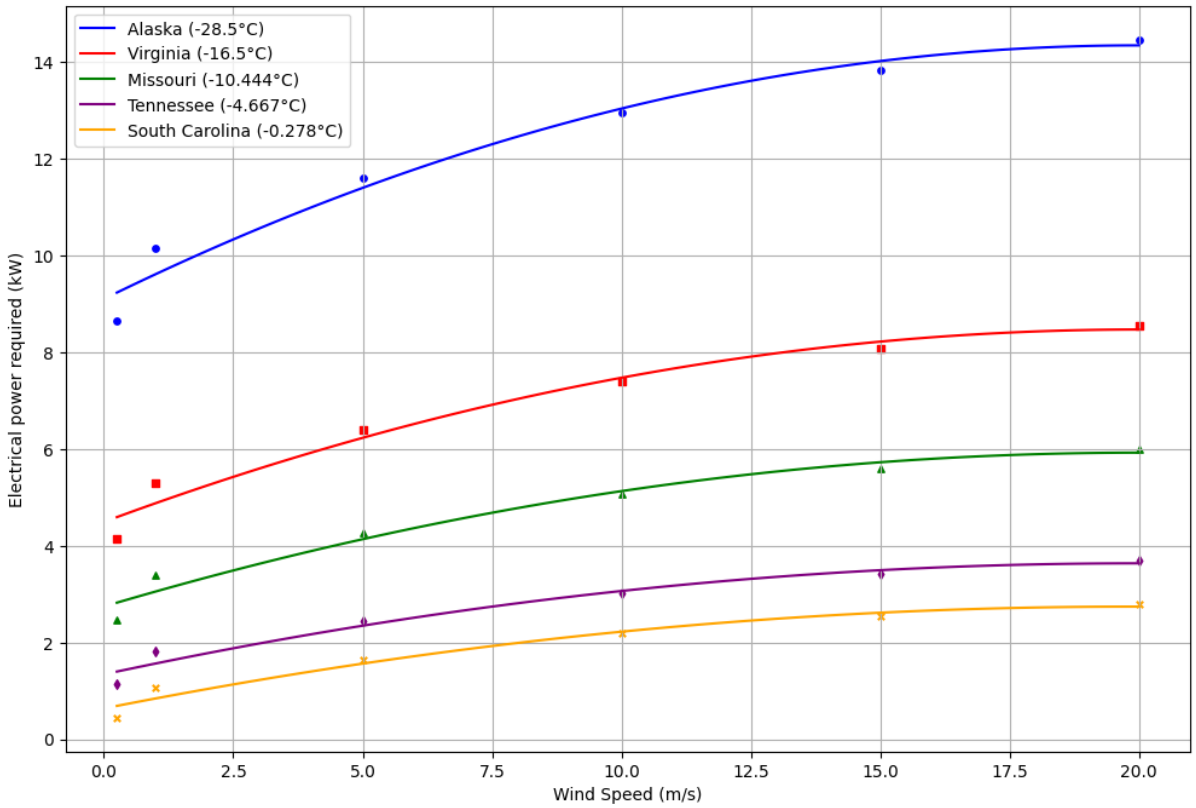

Figure 27. EPH required at different wind speeds – polynomial fit.

The polynomial approach corresponding to Figure 27 does not correctly address the data points at lower wind speeds; it is noted that particularly in between the 0.25m/s and 1m/s exists a discrepancy in the second degree polynomial fit, which is why more detailed simulations were performed for checking the behavior at this low wind speed settings, as shown in , usually when simulating or doing experimental work the wind speed will be a controlled parameter. It will be a lower value for simplicity purposes.

Table 13 , usually when simulating or doing experimental work the wind speed will be a controlled parameter. It will be a lower value for simplicity purposes.

Table 13. Electrical power in kW required for different small values of wind speeds at different temperatures.

Temperature (°C) / Wind speed (m/s)	Alaska (-28.5)	Virginia (-16.5)	Missouri (-10.444)	Tennessee (-4.667)	South Carolina (-0.278)
0.25	8.64	4.14	2.46	1.14	0.45
0.4	8.91	4.35	2.68	1.31	0.61
0.6	9.46	4.89	3.03	1.56	0.79
0.8	9.99	5.21	3.27	1.74	0.92
1	10.16	5.3	3.39	1.81	1.07
5	11.61	6.39	4.27	2.44	1.65
10	12.95	7.41	5.08	3.03	2.19
15	13.82	8.07	5.6	3.41	2.54
20	14.46	8.56	6	3.69	2.79

When including the data points at low wind speed levels, a better understanding of how much the EPH increase will be needed to mitigate the wind speed factor. Figure 28 shows the individual analysis for each state; higher wind speeds mean higher EPH to reach the target temperature, as expected. In colder climates, the necessity of increasing the EPH becomes more evident, meaning that colder climates will demand more energy connected to the transverse rebars to overcome the effect of wind speed.

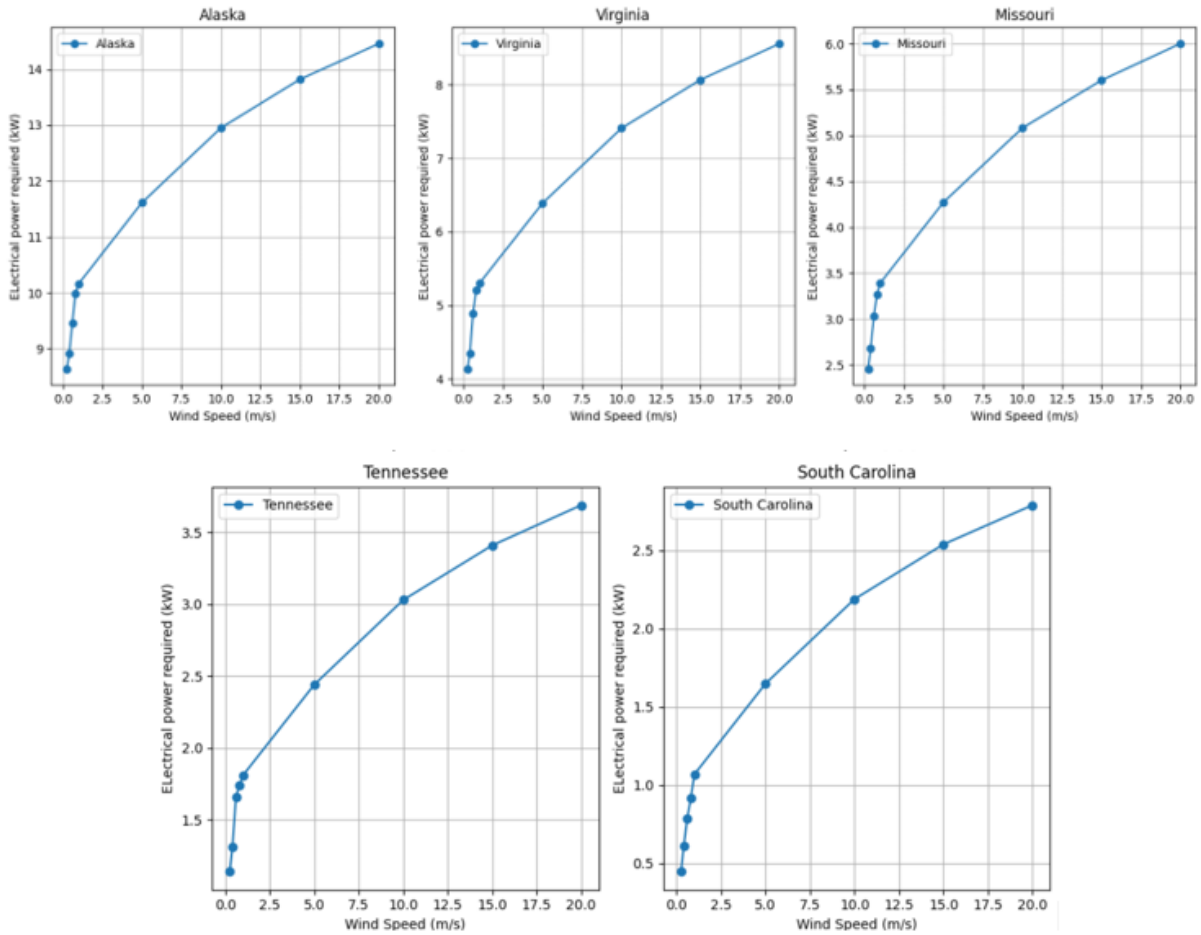

Figure 28. EPH required per state at different wind speeds.

The data exhibits a linear trend at lower wind speed levels; consequently, an independent analysis was conducted for wind speeds ranging from 0.25 m/s to 1 m/s. Figure 29 displays the corresponding linear equations and R-values for each state analyzed.

The independent analysis at lower wind speed levels is well-justified. In practical experimental setups, the wind speed parameter is more likely to be set below 1 m/s to simplify the experimentation process. Consequently, conducting a detailed analysis for wind speeds ranging from 0.25 m/s to 1 m/s ensures that the findings are relevant and applicable to these common conditions, providing valuable insights for experimental purposes.

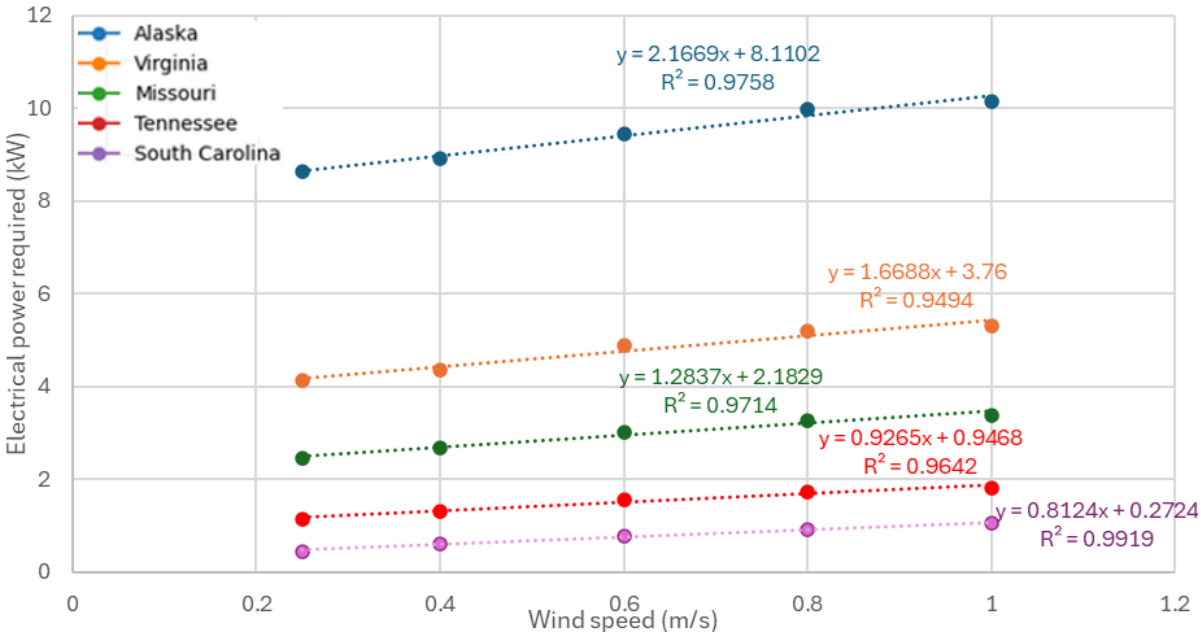

Figure 29. Trend analysis at lower wind speed velocities.

After incorporating additional data corresponding to low wind speeds, it has become evident that a logarithmic (ln) model is more suitable for accurately representing the relationship between wind speed and the EPH. Initially, a second-degree polynomial model was employed, which provided a reasonable fit for the existing dataset. The logarithmic model offers a better fit by more accurately reflecting the change in the EPH variable as wind speeds decrease. This adjustment ensures a more precise and reliable representation of the observed phenomena across the entire range of wind speeds, as shown in Figure 30.

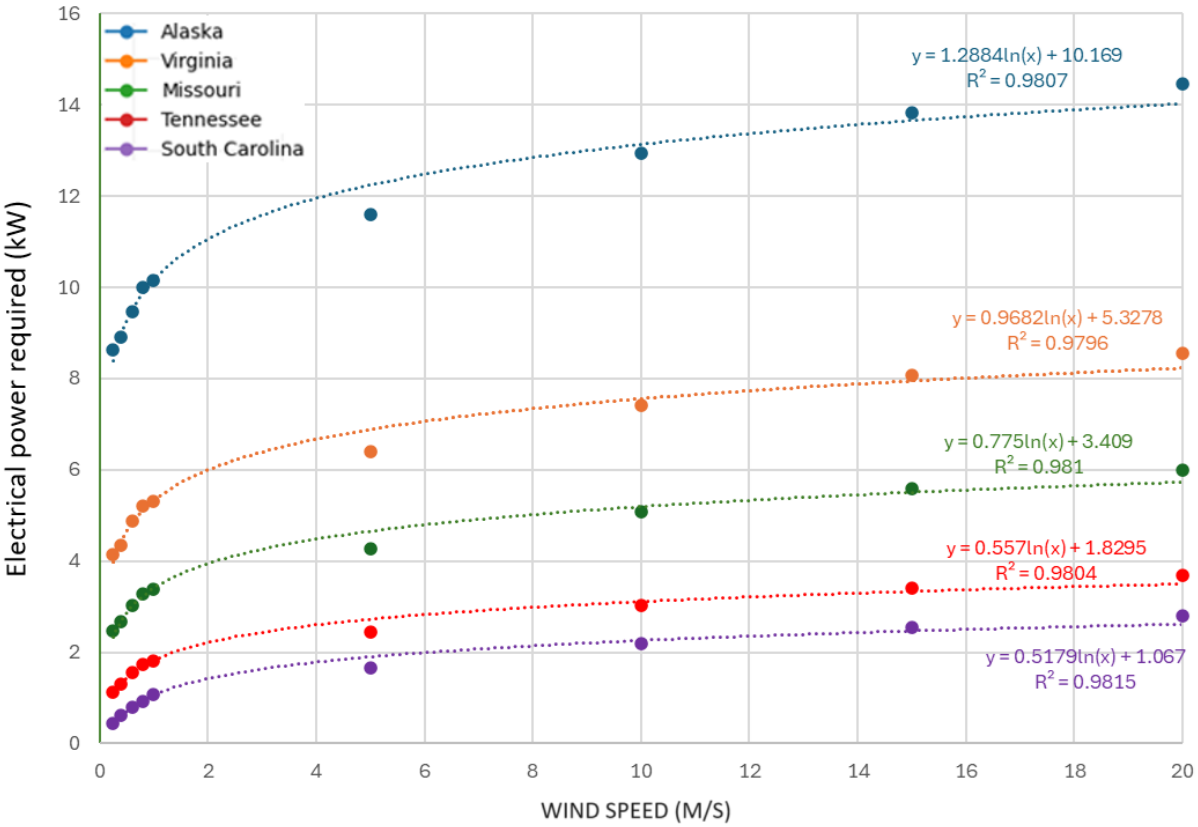

Figure 30. EPH required at different wind speeds – logarithmical fit.

The simulations' objective is to estimate the EPH required to avoid ice formation over bridges during the wintertime. Table 14 shows the amount of EPH required considering two crucial parameters: wind speed and temperature; the results presented are based on theoretical models and are intended to serve as a reference.

It is essential to address the limitations of the simulations. Usually, the simulations do not encompass all the variables of a real-world scenario, which is why the data presented in Table 14 should be interpreted cautiously and used as a reference for further investigation; in practical applications, the simulation results are used as a guideline for designing experimental setups and for evaluating the feasibility of preventing freezing over the bridge's decks. In this table, the parameters were calculated based on the properties of the air at 1 atm of pressure.

The result of this simulation offers valuable insights into preventing freezing on bridges, providing a framework for future research and engineering interventions.

Table 14. Table of EPH required (kW) according to wind speed and temperature.

		Wind speed (m/s)								
		Laminar flow					Turbulent flow			
		0.25	0.4	0.6	0.8	1	5	10	15	20
Temperature (°C)	-0.278	0.45	0.61	0.79	0.92	1.07	1.65	2.19	2.54	2.79
	-2	0.68	0.84	1.05	1.2	1.29	1.87	2.41	2.76	3.01
	-4	1.01	1.18	1.42	1.59	1.66	2.27	2.85	3.22	3.49
	-4.667	1.14	1.31	1.56	1.74	1.81	2.44	3.03	3.41	3.69
	-6	1.41	1.59	1.86	2.05	2.13	2.81	3.44	3.85	4.15
	-8	1.86	2.06	2.36	2.57	2.67	3.43	4.14	4.6	4.94
	-10	2.35	2.56	2.9	3.14	3.26	4.11	4.91	5.41	5.8
	-10.444	2.46	2.68	3.03	3.27	3.39	4.27	5.08	5.6	6
	-12	2.87	3.1	3.49	3.74	3.87	4.82	5.69	6.25	6.68
	-14	3.42	3.64	4.1	4.38	4.5	5.53	6.47	7.08	7.55
	-16	3.99	4.21	4.73	5.04	5.14	6.22	7.23	7.88	8.36
	-16.5	4.14	4.35	4.89	5.21	5.3	6.39	7.41	8.07	8.56
	-18	4.59	4.79	5.38	5.73	5.78	6.9	7.95	8.64	9.13
	-20	5.22	5.39	6.06	6.34	6.44	7.58	8.67	9.37	9.88
	-22	5.9	6.04	6.77	7.08	7.14	8.29	9.41	10.14	10.64
	-24	6.63	6.77	7.52	7.87	7.9	9.09	10.23	10.99	11.5
	-26	7.45	7.61	8.32	8.72	8.79	10.04	11.24	12.03	12.58
	-28	8.38	8.62	9.22	9.74	9.85	11.25	12.56	13.41	14.02
	-28.5	8.64	8.91	9.46	9.99	10.16	11.61	12.95	13.82	14.46

4.3 Location of the EPH.

During the simulations for this thesis, the focus was on applying the electrical power source to the 17 rebars corresponding to the analyzed segment of the bridge deck. As part of our optimization strategies to check the effects on the temperature distribution, an alternate rebar heating approach was conducted. Instead of heating 17 rebars, only 9 rebars were heated, resulting in a change in the spacing between the rebars to 12 inches (0.3048 m).

This approach is crucial in our efforts to maintain the desired temperature across the bridge deck. It allows us to assess the efficiency and effectiveness of different configurations, ensuring that the bridge deck remains at the optimal temperature. By reducing the number of rebars powered at any given time, potential energy savings can be made while still achieving the minimum temperature to avoid ice formation. The alternate connection strategy, utilizing 9 rebars or less, could offer insights into how the spatial distribution of heating elements impacts the overall temperature distribution and the system's ability to counteract environmental cooling effects.

Figure 31 displays the rebars that will be heated with electrical power for the alternate approach scenario. The method seeks to balance the need for maintaining safe surface temperatures against the goal of minimizing electrical consumption.

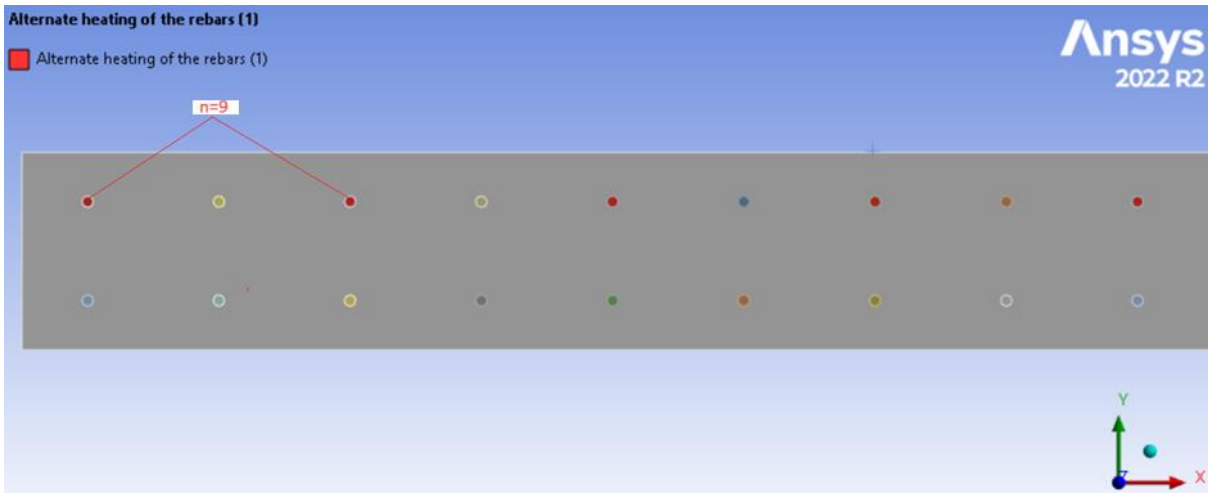

Figure 31. Alternate heating of rebars.

Alaska

The temperature is homogeneous in the coldest zone of the bridge; there is a difference of temperature of 0.02°C along the longitudinal direction, a positive outcome for the research because the objective is to keep the temperature surface of the deck homogeneous to avoid complications.

Figure 32 displays the temperature distribution for Alaska when implementing the strategy of alternating the application of the EPH to the rebars. The temperature difference of the first method is 0.3kW, as shown in Table 15. This is an exciting finding. With a slight increase in the power of the heat source in the alternate approach, the objective of reaching the target temperature can be achieved, meaning that the spacing strategy works well.

Table 15. Alternate heating method data in Alaska.

Alaska (-28.5°C)	
Power for archiving the target temperature (kW)	
All rebars	Alternate rebars
8.64	8.94

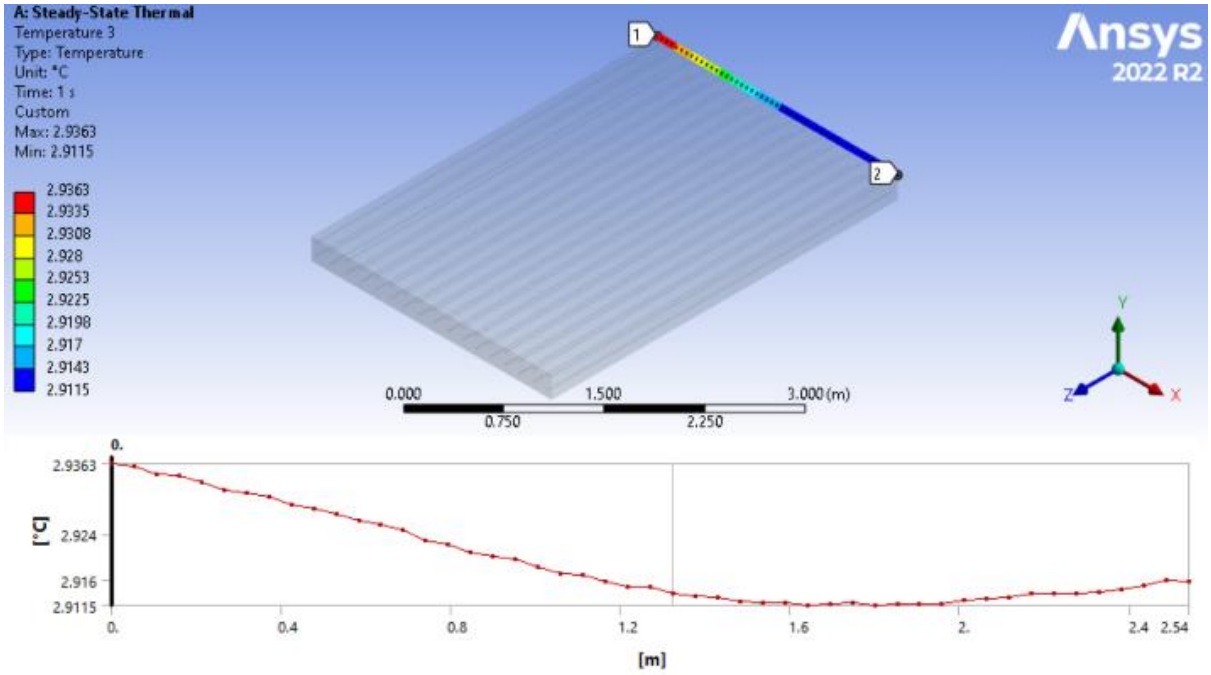

Figure 32.Surface temperature distribution in Alaska with alternate rebar heating.

Virginia

This analysis reveals that increasing the spacing in the rebars connected to the EPH can reduce energy consumption. Also, there are many benefits in the thermal

stresses avoided in the non-connected rebars. Data shows that when the alternate option is used, in Table 16, the increase of the EPH will be 210W.

When taking the approach of alternating two rebars, there is a significant difference in the power needed for the electric energy source; the increase in the value for the EPH goes to 2.9kW, which can potentially lead to failure of the model because of the stresses produced both in the rebars and the concrete layer, this is why alternating a space of 18inch is not viable for the model.

Table 16. Alternate heating method data in Virginia.

Virginia (-16.5°C)	
Power for archiving the target temperature (kW)	
All rebars	Alternate rebars
4.14	4.35

A slight enhancement in the heat source's power with the alternating method, shown in Figure 33, can fulfill the objective of reaching the desired temperature; by doing so, the power input for all the sections of the bridge's deck can be reduced, if counting the total heating power avoiding by this method, the value can round approximately 31.23kW.

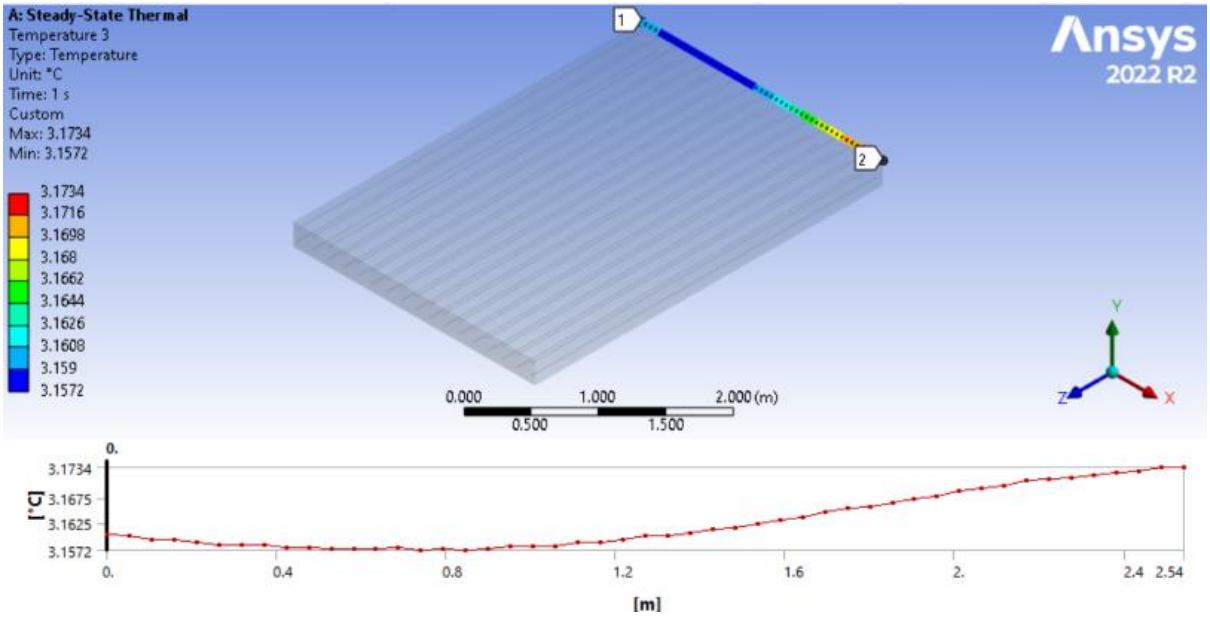

Figure 33. Surface temperature distribution in Virginia with alternate rebar heating.

Missouri.

The difference between the EPH value is shown in Table 17, the temperature distribution at this state is shown in Figure 34, the spacing of the application of the energy source is an essential factor, the homogeneous distribution of temperature in the surface of the bridge's deck is expected, the difference almost no noticeable, meaning that this type of method is a good option for both, saving power in the energy source and keeping the effects of homogeneous temperatures along the longitudinal direction of the bridge's deck.

Table 17. Alternate heating method data in Missouri.

Missouri (-10.444°C)	
Power for archiving the target temperature (kW)	
All rebars	Alternate rebars
2.46	2.58

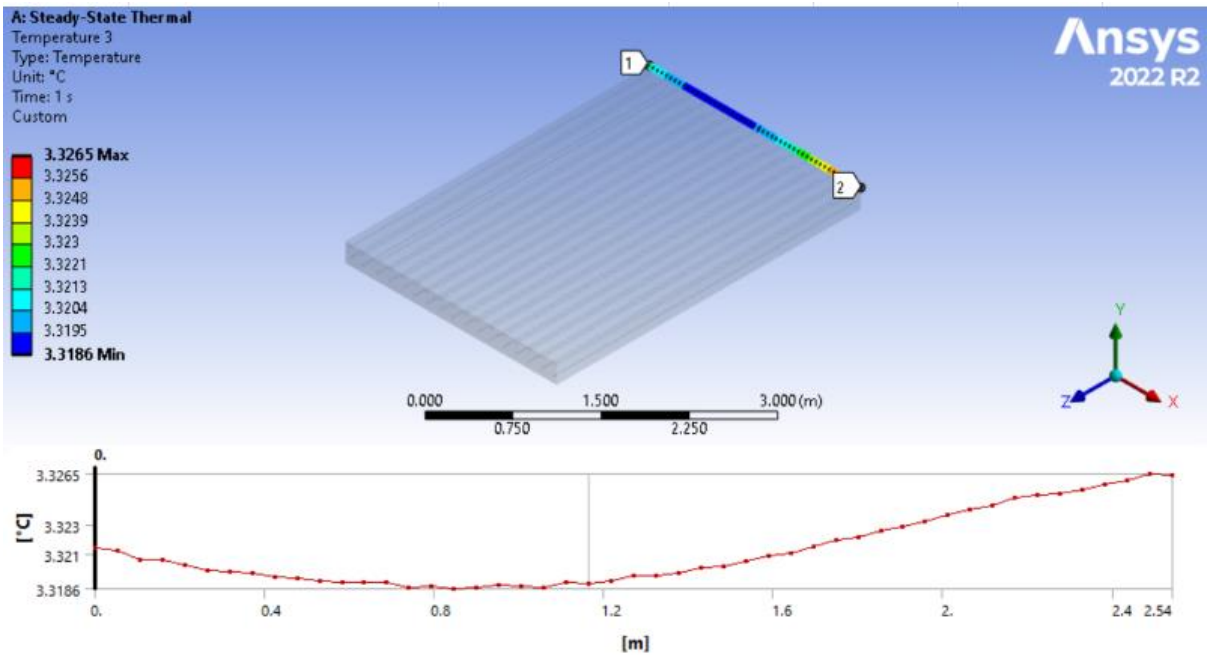

Figure 34. Surface temperature distribution in Missouri with alternate rebar heating.

Tennessee.

Table 18 demonstrates that a modest increase in power input, specifically of 80 W, can replicate the performance levels associated with the all-rebars method. Also, Figure 35 shows that the temperature distribution is still constant around the longitudinal axis.

Table 18. Alternate heating method data in Tennessee.

Tennessee (-4.667°C)	
Power for archiving the target temperature (kW)	
All rebars	Alternate rebars
1.14	1.22

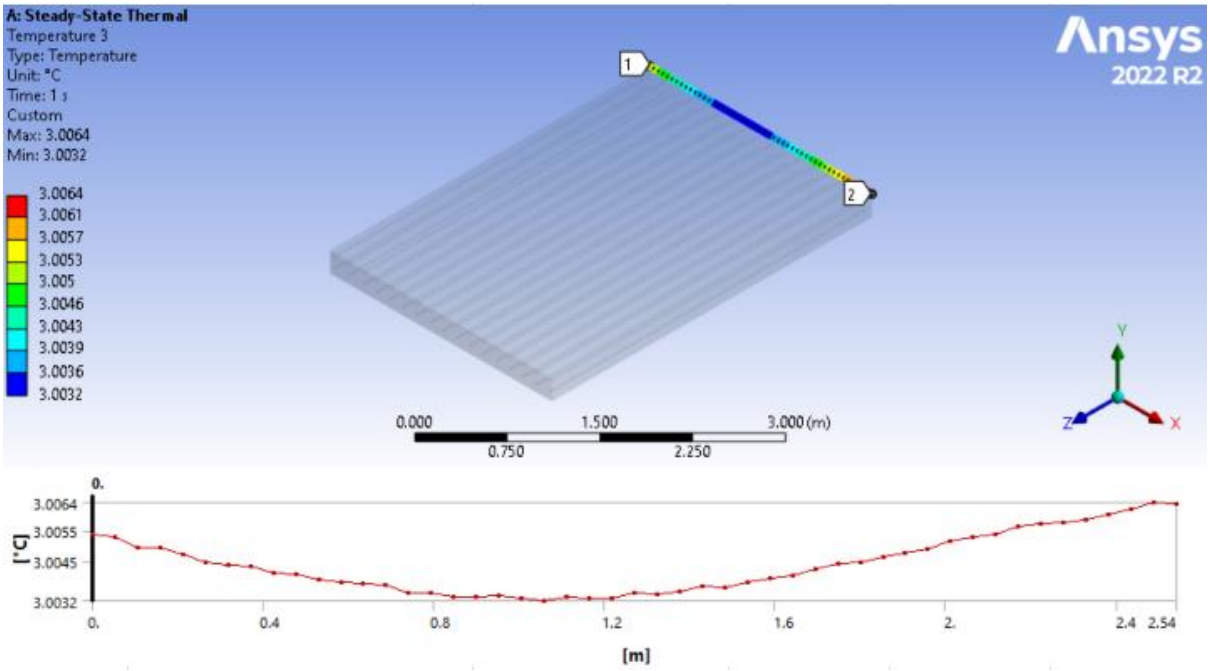

Figure 35. Surface temperature distribution in Tennessee with alternate rebar heating.

South Carolina.

Consistent with trends observed in other states, lower ambient temperatures reduce the need to increase the power of the electrical source. In this case, an increase of just 40W is sufficient for the alternate rebar approach to meet the requirements to prevent ice formation on the surface of the bridge's deck, according to Table 19. The approach saves a total of 8.4kW. Additionally, using the alternate rebar approach conserves energy and helps reduce the stress imposed on the rebars. This stress reduction contributes to the longevity and durability of the bridge's structural components. Reducing the mechanical stress typically experienced by the rebars during deicing operations enhances the overall structural integrity of the bridge. This dual benefit of energy efficiency and reduced structural stress makes the alternate rebar approach a highly advantageous strategy for maintaining bridge safety and functionality in colder climates.

Figure 36 shows the temperature distribution in South Carolina. Temperature remains constant in the longitudinal part of the bridge, and there is no significant difference in the analyzed heat line.

Table 19. Alternate heating method data in South Carolina.

South Carolina (-4.667°C)	
Power for archiving the target temperature (kW)	
All rebars	Alternate rebars
0.45	0.49

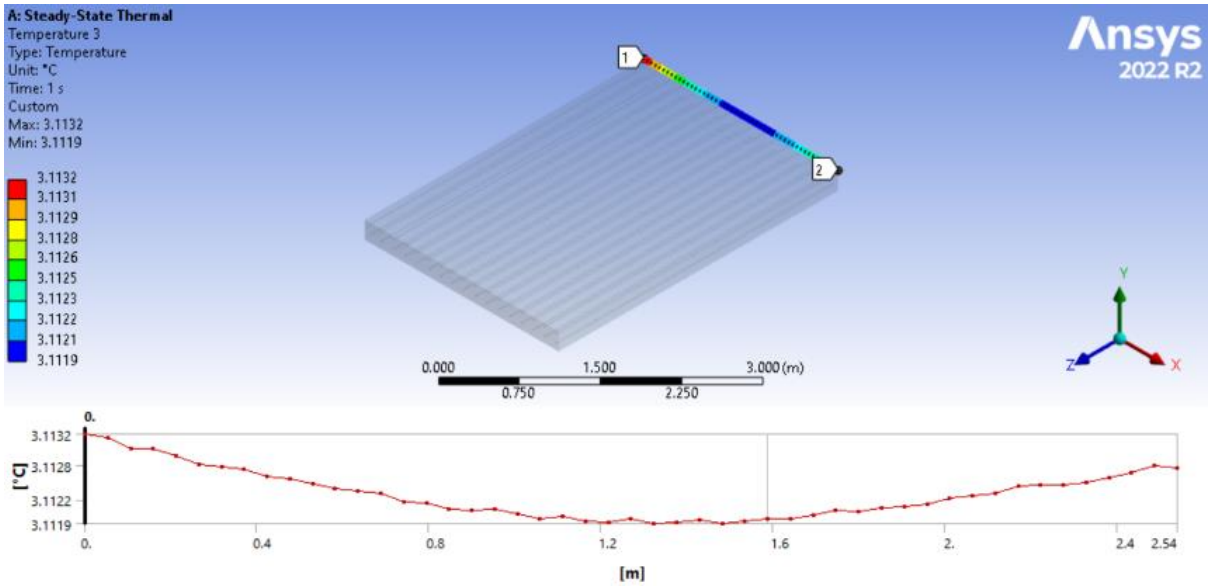

Figure 36. Surface temperature distribution in South Carolina with alternate rebar heating.

An analysis explored the feasibility of skipping two rebars when connecting the energy source. However, the outcomes of this approach could have been more favorable, as the energy demand from the source increased exponentially when the rebars were separated by 18 inches. This strategy's major limitations included a significant temperature increase in the rebars exposed to the EPH. This rise in temperature imposed additional stress on the rebars and the concrete, presenting considerable challenges to both structural integrity and energy efficiency.

The heightened temperatures could accelerate the degradation of both the rebars and the concrete, potentially leading to premature failure of structural components.

The increased energy consumption required to maintain deicing effectiveness at greater distances between powered rebars does not represent energy savings, making this approach unviable. The combination of higher operational costs, potential risks to structural safety, and decreased environmental efficiency highlights the critical need for optimizing the location of the EPH in deicing systems.

4.4 Stress analysis.

Rebars are a structural component of concrete bridges, and steel rebars strengthen the structure. When heating is applied to rebar, it will expand differently from the surrounding concrete because of the differences in the property materials, precisely because of the differences in their thermal expansion coefficients; this differential expansion will induce tension and compression stresses in the concrete, potentially leading to cracks or other forms of structural damage. Stress analysis helps in understanding and managing these effects to ensure the bridge's structural integrity.

Figure 37 illustrates the stress distribution in a transverse rebar embedded in concrete under an ambient temperature of -0.278°C, representing South Carolina's environmental conditions. The analysis reveals that the maximum stress occurs at 0.1524m in the transversal direction from the front face of the model; this point of maximum stress is defined as a critical value of stress. Thermal stresses produced by the application of the EPH will be the greatest among the structure and must be compared with the strength of the rebar to ensure structural integrity and safety; for theoretical purposes, the value should be lower than the tensile or compressive strength of the rebar for avoiding deformation. The stress magnitude decreases as one moves further along the

transverse direction. This reduction in stress can be attributed to the dissipation of energy away from the initial source, which is consistent with theoretical models predicting that stress concentrations are highest near the point of applied load or energy source; the decrease in stress as distance increases implies the rebar is less likely to experience critical stress levels further from the energy source, reducing the risk of structural failure in those regions.

This stress analysis is part of a broader effort to prevent ice formation on the concrete surface by ensuring the rebar does not compromise the structural integrity. The findings from this analysis can be used in the design process, as they help optimize the selection and placement of rebar to enhance the durability and resilience of the concrete structure under varying environmental conditions.

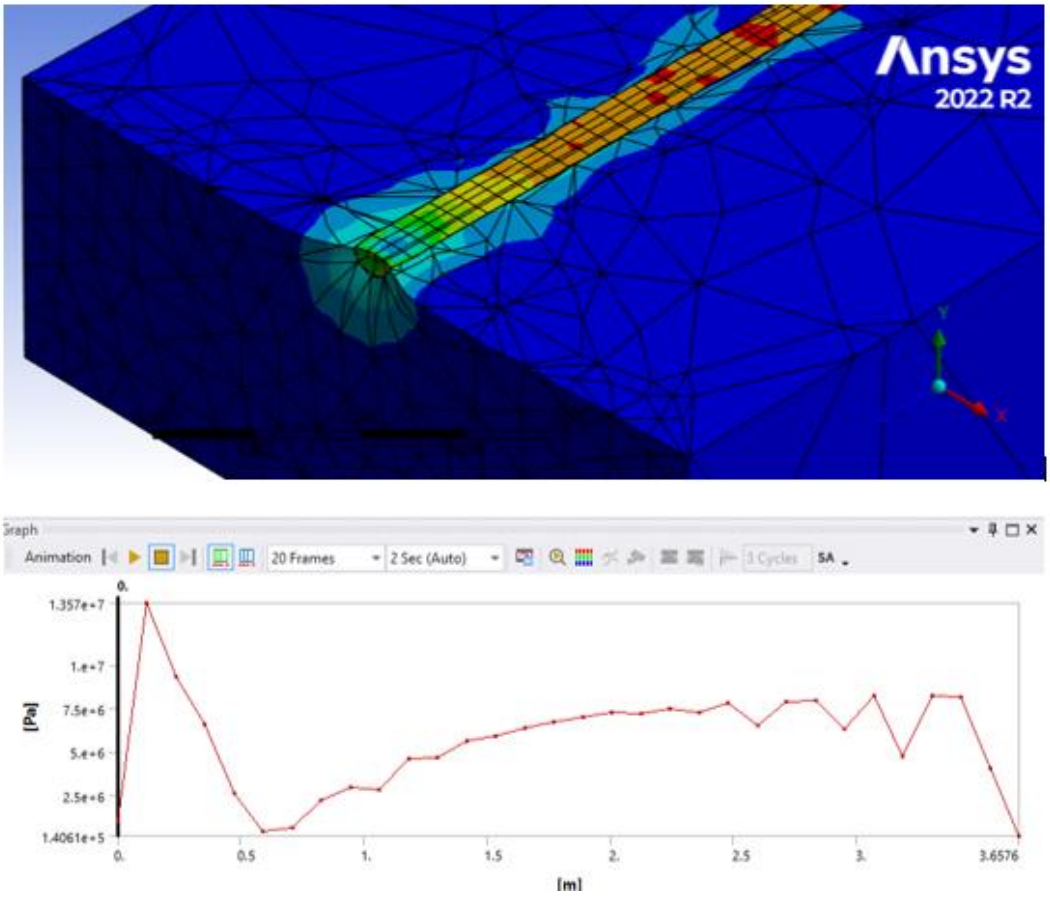

Figure 37. Von-Mises stress distribution in the transversal rebar.

Figure 38 shows the stress distribution in the concrete, which reveals significant stress concentrations near the interior walls where contact with the rebars exists. This phenomenon happens because there is a transfer of stress from the steel rebars to the concrete, and the embedded rebars produce tensile strength to the concrete because of the direct contact between them.

The maximum value found in the stress distribution of the concrete is 1.69MPa when considering the Von-Misses equivalent stress, the points of contact between the rebars and the concrete are areas of special attention; most likely that higher stresses in the rebars will produce stress in the concrete as well, that is why the maximum value can be found inside of the walls. The bond between rebars and concrete is essential, too; the contact zones between the rebars and the concrete are modeled as bonded, the rebars deform under loads and generate an additional force on the concrete as well, and the steel rebars have a much higher modulus of elasticity than the concrete, this is the reason there is different stress concentrations in both materials. The regions near the interior walls where the rebars are embedded are critical for evaluating the structural integrity and durability of the reinforced concrete structure.

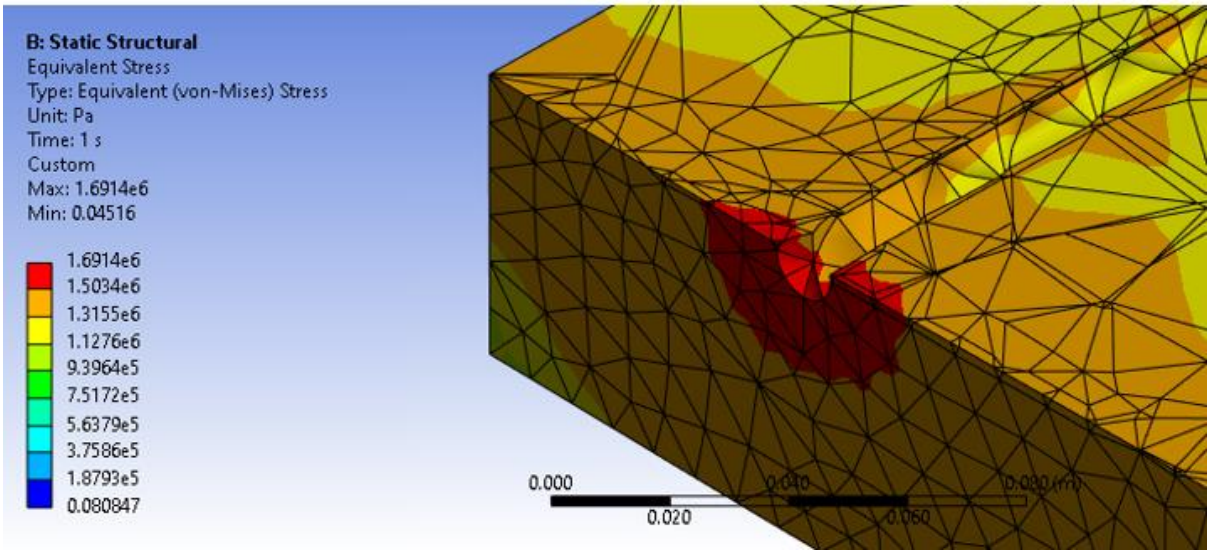

Figure 38. Stress distribution in the concrete.

Table 20 provides the critical stress concentration in both stress and transverse rebars for the two cases, all rebars method, and the alternate rebar approach method for the five states.

Table 20.Critical stress concentration in concrete and rebars.

State	Method	Stress in concrete (Pa)	Stress in rebars (Pa)
Alaska (-28.5 °C)	All rebars	3.3e7	6.6e8
	Alternate rebars	3.86e7	1.22e9
Virginia (-16.5 °C)	All rebars	2.99e7	2.39e8
	Alternate rebars	3.22e7	2.51e8
Missouri (-10.444 °C)	All rebars	9.39e6	1.2e8
	Alternate rebars	1.14e7	1.52e8
Tennessee (-4.667 °C)	All rebars	4.3e6	3.7e7
	Alternate rebars	4.8e6	4.06e7
South Carolina (-0.278 °C)	All rebars	1.69e6	1.28e7
	Alternate rebars	2.5e6	3.13e7

The data shows a trend of increasing stress with decreasing ambient temperatures because of the need for a higher EPH. Alaska, with the lowest temperature (-28.5°C), exhibits the highest stresses, mainly when using alternate rebars, where concrete stress reaches 3.86e7 Pa and rebar stress 1.22e9 Pa. In Virginia (-16.5°C), Missouri (-10.444°C), and Tennessee (-4.667°C), the stresses progressively decrease, with alternate rebars consistently showing higher values than all rebars. South Carolina, at -0.278°C, has the lowest stress values, with 1.69e6 Pa in concrete and 1.28e7 Pa in rebars using all rebars, and higher stresses of 2.5e6 Pa in concrete and 3.13e7 Pa in rebars using alternate rebars.

Considering the properties of the materials selected for this simulation, it is essential to note that concrete can handle a maximum tensile stress of 5 MPa. This limitation is due to the ultimate strength of the tensile concrete. Beyond this value, the material will crack and fail. The steel used for rebars in reinforced concrete structures has a tensile and compressive yield strength of 250 MPa. To maintain structural integrity and avoid plastic deformation of the steel, the stress in the rebars should not exceed 250 MPa. These stress limitations ensure that the concrete remains intact under tensile stress and that the rebars do not yield, preserving the overall durability and safety of the structure. Based on the previously analyzed data and the material properties, in extremely cold conditions such as in Alaska (-28.5 °C) and Virginia (-16.5 °C), the stresses in both concrete and rebars exceed their respective safe limits, indicating a high risk of structural failure. When the temperature is in relatively cold conditions such as Missouri (-10.444 °C), the stress exceeds the admissible limit of the concrete, but the rebar stress remains within safe conditions (120 MPa and 152 MPa, respectively); in this situation, safety problems related with concrete cracking will need to be taken in consideration. Finally, in milder conditions like Tennessee (-4.667 °C) and South Carolina (-0.278 °C), both materials remain within safe stress limits, indicating that the method can be

performed with no structural influence of the bridge. Considering these stress limits during structural design and analysis is essential to ensure safety and durability. The results try to give a preliminary concept of how to design and address the limitations of the simulation model.

CHAPTER 5

CONCLUSION.

5.1 ANSWER TO THE RESEARCH QUESTIONS.

It has been determined that a correlation exists between the EPH and the temperature on the surface of the bridge. Equation(14) establishes the mathematical relationship between these two variables studied; this equation is not universal and is only valid under the assumed circumstances of standardized air, 1 atm of pressure, and 0.25m/s wind speed.

Different parameters affect in different ways to the temperature distribution in the bridge's surface's deck; an increase in the EPH results in an increase in the temperature distribution, and higher wind speeds cool down the surface of the bridge faster and need higher values of the EPH for keeping the surface at the desired temperature, the location of the EPH into the rebars is also an important parameter, the more space between the rebars, the more EPH energy level will be needed.

By checking the thermo-mechanical properties of the model, the heat flow corresponding to the EPH should be less than 1.22kW for granting structural integrity.

5.2 GENERAL CONCLUSIONS.

A 3D FEA model was built to avoid ice formation over a bridge's deck. Influence factors on the temperature distribution and responses of the EPH were studied when heating the steel rebars of a concrete deck. The following conclusions are drawn from this study:

1. The model was developed to solve the problem of ice formation on the bridge's surface. It included using an external electrical energy source connected to the transverse steel rebars embedded in the concrete structure.
2. This study individually considered parameters such as outside temperature, EPH location, and wind speed. Additionally, a stress analysis was conducted to evaluate the feasibility of this method and provide guidelines for designers.
3. The location of the EPH is limited to the design of the bridge. In our case, the spacing in the alternate rebar approach is 12 inches (0.3048m) because of the regulations in the design of the bridges.
4. Alternate rebar heating is recommended. However, the EPH heat flow should not exceed 1.22kW at any time to ensure the bridge's structural integrity.

5.3 RECOMMENDATIONS.

It is recommended to implement adaptive power management systems, as this is for increasing the efficiency of the model and for economic advantages. By implementing these strategies, the EPH will be constantly subject to changes according to the conditions based on the input parameters studied in this thesis. It is of utmost importance to monitor the temperature distribution on the surface of the bridge to avoid complications related

to thermal stresses. Ideally, installing sensors across the surface of the bridge will allow the system to respond effectively to changes in environmental conditions.

Increasing the performance of the system by considering new methods related to advanced conductive materials and thermal insulation also needs to be further explored to enhance the efficiency of heating systems.

5.4 FUTURE WORK.

Future work will conduct experimental setups with the configuration proposed in the thesis's model, designing and implementing the physical systems that can achieve the conditions and parameters of the simulations to observe how the model will perform in real-world environments. It is highly recommended to use Table 12 as a reference for initial experimental setups. The table shows the EPH required under different scenarios of outside temperature and wind speeds. Any value can be obtained by doing a simple interpolation between the data presented.

While the thesis focused on heat transfer and thermal management, understanding the structural implications of the model is crucial for ensuring structural integrity, mainly because the rebars are a structural element. The potential effect of fatigue in the rebars and concrete needs to be addressed more deeply. While the focus was not exceeding critical values for ensuring structural safety, cycling loads can be harmful because of the fatigue of the components. The thesis will provide a comprehensive view of the proposed heating systems, from their thermal efficiency and energy use to their structural viability and environmental impact, giving a solid foundation for future innovations in sustainable building technologies.

References

[1] L. Fu and T. J. Kwon, “Mobility Effects of Winter Weather and Road Maintenance Operations,” in *Sustainable Winter Road Operations*, 2018. doi: 10.1002/9781119185161.ch8.

[2] S. Hyodo and K. Hasegawa, “Factors Affecting Analysis of the Severity of Accidents in Cold and Snowy Areas Using the Ordered Probit Model,” *Asian Transport Studies*, vol. 7. 2021. doi: 10.1016/j.eastsj.2021.100035.

[3] D. E. Yessentay, A. K. Kiyalbaev, S. N. Kiyalbay, and N. V. Borisyuk, “Reliability criterion and a model for determining the optimal speed of movement on automobile roads in winter sliding conditions,” *News of the National Academy of Sciences of the Republic of Kazakhstan, Series of Geology and Technical Sciences*, vol. 6, no. 444, 2020, doi: 10.32014/2020.2518-170X.138.

[4] fhwa.dot.gov, “Snow and Ice,” Snow and Ice. Accessed: Nov. 11, 2023. [Online]. Available: https://ops.fhwa.dot.gov/weather/weather_events/snow_ice.htm

[5] S. Knight, J. Hauxwell, and E. A. Haber, “Distribution and Abundance of Aquatic Plants – Human Impacts,” *Reference Module in Earth Systems and Environmental Sciences*, 2014, doi: 10.1016/B978-0-12-409548-9.09102-8.

[6] X. Liu, S. J. Rees, and J. D. Spitler, “Modeling snow melting on heated pavement surfaces. Part I: Model development,” *Appl Therm Eng*, vol. 27, no. 5–6, 2007, doi: 10.1016/j.applthermaleng.2006.06.017.

[7] D. B. McDonald, “Corrosion of epoxy-coated steel in concrete,” *Corrosion of Steel in Concrete Structures*, pp. 137–160, Jan. 2023, doi: 10.1016/B978-0-12-821840-2.00026-2.

[8] X. Han, D. Y. Yang, and D. M. Frangopol, “Risk-based life-cycle optimization of deteriorating steel bridges: Investigation on the use of novel corrosion resistant steel,” *Advances in Structural Engineering*, vol. 24, no. 8, 2021, doi: 10.1177/1369433220980529.

[9] H. L. Dai, K. L. Zhang, X. L. Xu, and H. Y. Yu, “The 18th Biennial Conference of International Society for Ecological Modelling Evaluation on the Effects of Deicing Chemicals on Soil and Water Environment,” *Procedia Environ Sci*, vol. 13, pp. 2148–2156, 2012, doi: 10.1016/j.proenv.2012.01.201.

[10] X. Wang, H. Fan, Y. Zhu, and M. Zhu, “Heat Transfer Simulation and Analysis of Ice and Snow Melting System Using Geothermy by Super-long Flexible Heat Pipes,” Energy Procedia, vol. 105, pp. 4724–4730, May 2017, doi: 10.1016/J.EGYPRO.2017.03.1026.

[11] H. Zhao, Z. Wu, S. Wang, J. Zheng, and G. Che, “Concrete pavement deicing with carbon fiber heating wires,” *Cold Reg Sci Technol*, vol. 65, no. 3, 2011, doi: 10.1016/j.coldregions.2010.10.010.

[12] H. Wang, L. Liu, and Z. Chen, “Experimental investigation of hydronic snow melting process on the inclined pavement,” *Cold Reg Sci Technol*, vol. 63, no. 1–2, 2010, doi: 10.1016/j.coldregions.2010.04.007.

[13] J. Chen, M. Zhang, H. Wang, and L. Li, “Evaluation of thermal conductivity of asphalt concrete with heterogeneous microstructure,” *Appl Therm Eng*, vol. 84, 2015, doi: 10.1016/j.applthermaleng.2015.03.070.

[14] R. Mehrabi, K. Atefi-Monfared, D. Kumar, A. A. Deshpande, and R. Ranade, “Thermo-mechanical assessment of heated bridge deck under internal cyclic thermal loading from various heating elements: pipe, cable, rebar,” *Cold Reg Sci Technol*, vol. 194, 2022, doi: 10.1016/j.coldregions.2021.103466.

[15] S. L. Abdelaziz, C. G. Olgun, and J. R. Martin, “Counterbalancing ambient interference on thermal conductivity tests for energy piles,” *Geothermics*, vol. 56, 2015, doi: 10.1016/j.geothermics.2015.03.005.

[16] K. Liu, S. Huang, C. Jin, H. Xie, and F. Wang, “Prediction models of the thermal field on ice-snow melting pavement with electric heating pipes,” *Appl Therm Eng*, vol. 120, 2017, doi: 10.1016/j.applthermaleng.2017.04.008.

[17] R. Mehrabi, K. Atefi-Monfared, D. Kumar, A. A. Deshpande, and R. Ranade, “Thermo-mechanical assessment of heated bridge deck under internal cyclic thermal loading from various heating elements: pipe, cable, rebar,” *Cold Reg Sci Technol*, vol. 194, 2022, doi: 10.1016/j.coldregions.2021.103466.

[18] “Radiation Heat Transfer,” 2018, doi: 10.1016/B978-0-12-812024-8.00003-5.

[19] J. Liu, Q. Yu, J. Peng, X. Hu, and W. Duan, “Thermal energy recovery from high-temperature blast furnace slag particles,” *International Communications in Heat and Mass Transfer*, vol. 69, 2015, doi: 10.1016/j.icheatmasstransfer.2015.10.013.

[20] Y. Blikharskyy, J. Selejdak, and N. Kopiika, “Specifics of corrosion processes in thermally strengthened rebar,” *Case Studies in Construction Materials*, vol. 15, 2021, doi: 10.1016/j.cscm.2021.e00646.

[21] L. D. Hung Anh and Z. Pásztory, “An overview of factors influencing thermal conductivity of building insulation materials,” *Journal of Building Engineering*, vol. 44. 2021. doi: 10.1016/j.jobe.2021.102604.

[22] P. K. et Al, “Convection Heat Transfer Coefficient Convection Heat Transfer Coefficient Mechanical Engineering,” *Design and performance optimization of renewable energy systems*, 2021.

[23] S. Hatte and R. Pitchumani, “Analysis of convection heat transfer on multiscale rough superhydrophobic and liquid infused surfaces,” *Chemical Engineering Journal*, vol. 424, 2021, doi: 10.1016/j.cej.2021.130256.

[24] K. J. Kinnari *et al.*, “Flow Assurance Challenges for Hydrate Deposition in Pipes with Stagnant Flow,” in *9th International Conference on Gas Hydrates*, 2017.

[25] M. S. Fernandes, E. Rodrigues, and J. J. Costa, “A new wind direction-driven heat convection model is needed in dynamic simulation: What, why, and how,” *Energy Build*, vol. 256, 2022, doi: 10.1016/j.enbuild.2021.111716.

[26] K. S. Reddy, G. Veershetty, and T. Srihari Vikram, “Effect of wind speed and direction on convective heat losses from solar parabolic dish modified cavity receiver,” *Solar Energy*, vol. 131, 2016, doi: 10.1016/j.solener.2016.02.039.

[27] C. French, A. Mokhtarzadeh, T. Ahlborn, and R. Leon, “High-strength concrete applications to prestressed bridge girders,” *Constr Build Mater*, vol. 2–3, no. 2–4, 1998, doi: 10.1016/s0950-0618(97)00012-3.

[28] V. Rajnath Singh and N. Netam, “Effect of convective heat transfer coefficient on estimation of effective thermal conductivity of two-phase material,” in *Materials Today: Proceedings*, 2020. doi: 10.1016/j.matpr.2020.04.534.

[29] B. C. Sakiadis, “Boundary-layer behavior on continuous solid surfaces: II. The boundary layer on a continuous flat surface,” *AIChE Journal*, vol. 7, no. 2, 1961, doi: 10.1002/aic.690070211.

[30] B. Jayaraman and J. G. Brasseur, “Transition in atmospheric boundary layer turbulence structure from neutral to convective, and large-scale rolls,” *J Fluid Mech*, vol. 913, 2021, doi: 10.1017/jfm.2021.3.

[31] K. H. B. Toh and E. W. C. Lim, “Dimensionless numbers and correlations for characterizing heat transfer in a pulsating fluidized bed,” *Appl Therm Eng*, vol. 153, 2019, doi: 10.1016/j.applthermaleng.2019.03.039.

[32] A. V. Dmitrenko, “Prediction of laminar–turbulent transition on flat plate on the basis of stochastic theory of turbulence and equivalence of measures,” *Continuum Mechanics and Thermodynamics*, vol. 34, no. 2, 2022, doi: 10.1007/s00161-021-01078-0.

[33] L. Laloui and A. F. Rotta Loria, “Analytical modelling of steady heat and mass transfers,” *Analysis and Design of Energy Geostructures*, pp. 333–408, 2020, doi: 10.1016/B978-0-12-816223-1.00008-4.

[34] C. B. Rocha, N. C. Constantinou, S. G. Llewellyn Smith, and W. R. Young, “The Nusselt numbers of horizontal convection,” *J Fluid Mech*, vol. 894, 2020, doi: 10.1017/jfm.2020.269.

[35] L.-Z. Zhang, “Heat and Mass Transfer in Plate-Fin Membrane Ducts,” *Conjugate Heat and Mass Transfer in Heat Mass Exchanger Ducts*, pp. 125–156, Jan. 2013, doi: 10.1016/B978-0-12-407782-9.00005-8.

[36] A. P. Colburn, “A method of correlating forced convection heat-transfer data and a comparison with fluid friction,” *Int J Heat Mass Transf*, vol. 7, no. 12, 1964, doi: 10.1016/0017-9310(64)90125-5.

[37] T. Kodama, “High-temperature solar chemistry for converting solar heat to chemical fuels,” *Progress in Energy and Combustion Science*, vol. 29, no. 6. 2003. doi: 10.1016/S0360-1285(03)00059-5.

[38] J. N. Bahcall and E. E. Salpeter, “On the Interaction of Radiation from Distant Sources with the Intervening Medium.,” *Astrophys J*, vol. 142, 1965, doi: 10.1086/148460.

[39] M. Karami, M. Bozorgi, and S. Delfani, “Effect of design and operating parameters on thermal performance of low-temperature direct absorption solar collectors: a review,” *Journal of Thermal Analysis and Calorimetry*, vol. 146, no. 3. 2021. doi: 10.1007/s10973-020-10043-z.

[40] L. M. A. Gontijo and C. G. Rodrigues, “THERMAL RADIATION AND PLANCK’S FORMULA,” *Quim Nova*, vol. 45, no. 10, 2022, doi: 10.21577/0100-4042.20170942.

[41] “Broadband albedo,” *Advanced Remote Sensing*, pp. 193–250, Jan. 2020, doi: 10.1016/B978-0-12-815826-5.00006-4.

[42] G. Tanda and M. Misale, “Effects of surface irregularities and coatings on thermal emittance of selected metals between 373 and 1073 k,” *J Heat Transfer*, vol. 143, no. 4, 2021, doi: 10.1115/1.4049636.

[43] S. X. Liu, J. Rees., and J. D. Spitler, “Simulation of a geothermal bridge deck anti-icing system and experimental validation,” *Proceedings of the Transportation Research Board 82nd Annual Meeting*, pp. 12–16, 2003.

[44] Shuo Han, Jinliang Xu, Menghua Yan, and Zhaoxin Liu, “Using multiple linear regression and BP neural network to predict critical meteorological conditions of expressway bridge pavement icing,” *PlosOne*, 2022.

[45] “ANSYS.” ANSYS, Inc.

[46] American Association of State Highway and Transportation Officials, “AASHTO LRFD Bridge Design Specifications. .” Washington, D.C, 2008.

[47] ACI Committee 318, “ACI 318-19: Building Code Requirements for Structural Concrete,” Farmington Hills, MI, 2019.

[48] FHWA, “Lane Width,” A Policy on Geometric Design of Highways and Streets.

[49] American Society of Mechanical Engineers, “1998 asme bpv code.”

[50] National Weather Service, US Dept of Commerce, and National Oceanic and Atmospheric Administration, “National Weather Service.”

[51] Yunus Cengel and Michael Boles, *Thermodynamics: An Engineering Approach*, 8th Edition. 2014.

[52] A. Blog, “The Fundamentals of FEA Meshing for Structural Analysis,” Ansys Blog

APPENDIX A

Temperature distribution with the recommended EPH across the states of USA.

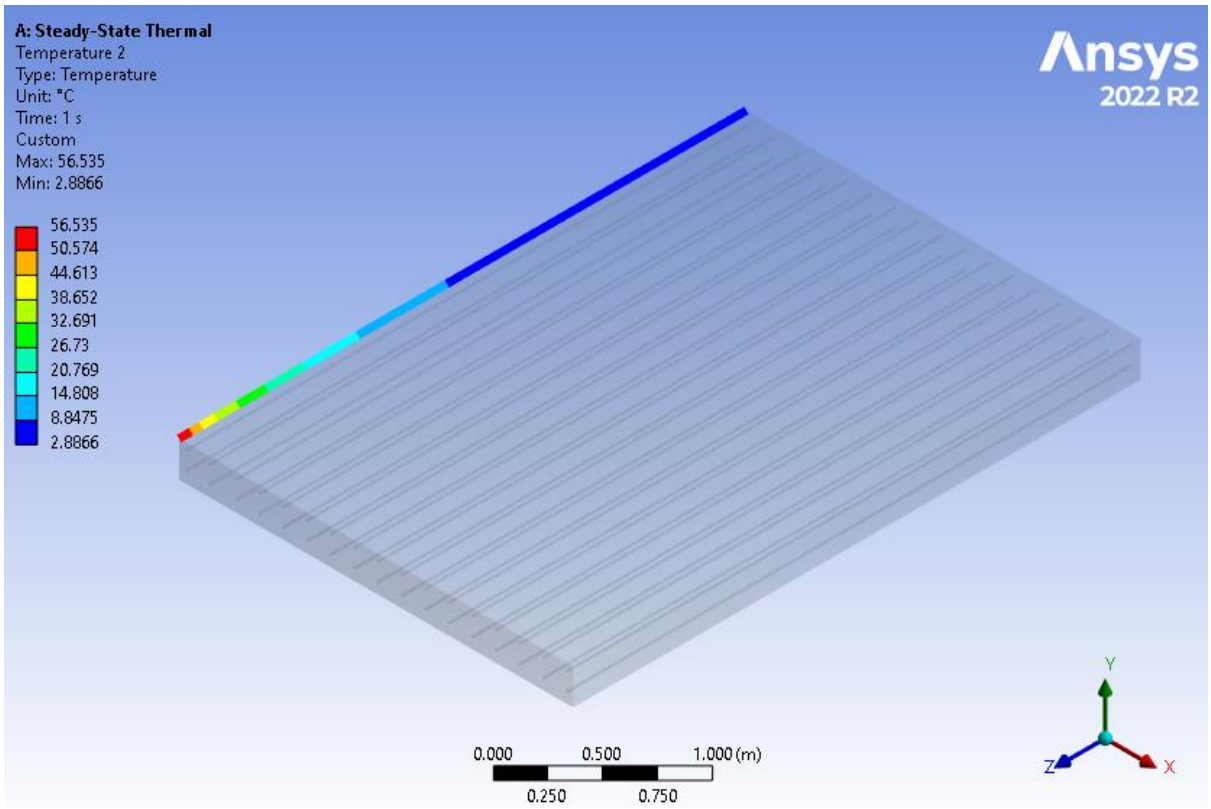

Figure 39. Temperature distribution in the left edge of the deck in Alabama using a 648.28W power energy source.

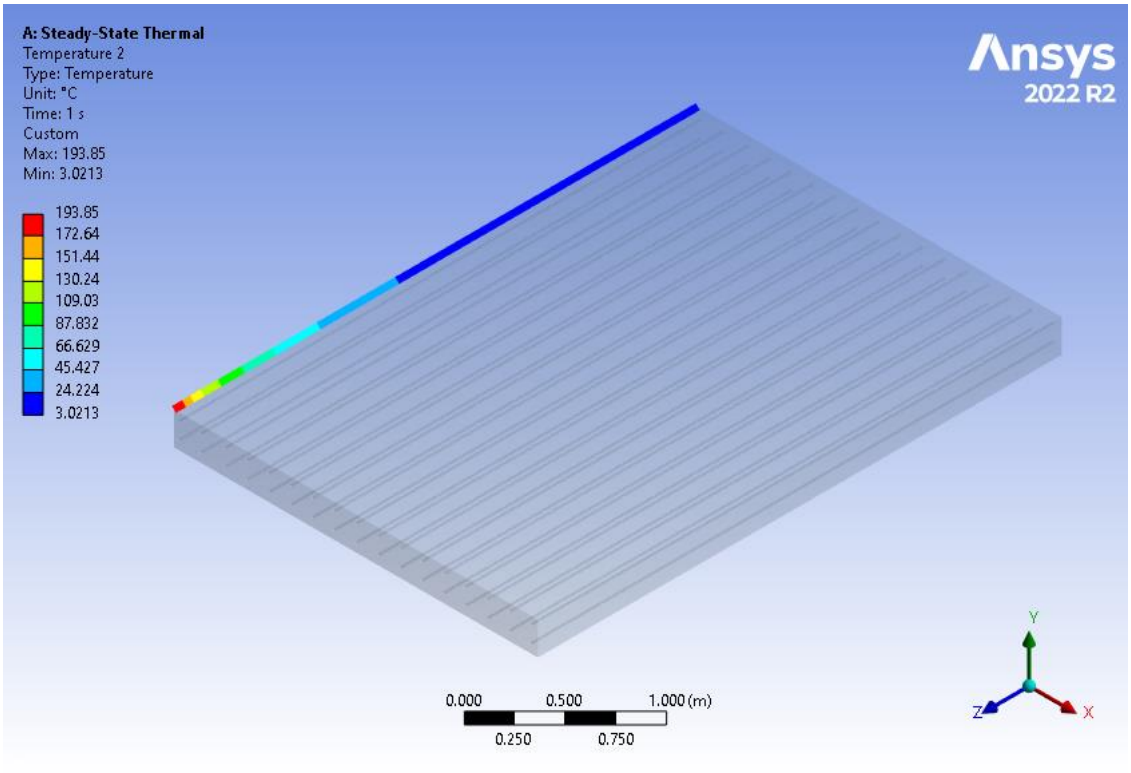

Figure 40. Temperature distribution in the left edge of the deck in Arizona using a 2660.15W power energy source.

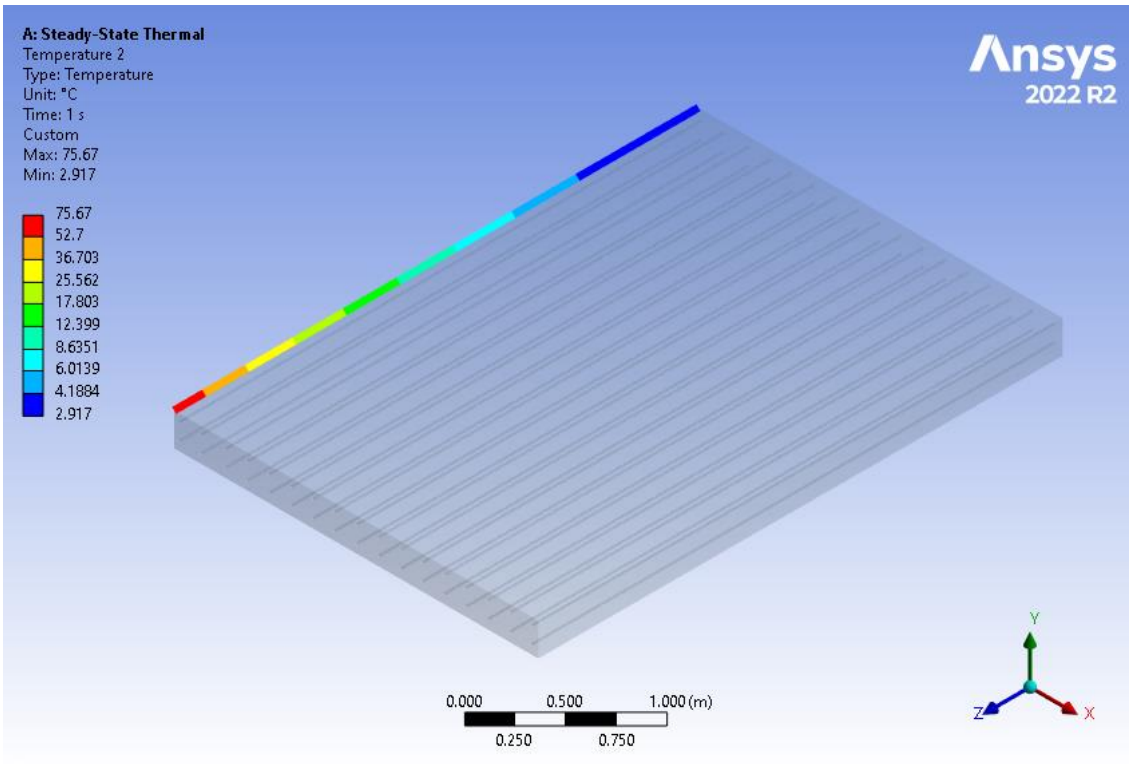

Figure 41. Temperature distribution in the left edge of the deck in Arkansas using a 901.64W power energy source.

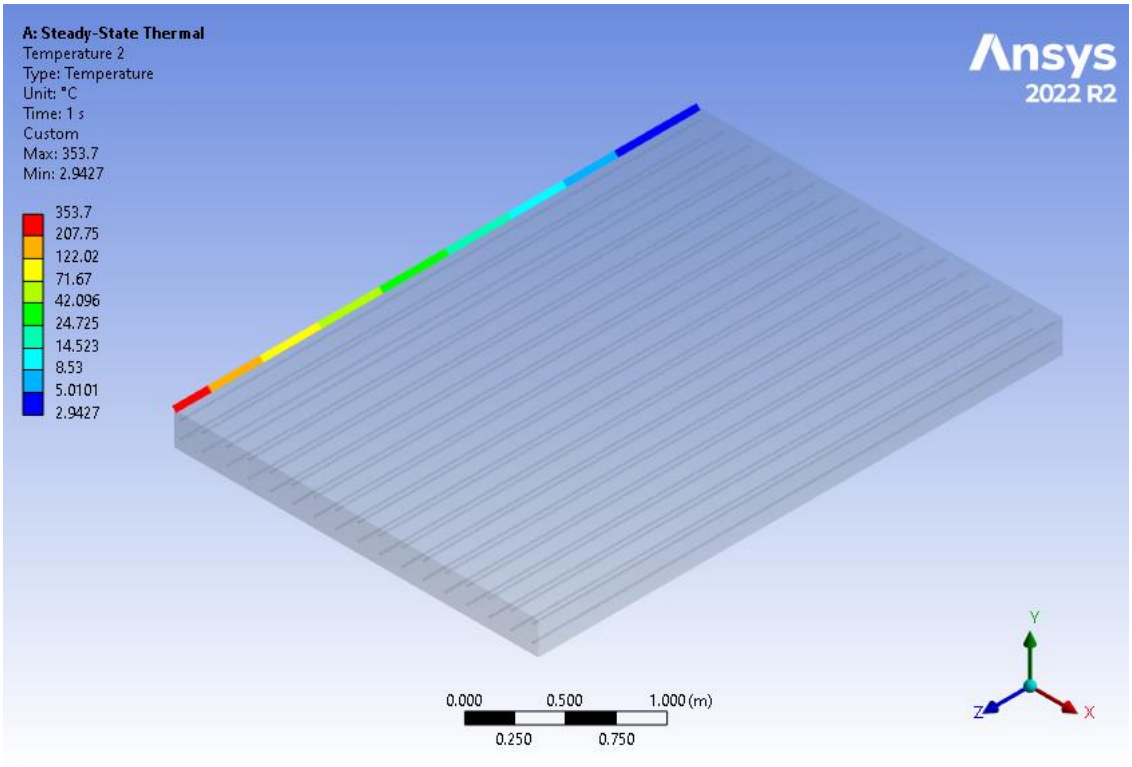

Figure 42. Temperature distribution in the left edge of the deck in California using a 5402.38W power energy source.

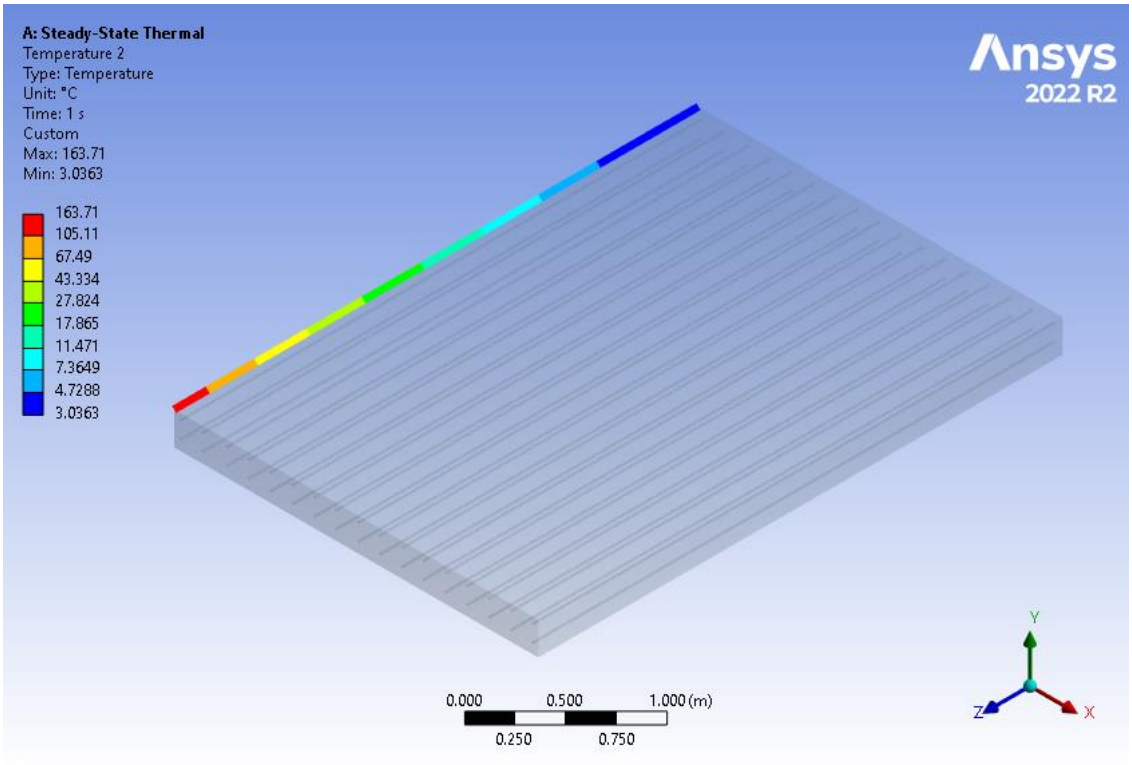

Figure 43. Temperature distribution in the left edge of the deck in Connecticut using a 2181.48W power energy source.

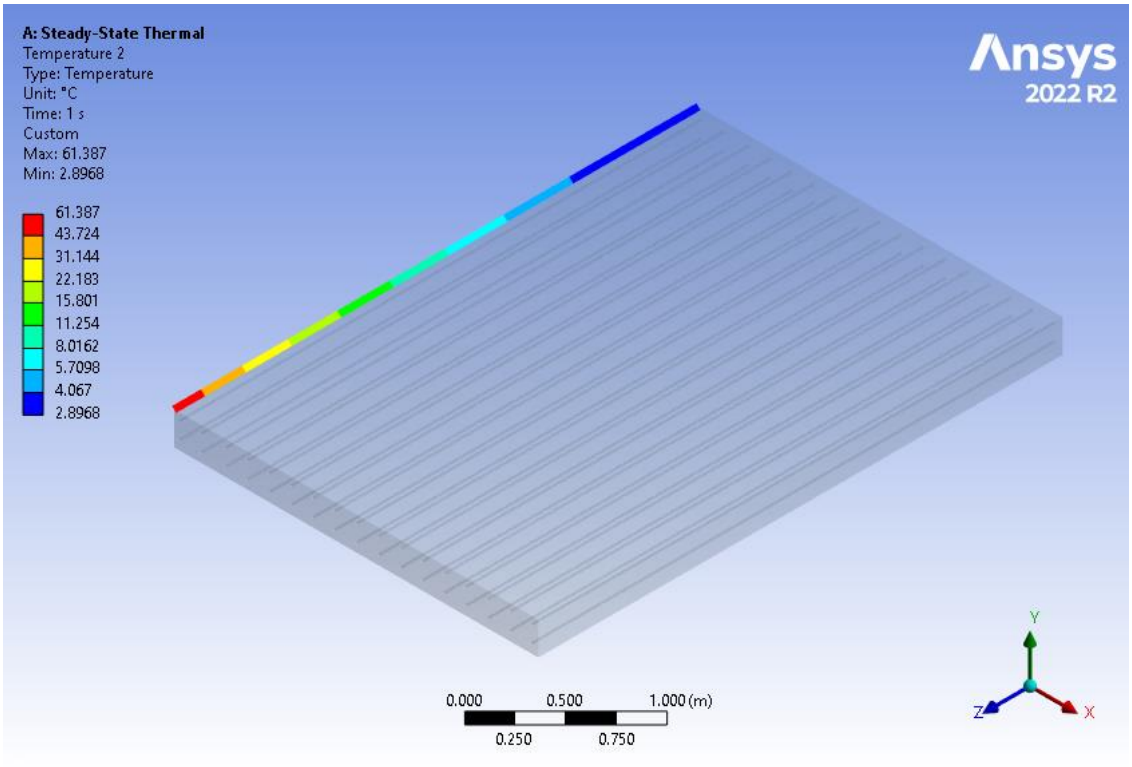

Figure 44. Temperature distribution in the left edge of the deck in Delaware using a 711.58W power energy source.

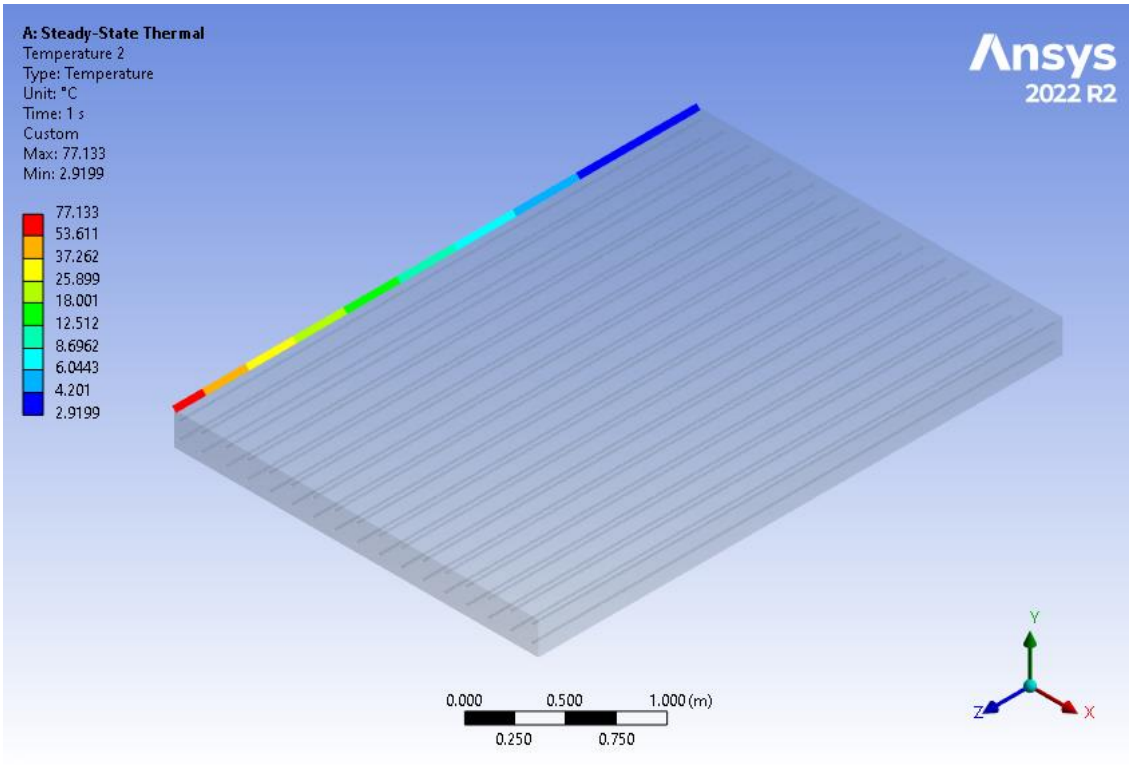

Figure 45. Temperature distribution in the left edge of the deck in Georgia using a 921.38W power energy source.

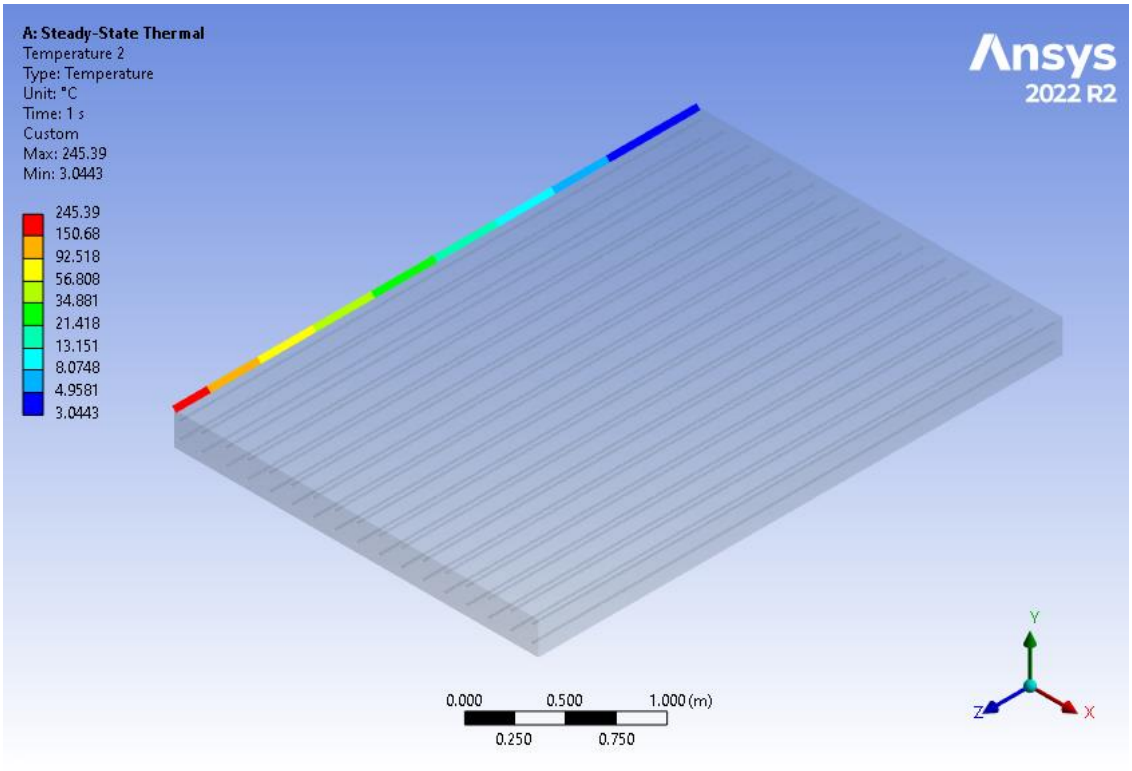

Figure 46. Temperature distribution in the left edge of the deck in Idaho using a 3516.86W power energy source.

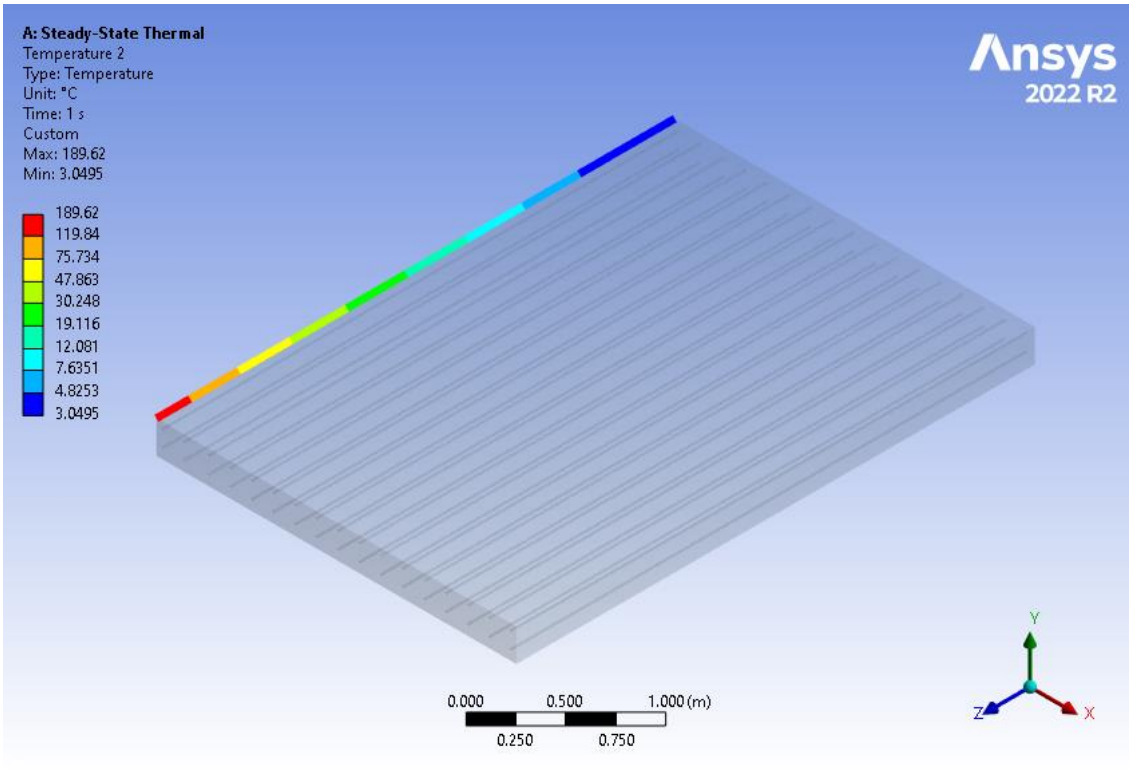

Figure 47. Temperature distribution in the left edge of the deck in Illinois using a 2591.7W power energy source.

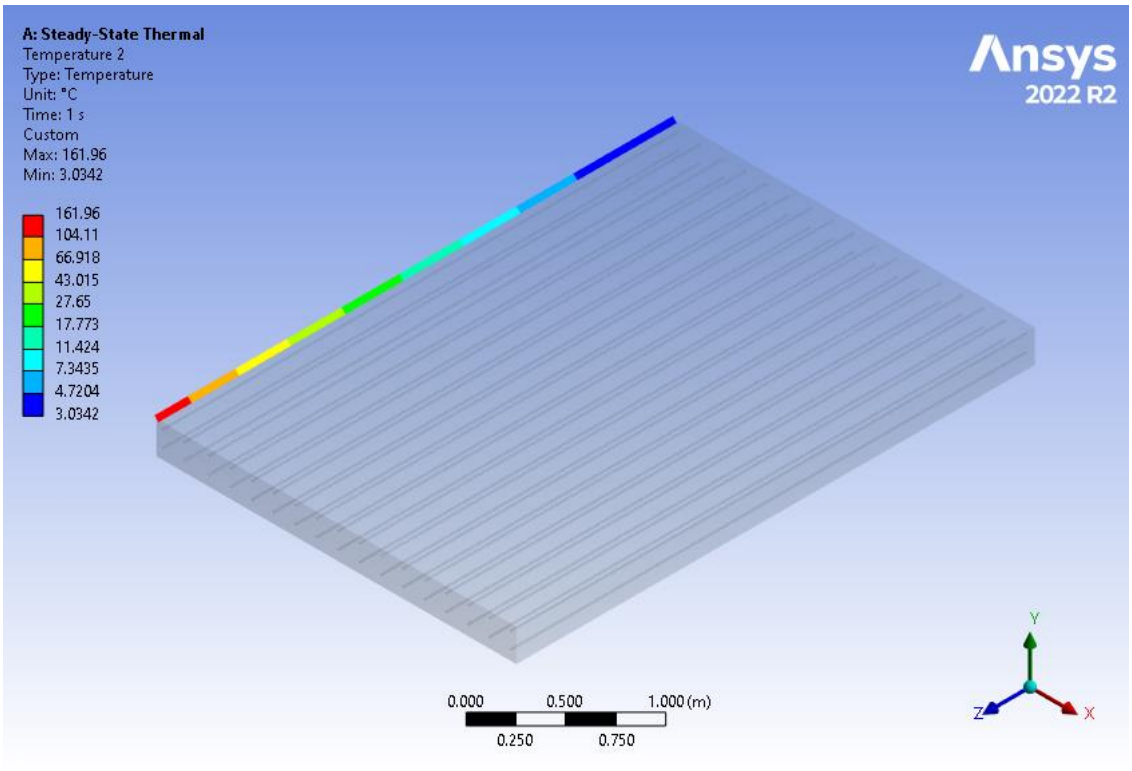

Figure 48. Temperature distribution in the left edge of the deck in Indiana using a 2154.29W power energy source.

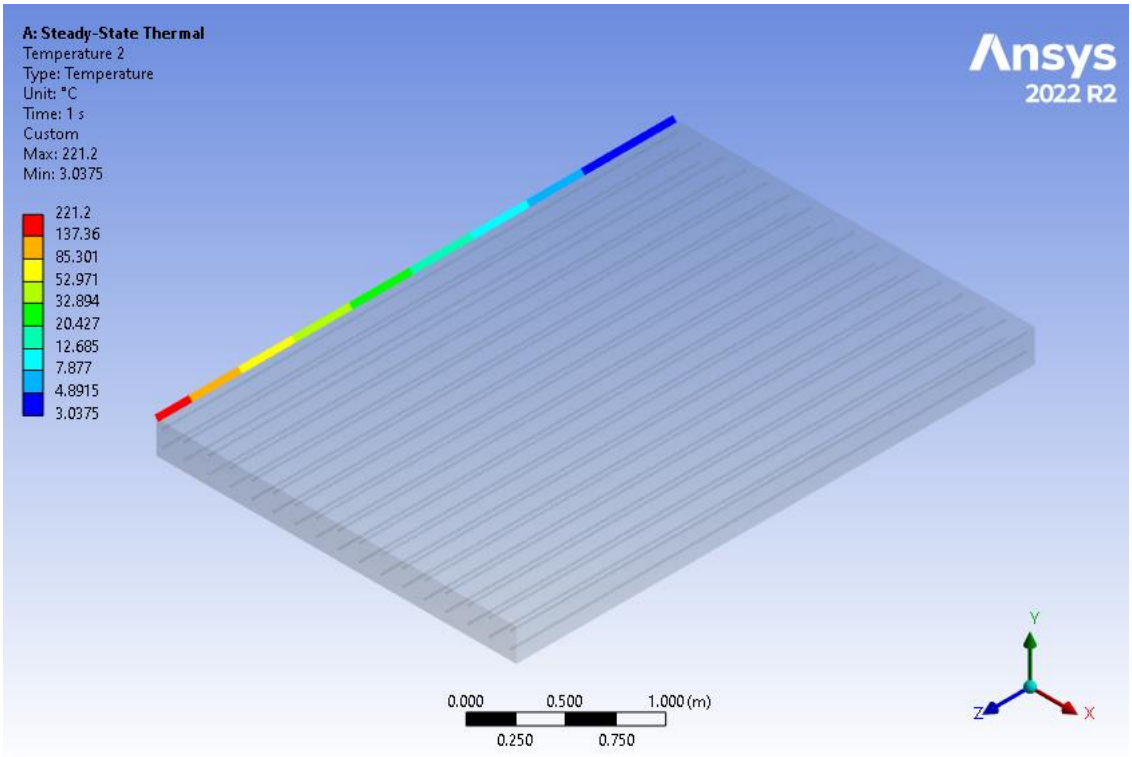

Figure 49. Temperature distribution in the left edge of the deck in Iowa using a 3110.03W power energy source.

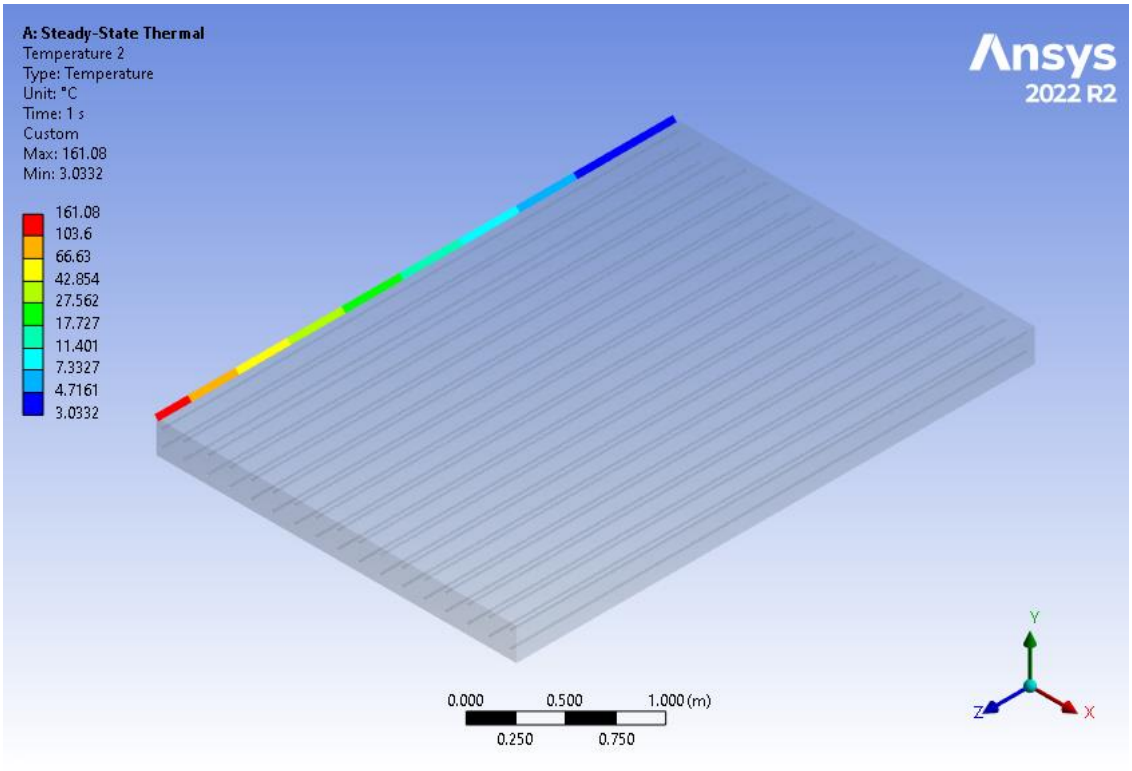

Figure 50. Temperature distribution in the left edge of the deck in Kansas using a 2140.63W power energy source.

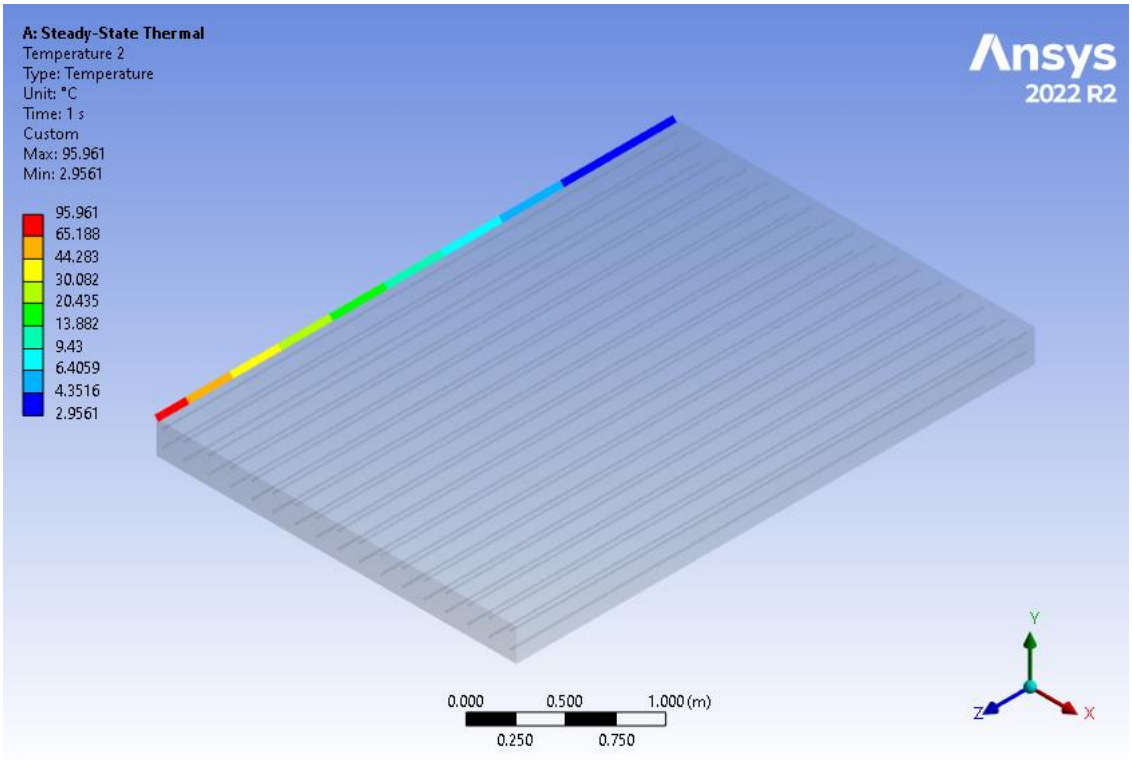

Figure 51. Temperature distribution in the left edge of the deck in Kentucky using a 1180.13W power energy source.

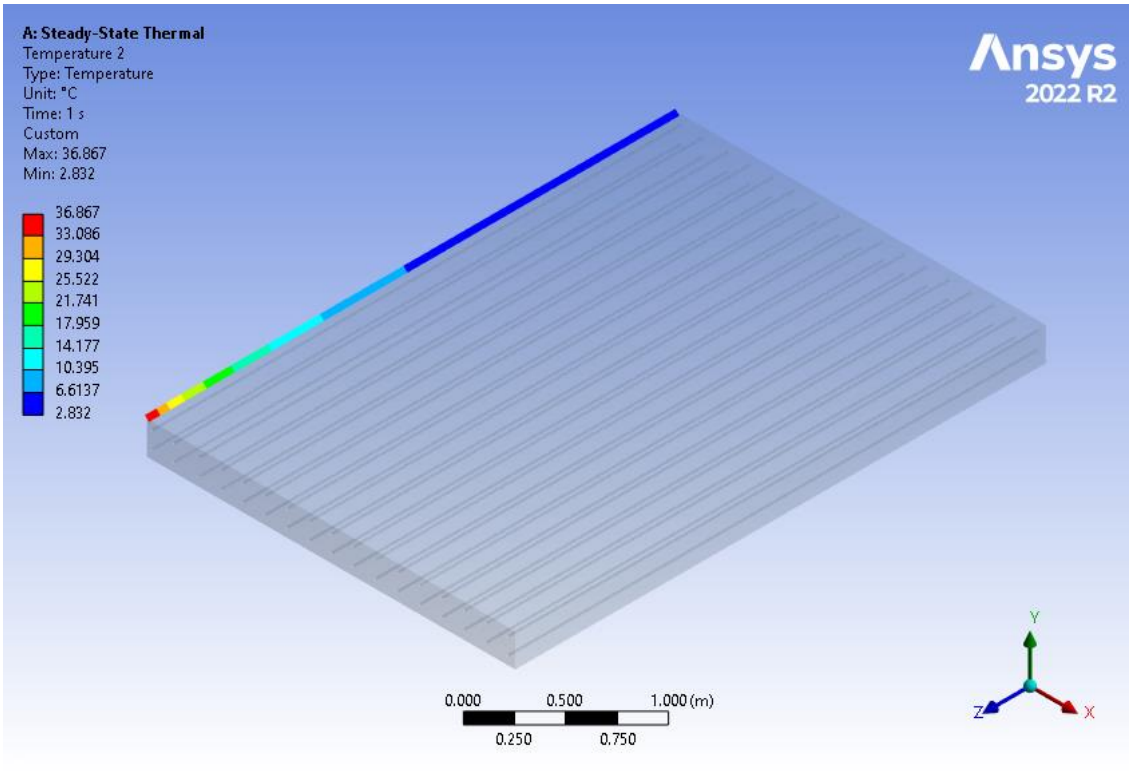

Figure 52. Temperature distribution in the left edge of the deck in Louisiana using a 397.08W power energy source.

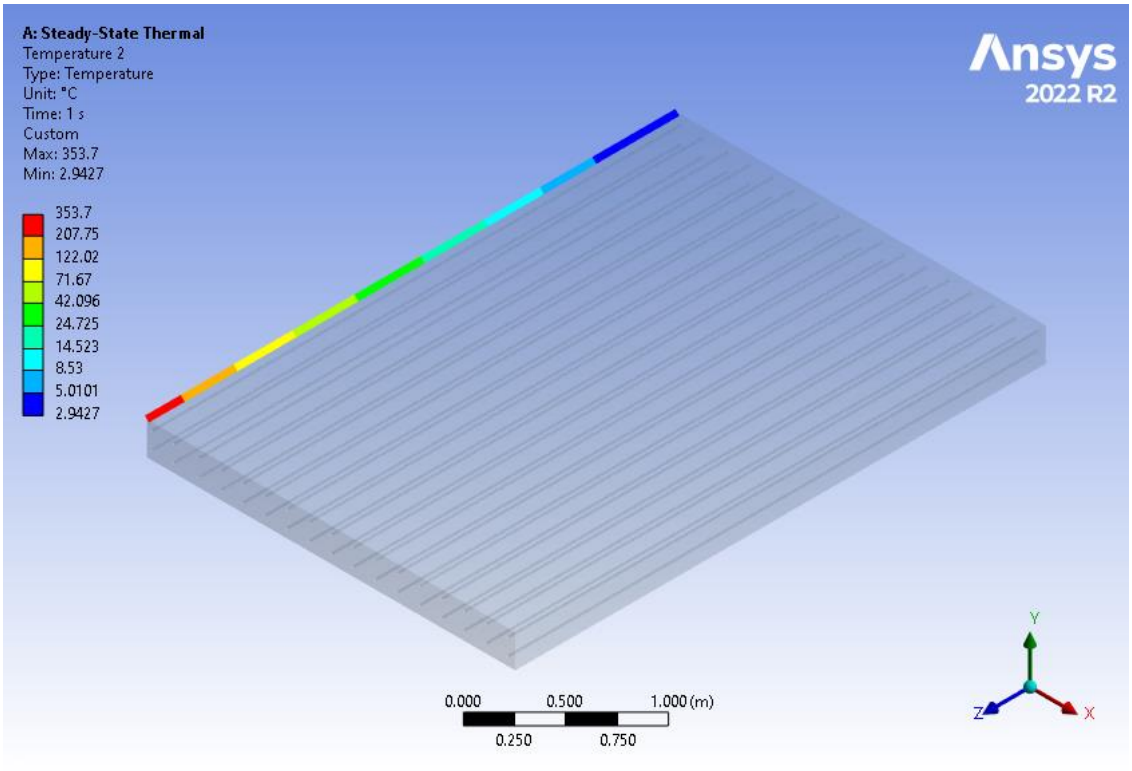

Figure 53. Temperature distribution in the left edge of the deck in Maine using a 5402.38W power energy source.

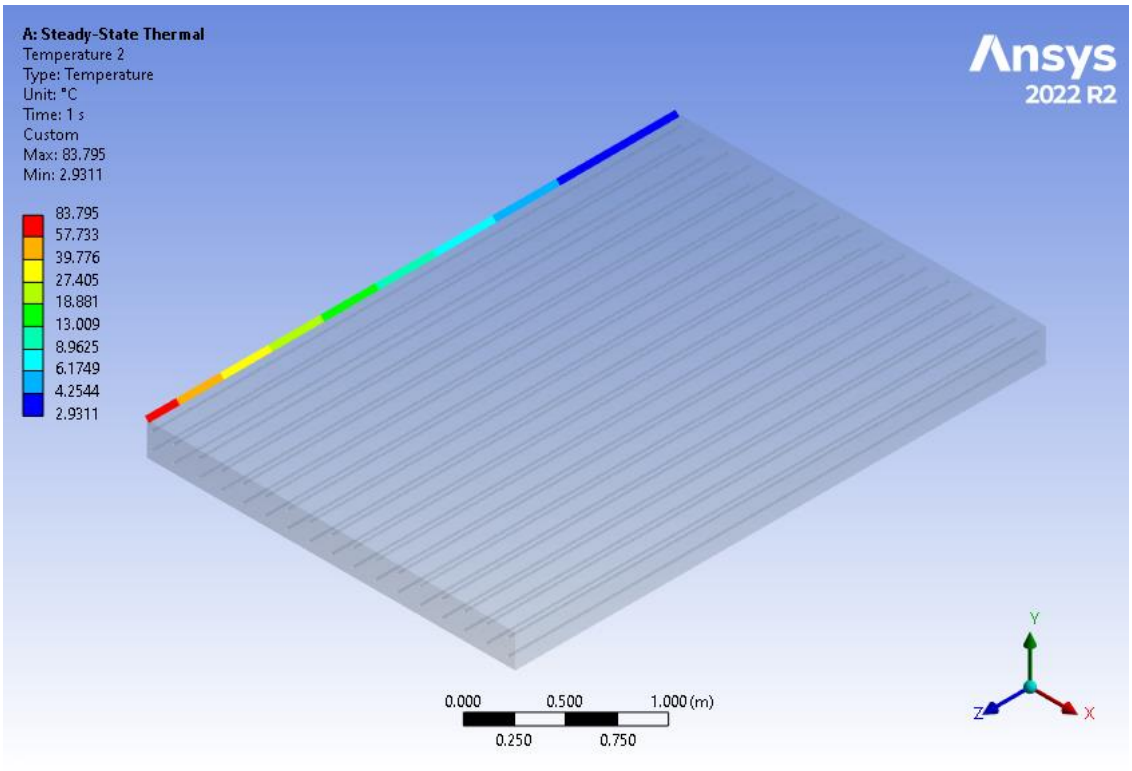

Figure 54. Temperature distribution in the left edge of the deck in Maryland using a 1012.01W power energy source.

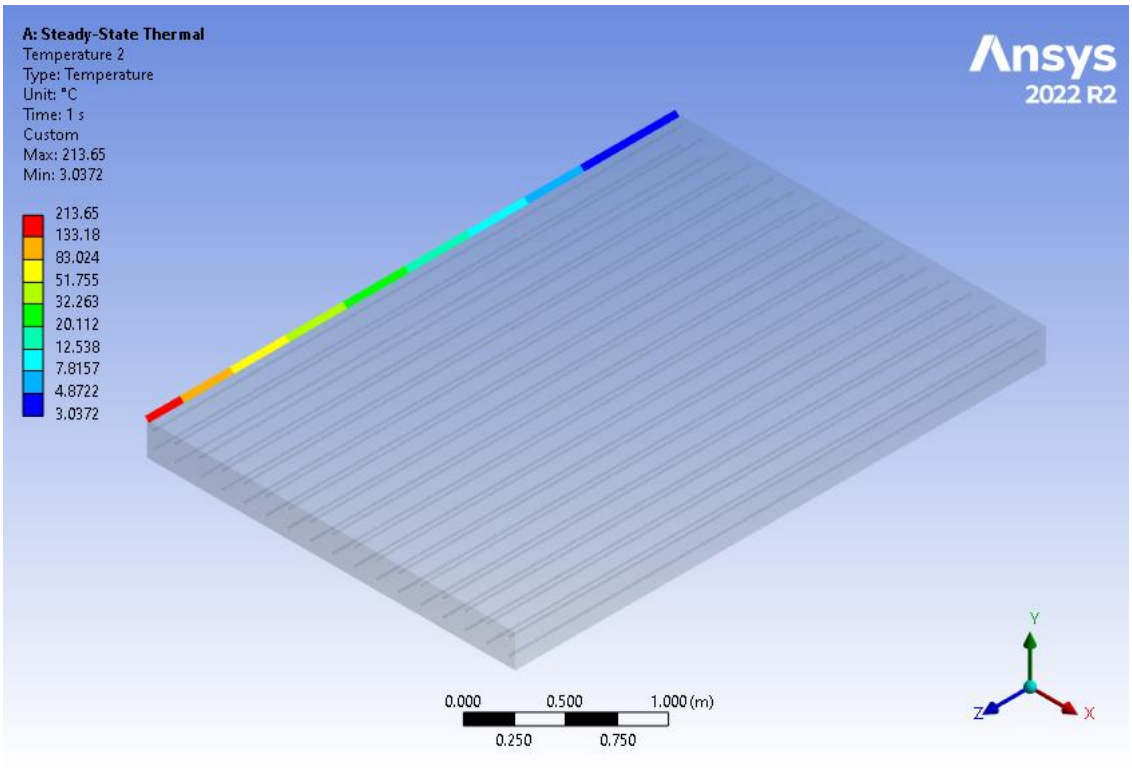

Figure 55. Temperature distribution in the left edge of the deck in Massachusetts using a 2984.58W power energy source.

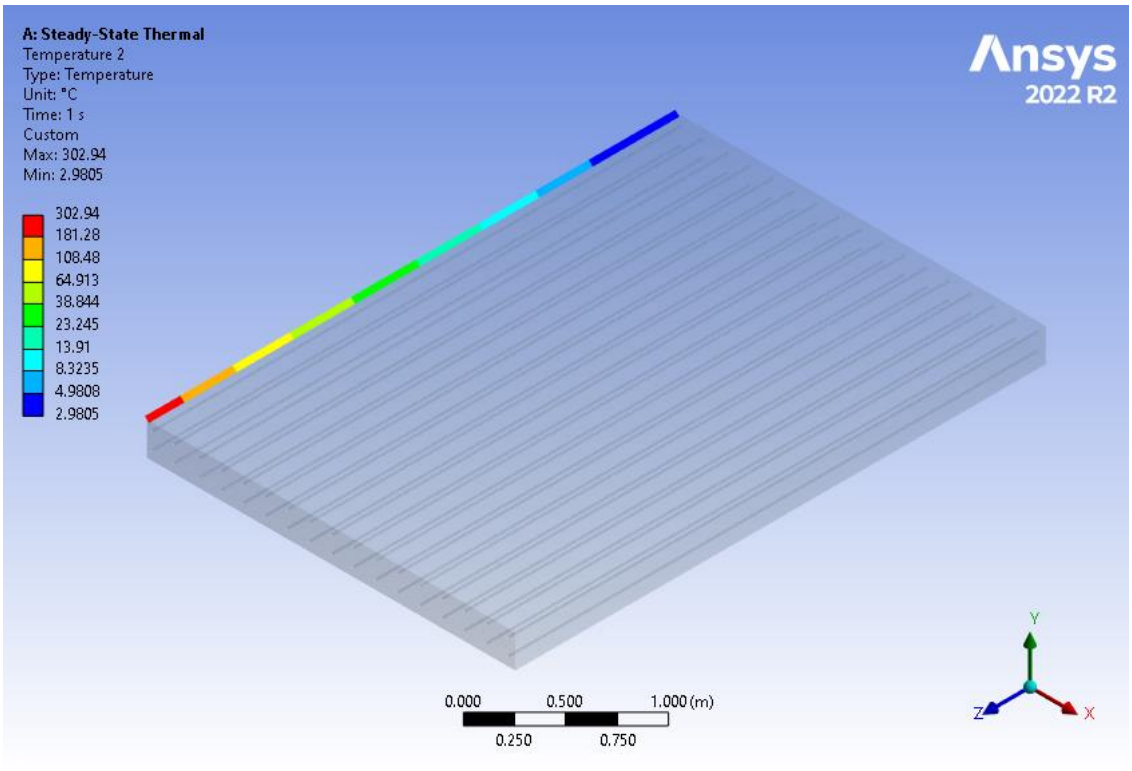

Figure 56. Temperature distribution in the left edge of the deck in Michigan using a 4507.06W power energy source.

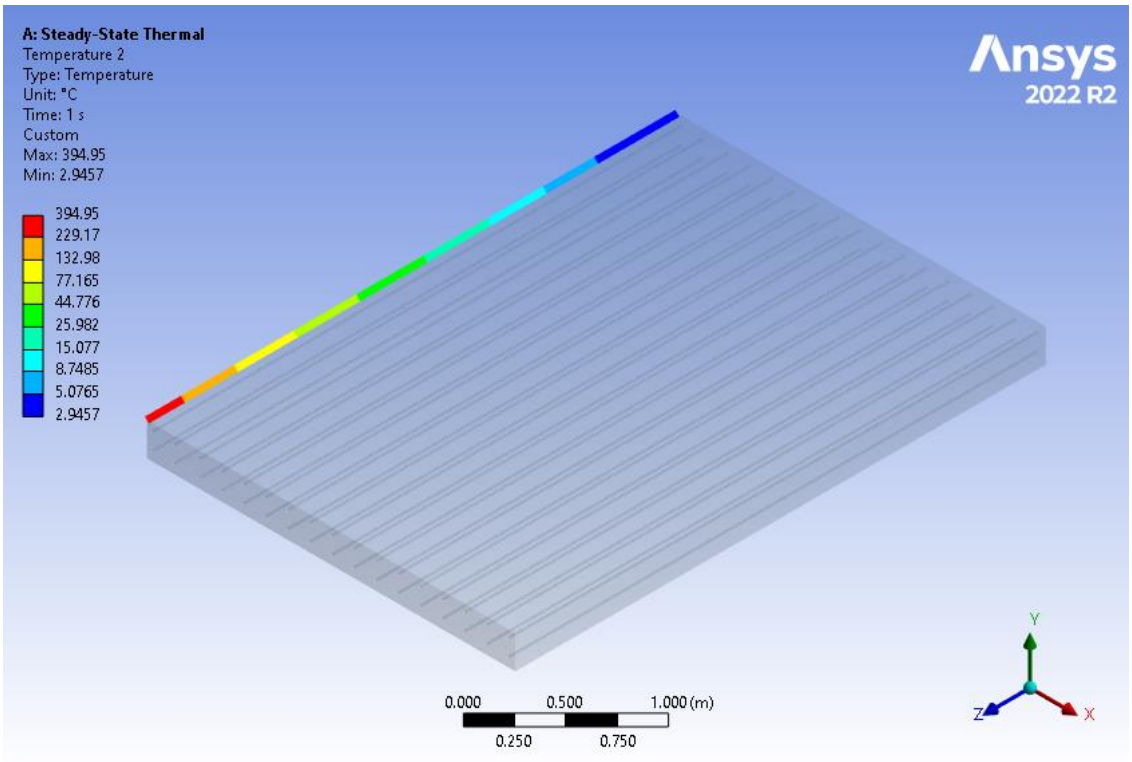

Figure 57. Temperature distribution in the left edge of the deck in Minnesota using a 6132.69W power energy source.

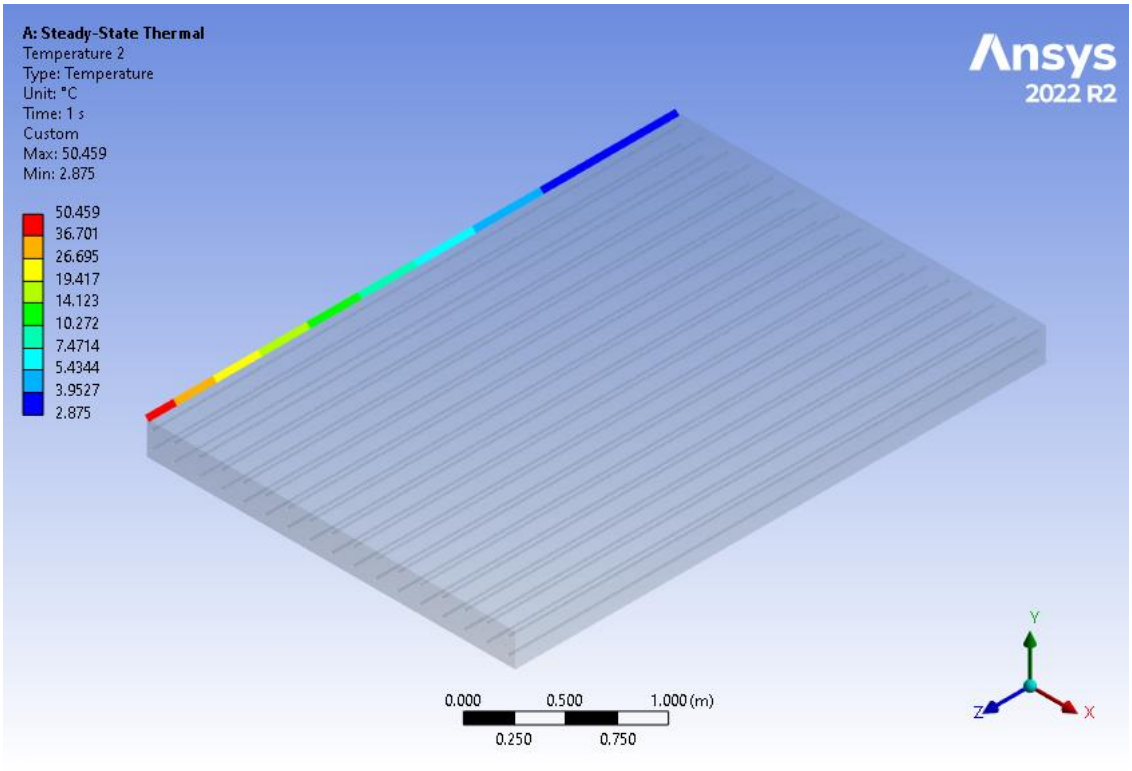

Figure 58. Temperature distribution in the left edge of the deck in Mississippi using a 569.83W power energy source.

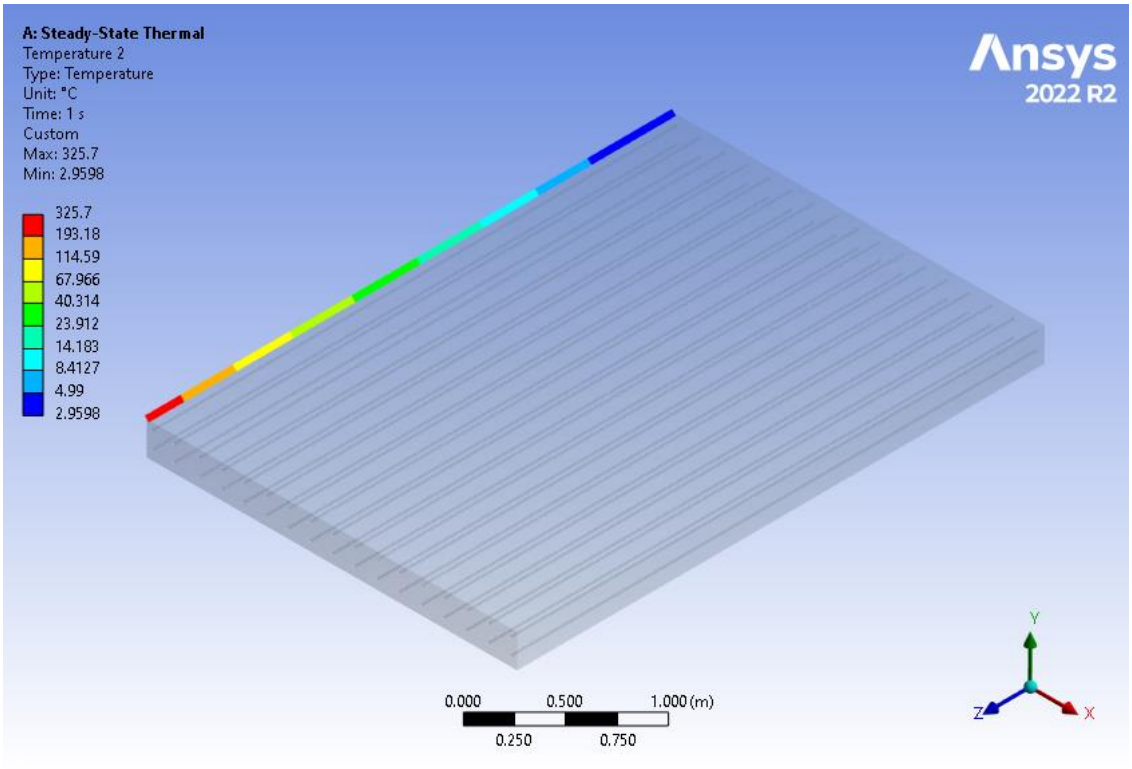

Figure 59. Temperature distribution in the left edge of the deck in Montana using a 4906.69W power energy source.

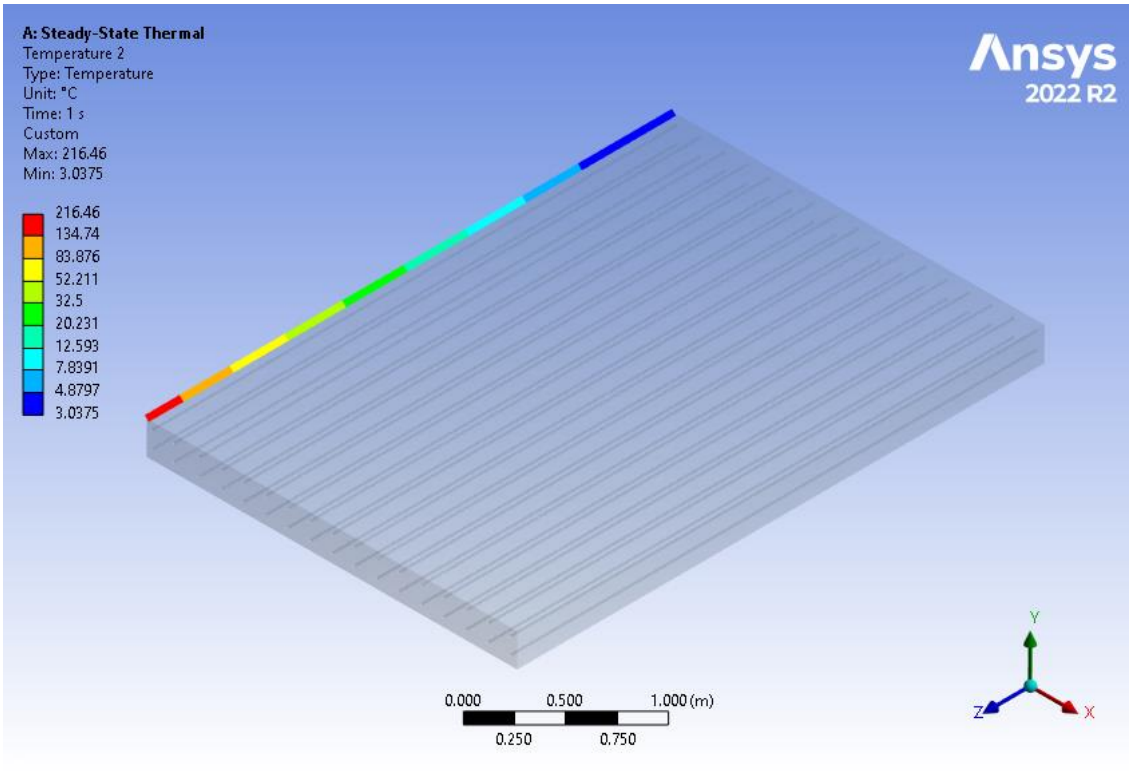

Figure 60. Temperature distribution in the left edge of the deck in Nebraska using a 3031.22W power energy source.

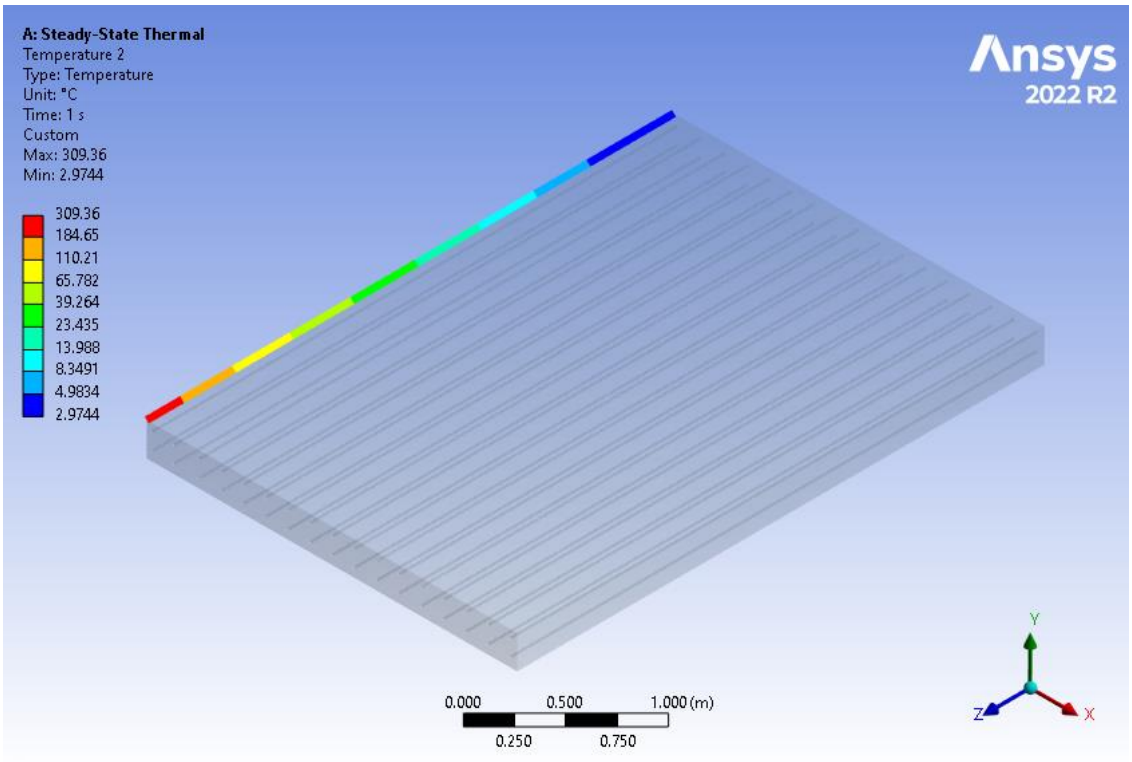

Figure 61. Temperature distribution in the left edge of the deck in New Hampshire using a 4619.53W power energy source.

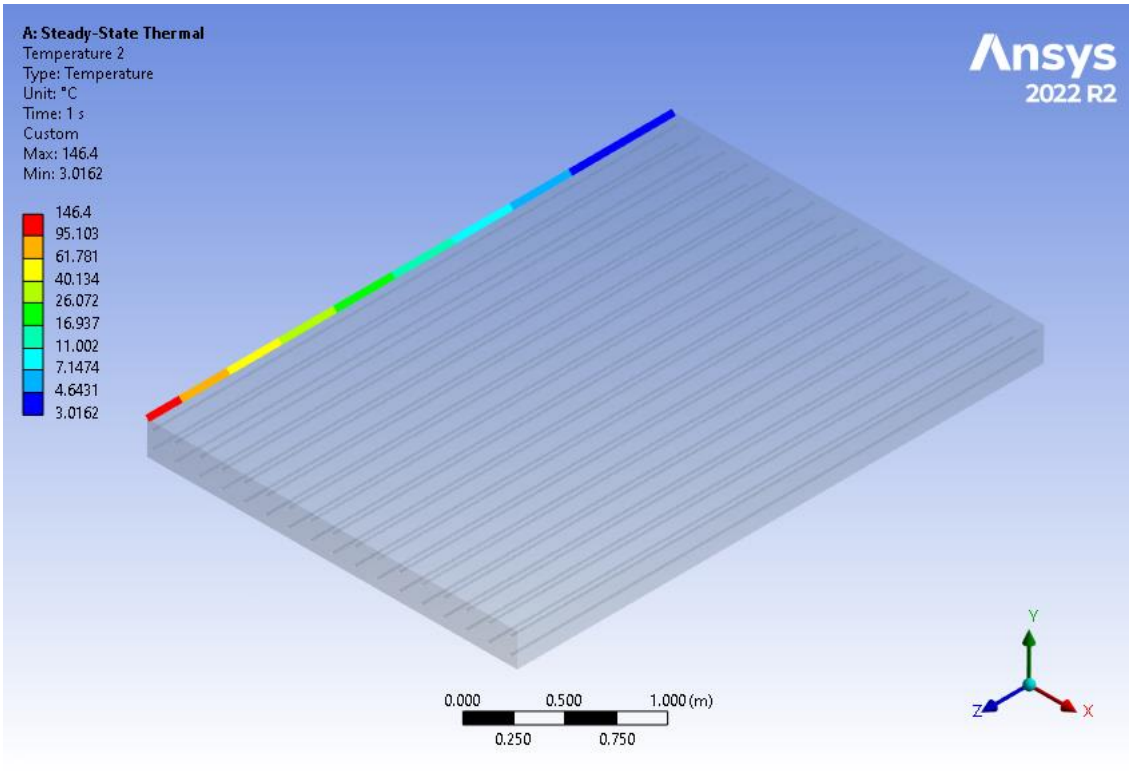

Figure 62. Temperature distribution in the left edge of the deck in New Jersey using a 1915.65W power energy source.

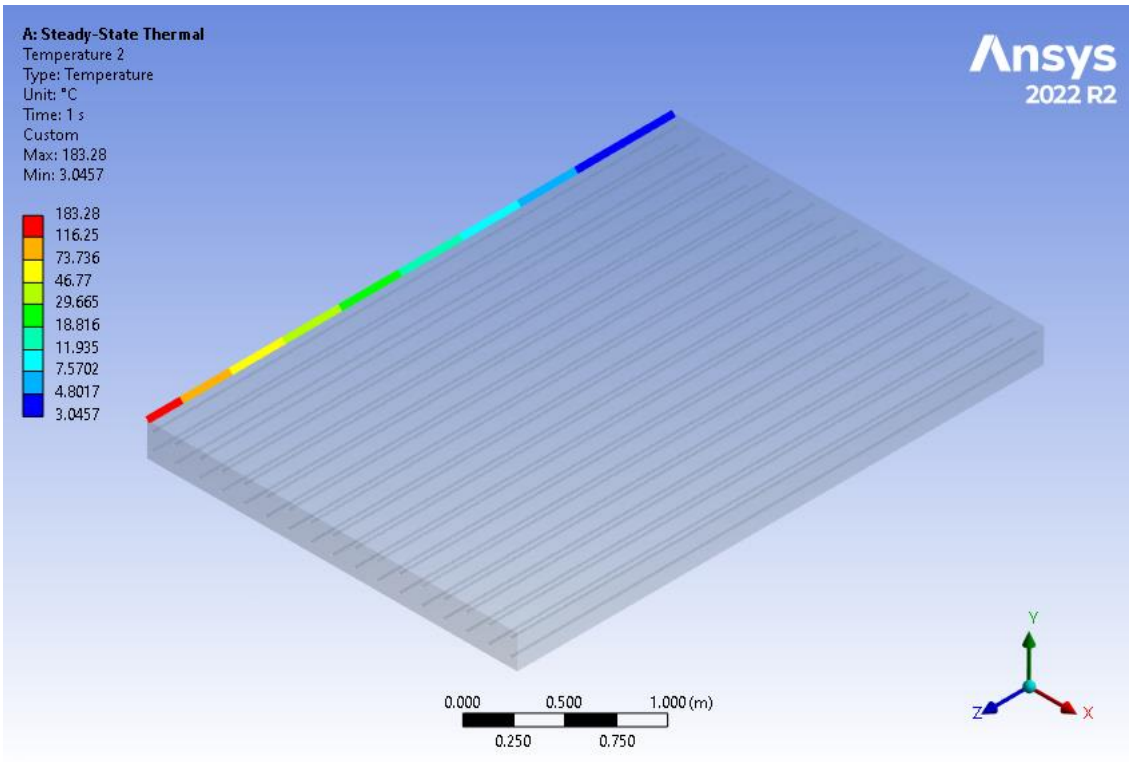

Figure 63. Temperature distribution in the left edge of the deck in New Mexico at 2489.96W power energy source.

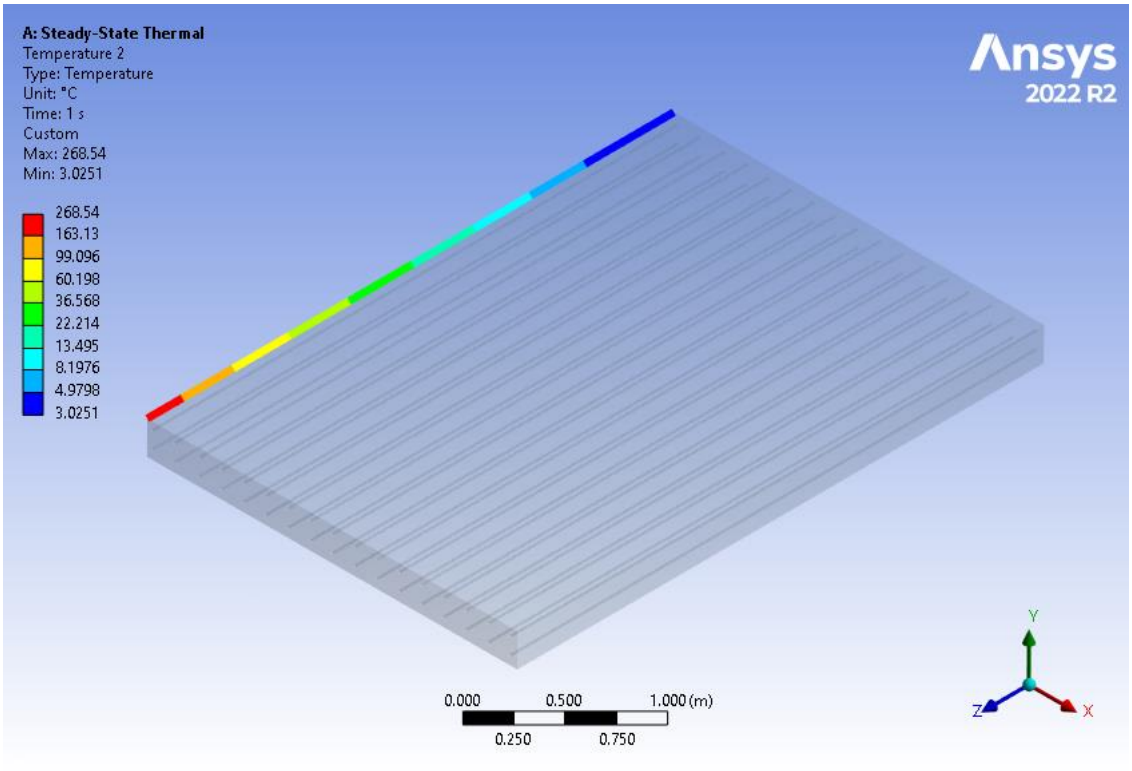

Figure 64. Temperature distribution in the left edge of the deck in New York using a 3910.41W power energy source.

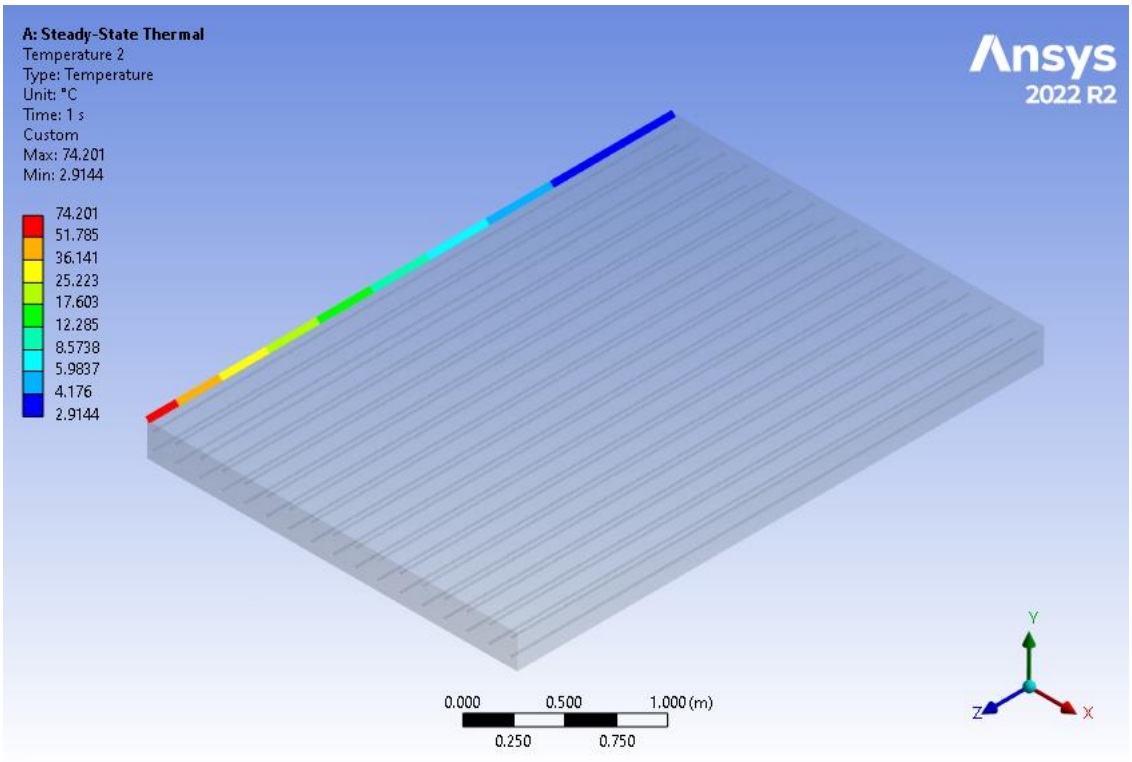

Figure 65. Temperature distribution in the left edge of the deck in North Carolina using a 881.87W power energy source.

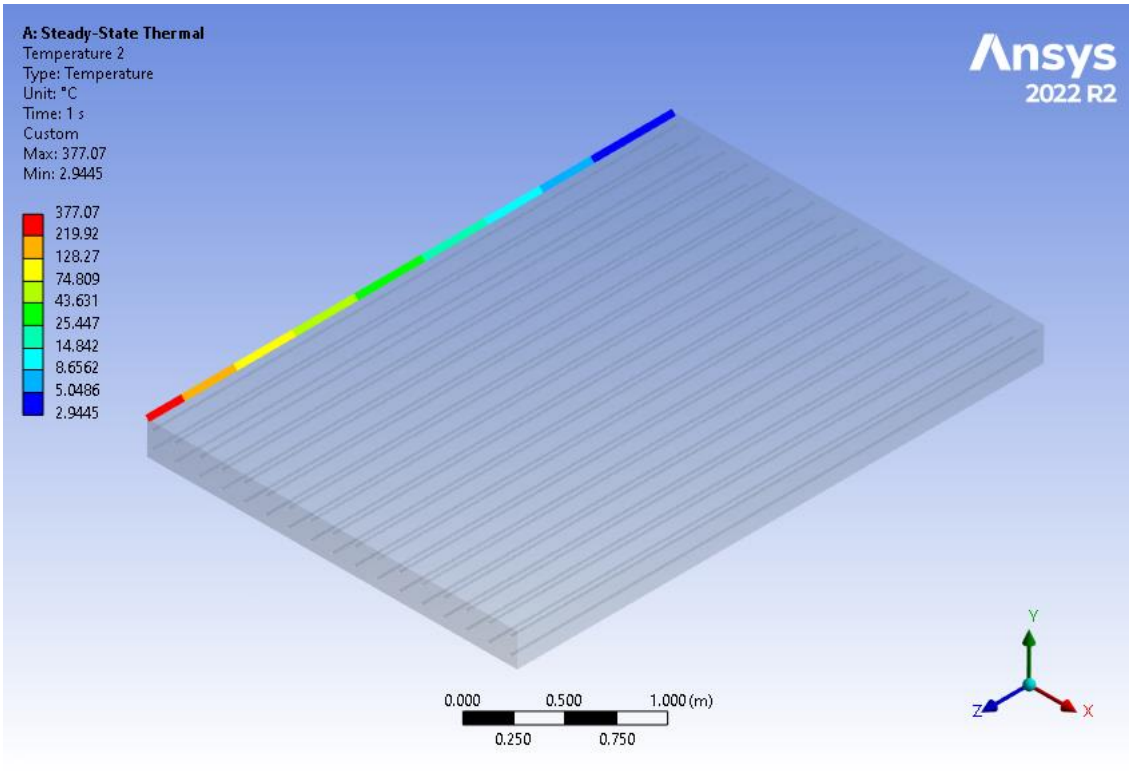

Figure 66. Temperature distribution in the left edge of the deck in North Dakota using a 5814.53W power energy source.

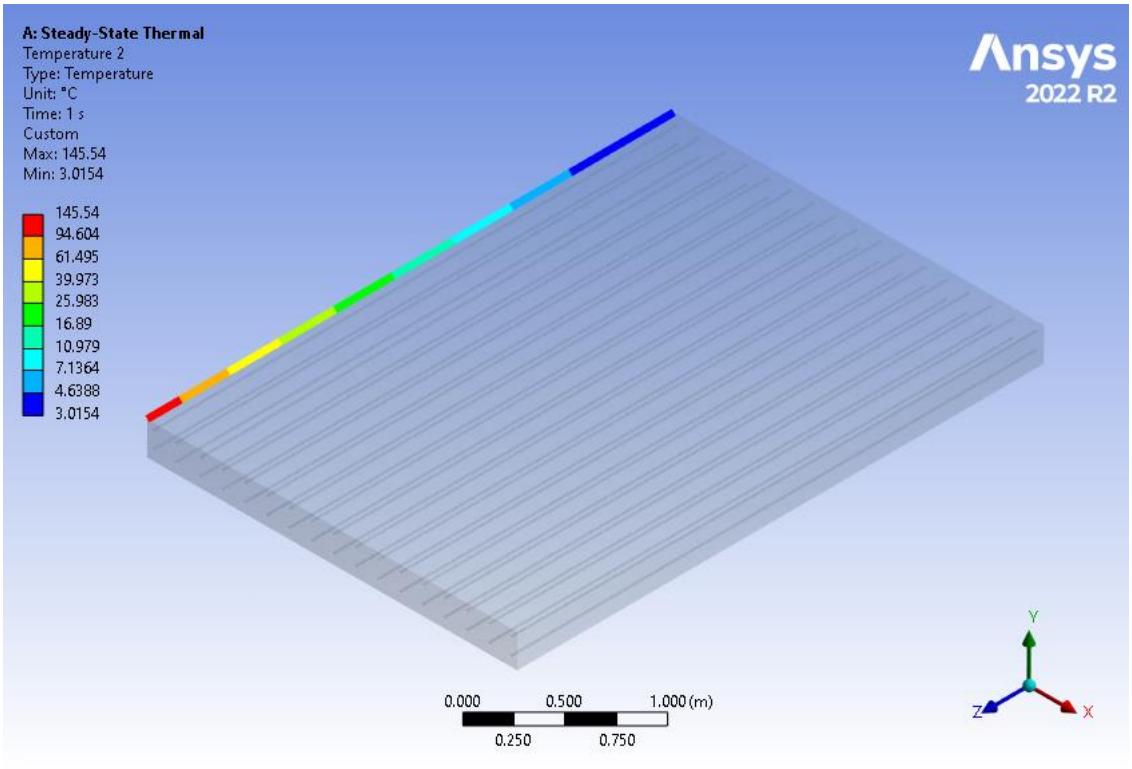

Figure 67. Temperature distribution in the left edge of the deck in Ohio using a 1902.62W power energy source.

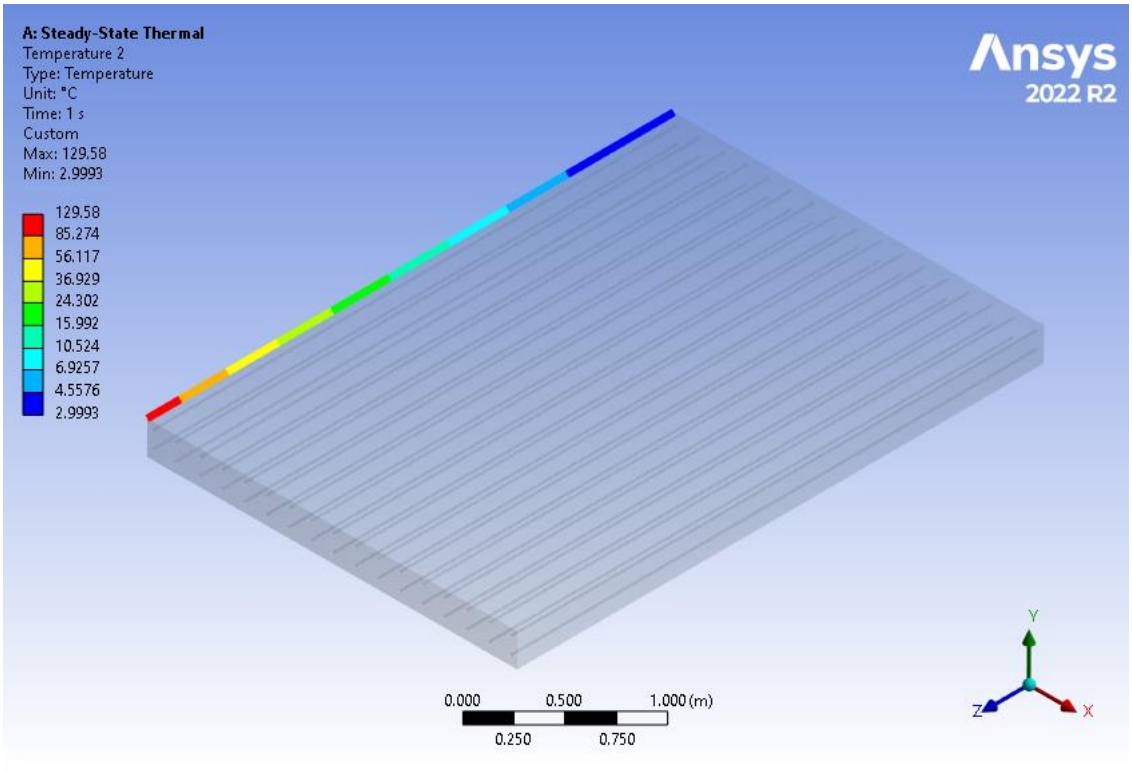

Figure 68. Temperature distribution in the left edge of the deck in Oklahoma using a 1663.75W power energy source.

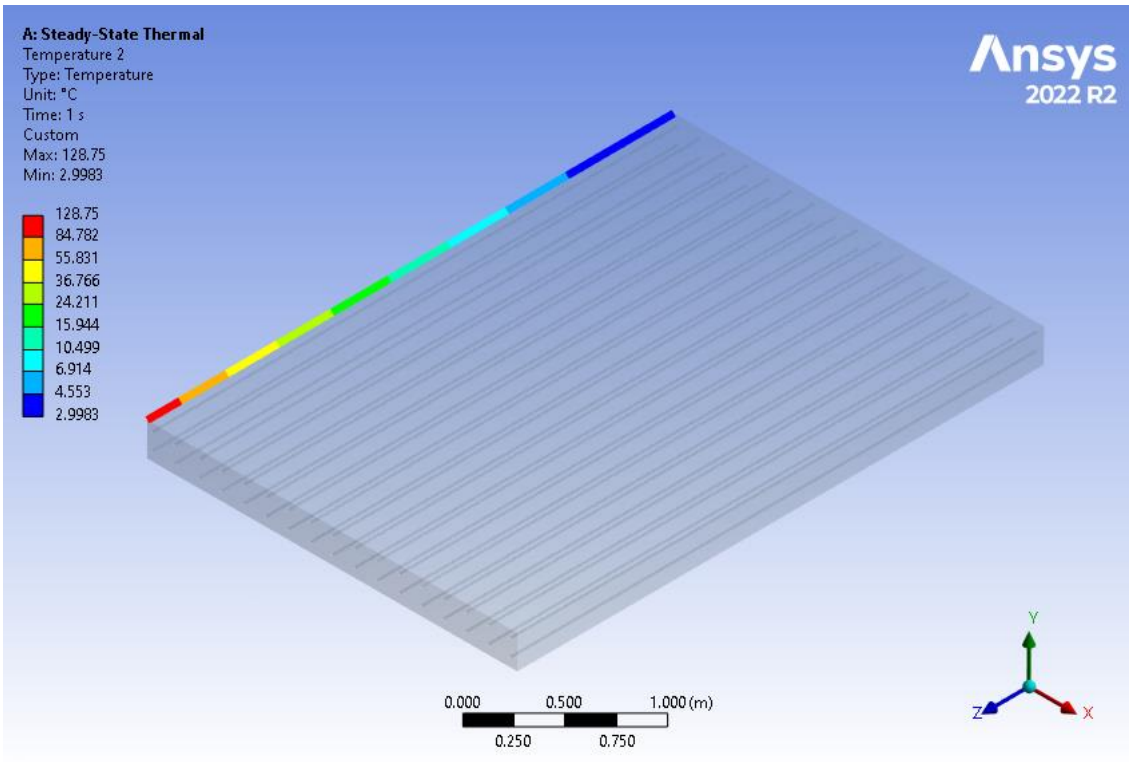

Figure 69. Temperature distribution in the left edge of the deck in Oregon using a 1651.42W power energy source.

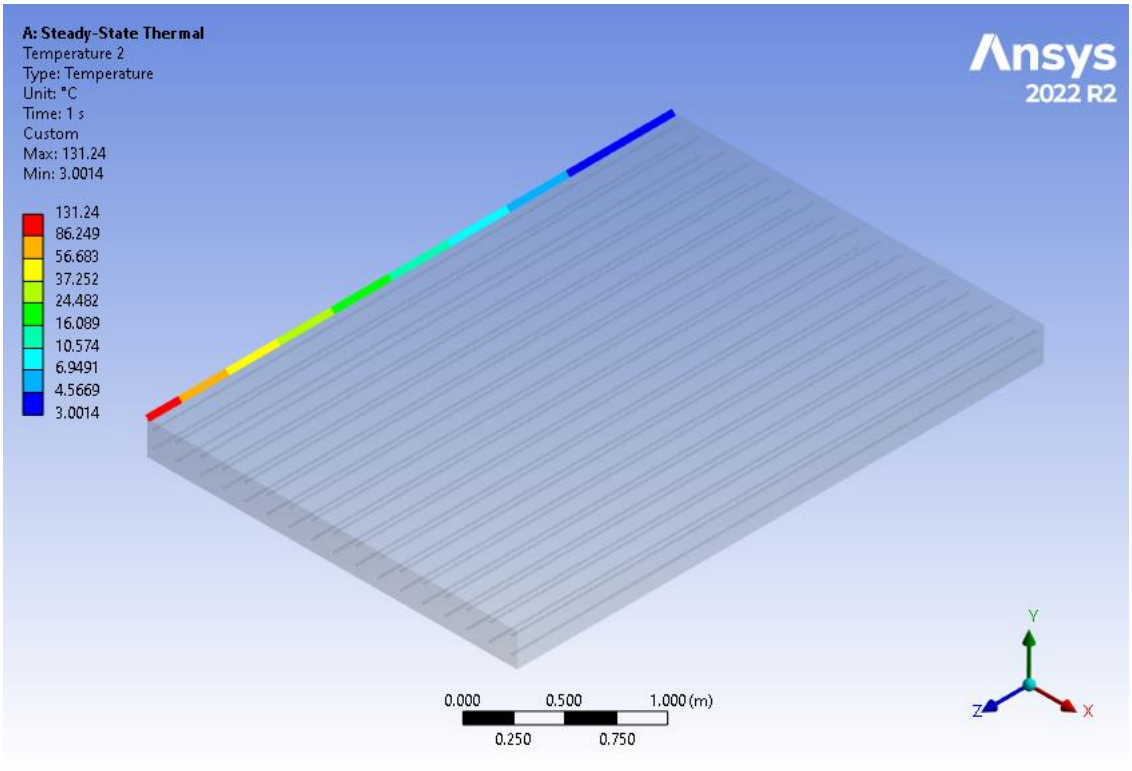

Figure 70. Temperature distribution in the left edge of the deck in Rhode Island using a 1688.29W power energy source.

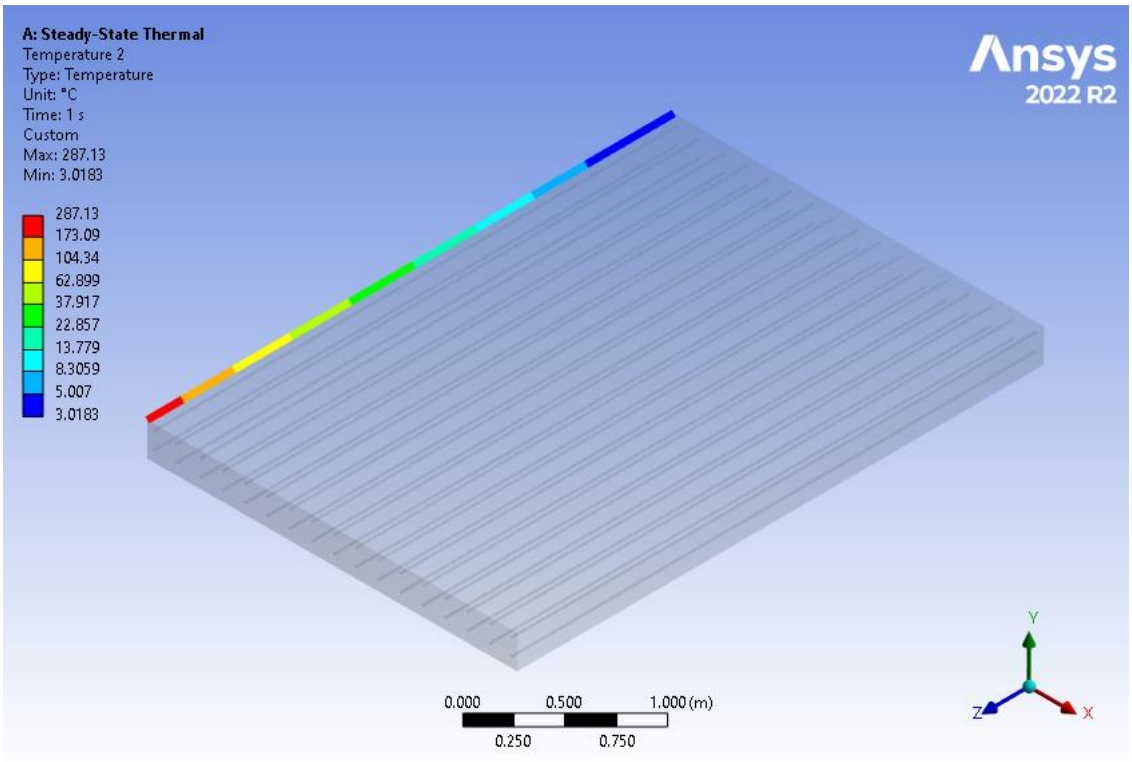

Figure 71. Temperature distribution in the left edge of the deck in South Dakota using a 4231.22W power energy source.

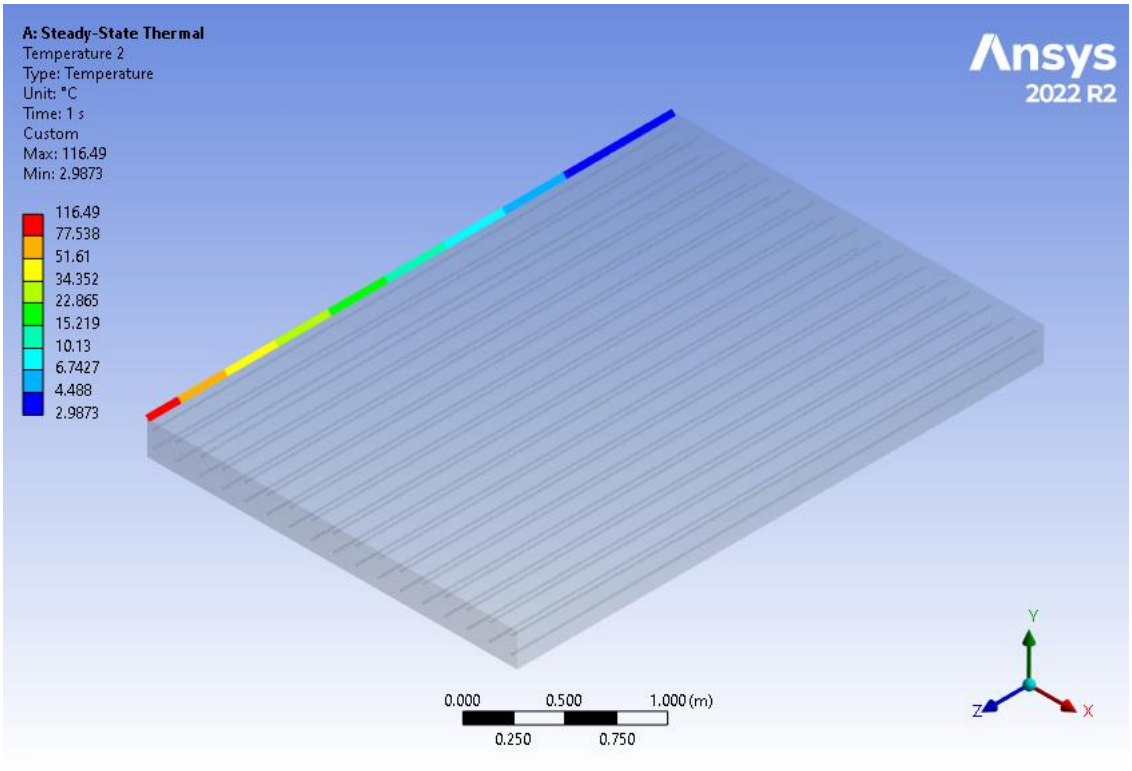

Figure 72. Temperature distribution in the left edge of the deck in Texas using a 1472.22W power energy source.

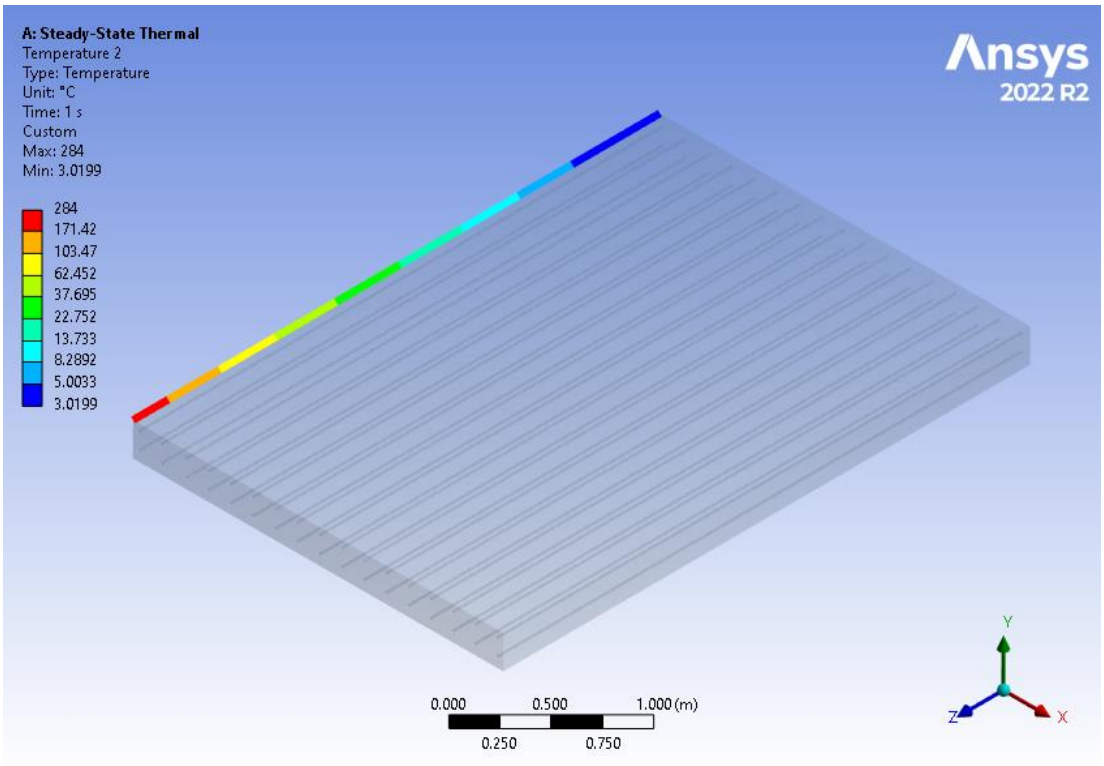

Figure 73. Temperature distribution in the left edge of the deck in Utah using a 4176.86W power energy source.

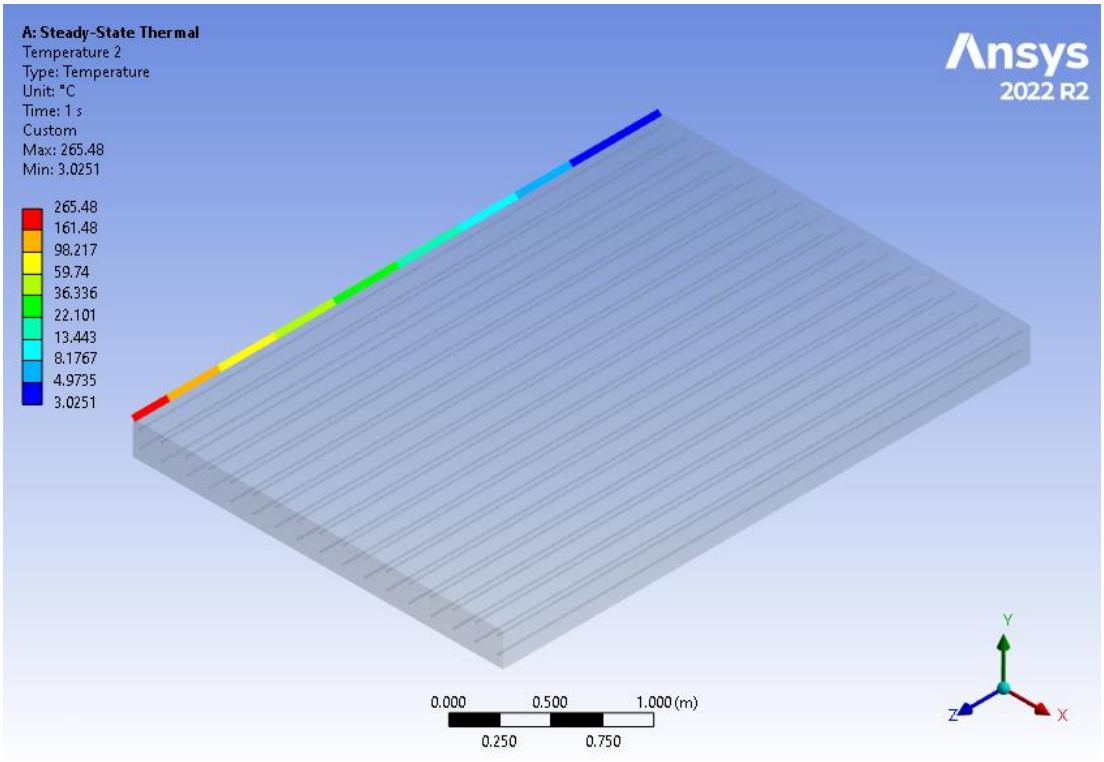

Figure 74. Temperature distribution in the left edge of the deck in Vermont using a 3857.94W power energy source.

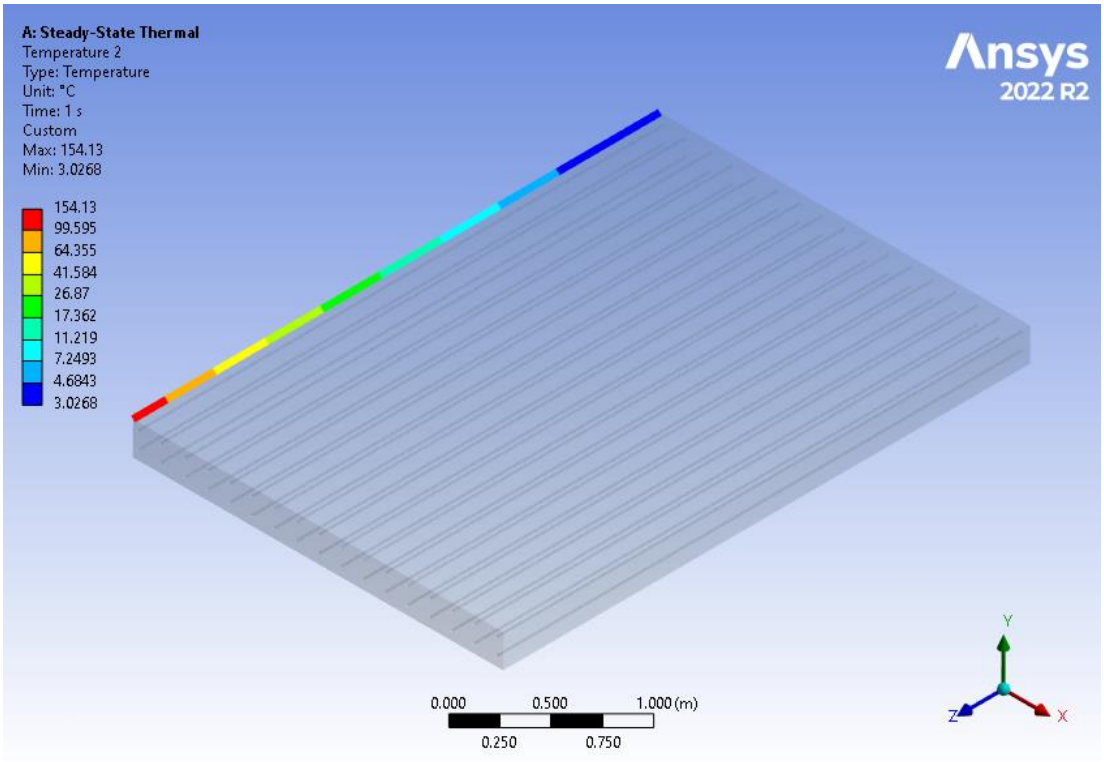

Figure 75. Temperature distribution in the left edge of the deck in Washington using a 2033.56W power energy source.

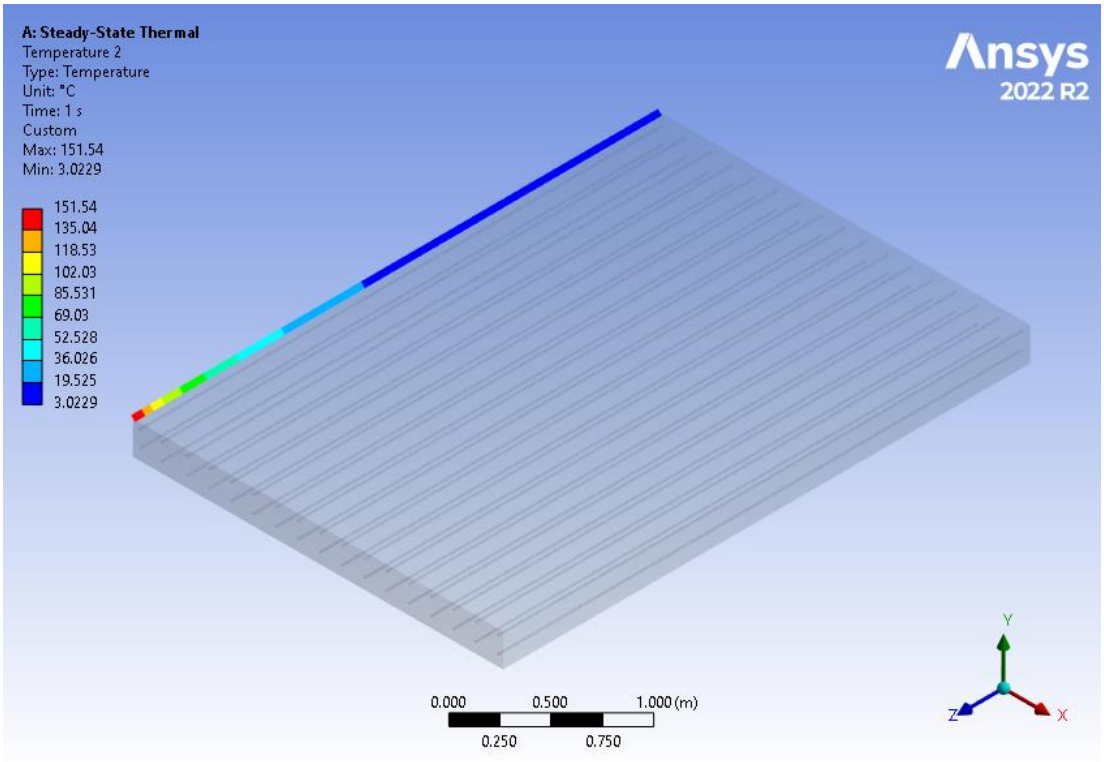

Figure 76. Temperature distribution in the left edge of the deck in West Virginia using a 1993.86W power energy source.

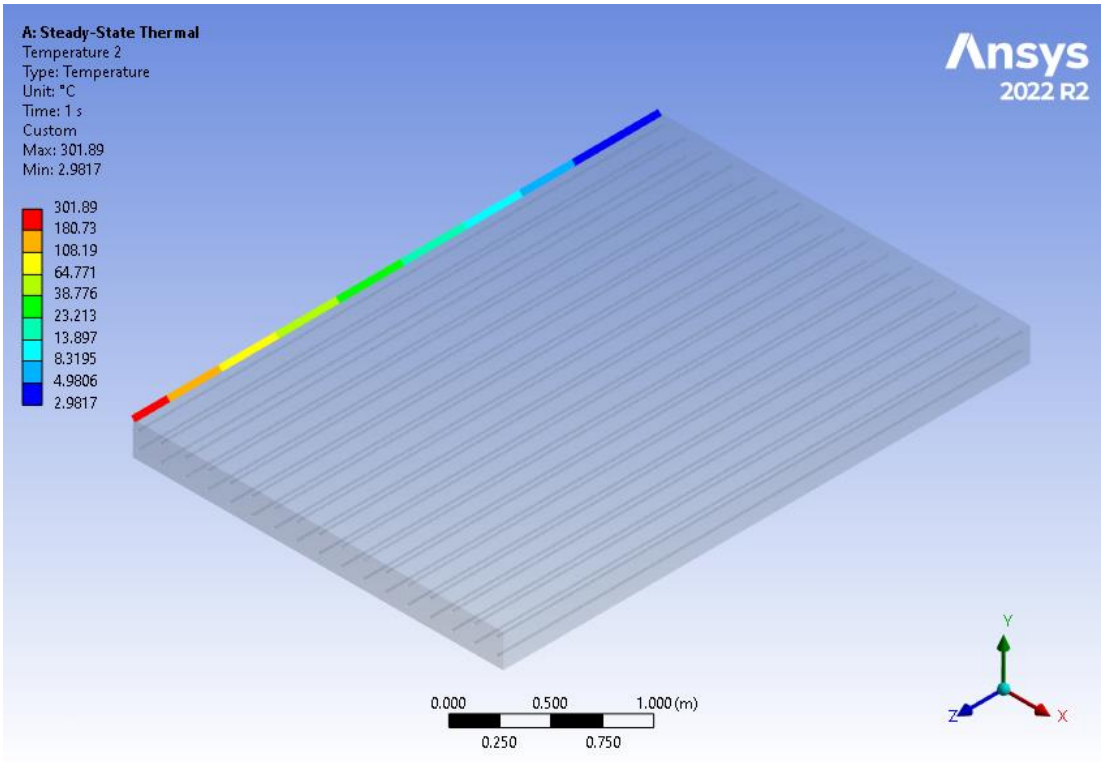

Figure 77. Temperature distribution in the left edge of the deck in Wisconsin using a 4488.61W power energy source.

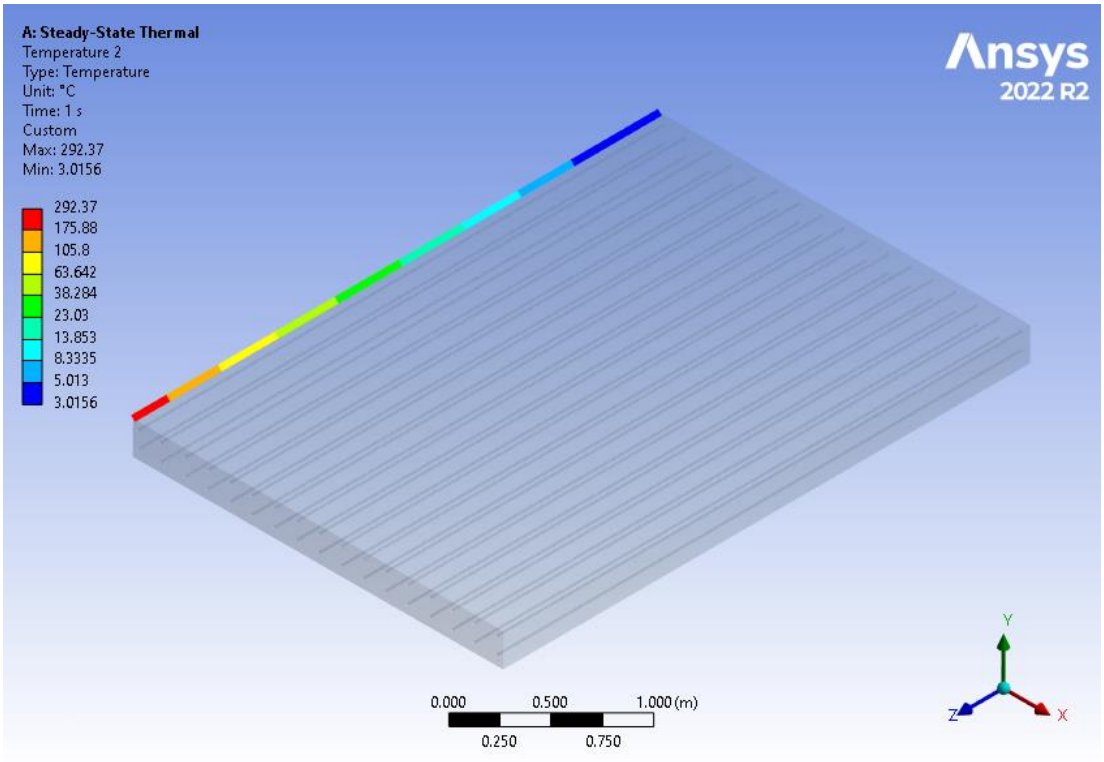

Figure 78. Temperature distribution in the left edge of the deck in Wyoming using a 4322.41W power energy source.

APPENDIX B

Table of ideal EPH for each state.

Table 21. Ideal EPH for state.

State	Temperature (°C)	EPH (W)
Alabama	-2.055	648.29
Alaska	-28.5	8798.85
Arizona	-11.5	2660.15
Arkansas	-3.556	901.24
California	-0.444	404.88
Colorado	-20.167	5385.36
Connecticut	-9.611	2177.85
Delaware	-2.444	711.42
Georgia	-3.667	920.95
Idaho	-14.5	3508.25
Illinois	-11.222	2586.66
Indiana	-9.5	2150.75
Iowa	-13.111	3103.05
Kansas	-9.444	2137.13
Kentucky	-5.056	1179.23
Louisiana	-0.389	397.08
Maine	-20.167	5385.36
Maryland	-4.167	1011.43
Massachusetts	-12.667	2978.08
Michigan	-17.611	4494.19
Minnesota	-22.111	6112.14

Mississippi	-1.556	569.79
Missouri	-10.444	2385.60
Montana	-18.778	4892.00
Nebraska	-12.833	3024.55
New Hampshire	-17.944	4606.15
New Jersey	-8.5	1912.85
New Mexico	-10.833	2485.29
New York	-15.778	3900.16
North Carolina	-3.444	881.49
North Dakota	-21.278	5795.53
Ohio	-8.444	1899.86
Oklahoma	-7.389	1661.68
Oregon	-7.333	1649.38
Pennsylvania	-10.444	2385.60
Rhode Island	-7.5	1686.15
South Carolina	-0.278	381.45
South Dakota	-16.778	4219.57
Tennessee	-4.667	1104.72
Texas	-6.5	1470.65
Utah	-16.611	4165.45
Vermont	-15.611	3847.91
Virginia	-16.5	4129.65
Washington	-9	2030.40
West Virginia	-8.833	1990.83
Wisconsin	-17.556	4475.82
Wyoming	-17.056	4310.36